

Technische Universität München
Lehrstuhl für Angewandte Mechanik

**Flexible Multi-Body Systems with
Set-Valued Force Laws**

Dipl.-Ing. Univ. Roland Zander

Vollständiger Abdruck der von der Fakultät für Maschinenwesen der
Technischen Universität München zur Erlangung des akademischen Grades eines

Doktor-Ingenieurs

genehmigten Dissertation.

Vorsitzender:

Univ.-Prof. Dr.-Ing. Wolfgang A. Wall

Prüfer der Dissertation:

1. Univ.-Prof. Dr.-Ing. habil. Heinz Ulbrich
2. Univ.-Prof. Dr.-Ing. habil. Peter Eberhard, Universität Stuttgart

Die Dissertation wurde am 03.07.2008 bei der Technischen Universität München
eingereicht und durch die Fakultät für Maschinenwesen am 07.11.2008 angenommen.

Für Roswitha

Acknowledgment – Danksagung

Die vorliegende Arbeit entstand während meiner Tätigkeit als wissenschaftlicher Assistent am Lehrstuhl für Angewandte Mechanik der TU München unter der Leitung von meinem Doktorvater Prof. Heinz Ulbrich. Ihm gilt mein herzlicher Dank besonders für seine Unterstützung wie auch die Freiheiten, die ich innerhalb meiner Lehr- und Forschungstätigkeiten genießen durfte. Die Zeit an seinem Lehrstuhl wird mir als abwechslungsreich und lehrreich, aber auch als im positiven Sinne anstrengend in Erinnerung bleiben.

Bei Herrn Prof. Peter Eberhard bedanke ich mich für das meiner Arbeit von Beginn an entgegen gebrachte Interesse und für die Übernahme des Zweitgutachtens. Mit besonderer Freude erinnere ich mich an das erste Zusammentreffen im Rahmen der Ferienakademie 2002 und an das IUTAM Symposium 2006 in Stuttgart.

Ein wesentlicher Beitrag zum Gelingen meiner Arbeit bestand in dem freundschaftlichen Arbeitsklima, das auf den gesamten Kollegenkreis zurück geht, und der allgemein vorherrschenden großen Hilfsbereitschaft am Lehrstuhl. Hier gilt ein besonderer Dank all meinen Zimmerkollegen: Martin Förg, Lucas Ginzinger, Mathias Bachmayer und Daniela Jensen schafften es alle auf ihre jeweils eigene Art, dieses Klima weiter zu intensivieren. Bei Sebastian Lohmeier bedanke ich mich dafür, zu nahezu jeder L^AT_EX-Frage die passende Antwort zu bieten. Die unzähligen privaten Sport- und Freizeit-Betätigungen mit vielen Kollegen sind legendär!

Über die akribische Durchsicht meines Manuskripts und die konstruktiven Anregungen hinaus bin ich meinen Probelesern zutiefst dankbar: Martin Förg vor allem für seine Freundschaft und Unterstützung in allen Belangen; Markus Friedrich dafür, sein überragendes Können am Computer auch seinen unbeholfenen Kollegen zum Vorteil werden zu lassen; Thorsten Schindler für sein eifriges Hinterfragen bei neuen wie alten Aufgaben; Rainer Britz für lange und vielfältige Gespräche bei leckerem Café; Robert Huber für das Engagement, in Lehre und Projekt auch unkonventionelle Wege zu beschreiten.

Meinen Freunden von der Deutschen Lebens-Rettungs-Gesellschaft und vor allem meinem engsten Freundeskreis „Furx“ danke ich für die Ablenkung von der fachlichen Einspurigkeit: Abseits des Alltages war und ist mir dort Ausgleich gewiss.

Meinen Eltern Veronika und Jürgen Zander danke ich für ihre Liebe und ihre Unterstützung. Das durch sie in mich gesetzte Vertrauen hat mich gelehrt, mir selbst etwas zuzutrauen und mein Ziel dann auch zu erreichen.

Ganz besonders großer Dank gebührt meiner Freundin Roswitha Ebner für ihr Vertrauen und ihre Liebe, die mir Kraft für meine Promotion gegeben haben, sowie für ihre Geduld besonders während der letzten Monate meiner Dissertation.

München, im November 2008

Roland Zander

Si tu veux construire un bateau, ne rassemble pas des hommes pour aller chercher du bois, préparer des outils, répartir les tâches, alléger le travail mais enseigne aux gens la nostalgie de l'infini de la mer.

If you want to build a ship, don't drum up people to collect wood and don't assign them tasks and work, but rather teach them to long for the endless immensity of the sea.

Wenn Du ein Schiff bauen willst, so trommle nicht Männer zusammen, um Holz zu beschaffen, Werkzeuge vorzubereiten, die Arbeit einzuteilen und Aufgaben zu vergeben, sondern lehre die Männer die Sehnsucht nach dem endlosen weiten Meer.

accredited to Antoine DE SAINT-EXUPÉRY

Contents

| | | |
|----------|--|-----------|
| 1 | Introduction | 1 |
| 1.1 | Problem Formulation | 1 |
| 1.2 | Literature Survey | 2 |
| 1.3 | Aspects and Outline | 6 |
| 2 | Non-Smooth Multi-Body Systems | 7 |
| 2.1 | Equations of Motion | 7 |
| 2.1.1 | Energetic Principles | 8 |
| 2.1.2 | Measure Differential Equations of Motion | 12 |
| 2.2 | Kinematics of Constraints | 15 |
| 2.3 | Contact Force Laws | 19 |
| 2.3.1 | Single-Valued Force Laws | 19 |
| 2.3.2 | Set-Valued Force Laws | 21 |
| 2.4 | Numerical Methods for Non-Smooth Systems | 25 |
| 3 | Flexible Bodies in Non-Smooth Multi-Body Systems | 27 |
| 3.1 | Analytical Framework | 27 |
| 3.1.1 | Continuum Kinematics | 28 |
| 3.1.2 | Constitutive Laws and Kinetics | 31 |
| 3.2 | Remarks on Time and Local Continuity | 35 |
| 3.3 | Discretization of Flexible Bodies with Discontinuities | 37 |
| 3.3.1 | Discretization | 37 |
| 3.3.2 | Common Formulations | 43 |
| 3.3.3 | Contact and Discontinuity | 46 |
| 3.4 | Contact Kinematics of Flexible Systems | 50 |
| 3.4.1 | Contour Description | 50 |
| 3.4.2 | Contact Conditions | 54 |
| 3.5 | Remarks on Implementation | 55 |
| 4 | Analytic System Reduction | 57 |
| 4.1 | Relative Kinematics | 57 |
| 4.1.1 | General System Description | 58 |
| 4.1.2 | Rigid Bodies on Flexible Structures | 60 |
| 4.2 | The Redundant Coordinate Method | 64 |
| 4.2.1 | Transformations between Coordinate Sets | 64 |
| 4.2.2 | A One-Dimensional Example | 66 |
| 4.2.3 | A Formulation for Planar Slender Beams | 67 |

| | |
|--|-----------|
| 5 Numerical Aspects | 73 |
| 5.1 Time Integration | 73 |
| 5.2 Contact Point Search | 76 |
| 6 Examples | 79 |
| 6.1 Cantilever Beam with Impacts | 79 |
| 6.2 The Elastic Rocking Rod | 81 |
| 6.3 The Woodpecker Toy | 84 |
| 6.4 Elastic Bowl of Dice | 87 |
| 6.5 Push-Belt Continuous Variable Transmission | 89 |
| 7 Conclusion | 93 |
| Bibliography | 95 |

Abstract

Set-valued force laws are commonly used in multi-body simulations for modeling constraints. Here, contacts implying structural variance are of special interest since these might induce jumps to the system velocities. The current work extends and applies the methods developed for rigid body systems to the simulation of flexible systems: particularly the discretization of a flexible continuum with spatial discrete contacts in mind is addressed. Thereby, special systems allow for minimal coordinate representations. Numerical methods and program algorithms are presented aside. Closing up examples span the field from academic systems up to the modeling of industrial component assemblies.

Kurzfassung

In der Mehrkörpersimulation werden mengenwertige Kraftgesetze zur Beschreibung von Nebenbedingungen verwendet. Hierbei sind insbesondere Bindungen von Interesse, die zu Strukturvarianzen führen und somit Sprünge in den Systemgeschwindigkeiten bewirken können. Die vorliegende Arbeit erweitert die für Starrkörpersysteme entwickelten Methoden auf die Simulation von flexiblen Mehrkörpersystemen: insbesondere die Diskretisierung eines flexiblen Kontinuums vor dem Hintergrund ortsdiskreter Kontakte wird diskutiert. Dabei erlauben spezielle Systeme eine Formulierung in Minimalkoordinaten. Begleitend werden Fragen der Numerik und Programm-Algorithmik behandelt. Die abschließenden Beispiele erstrecken sich von einfachen akademischen Systemen bis hin zur Modellierung industrieller Baugruppen.

1 Introduction

Multi-body simulation, mainly being devoted to the dynamics of machinery, is an important method of computational engineering. The increasing complexity of technical systems raises the demand for highly sophisticated simulations. This is reflected directly by the development during the last decades: both theory and numerics for multi-body system (MBS) modeling are subject of intensive research. Thereby, the description of structural flexibilities as well as the inclusion of arbitrary contact situations form self-contained working fields of great importance. Concurrently, the description of flexible bodies as well as the investigation of systems with contacts find their way into commercial simulation environments but usually are of limited applicability when regarding both simultaneously but excluding contact flexibility.

1.1 Problem Formulation

Classically, MBS were conceived as systems of rigid bodies undergoing large spatial motion. The resulting mathematical models are commonly nonlinear. The bodies are coupled by interaction forces describing joints, discrete flexible elements like springs and dampers or active subsystems of control. Partly, kinematic constraints can be regarded without evaluating force laws by the use of an adapted parametrization for tree structured systems. In setting up the simulation model by these standard elements of multi-body simulation and applying additional loads and boundary conditions, even complex system designs can be investigated concerning the long-term dynamical behavior.

The incorporation of structural flexibilities in MBS is the consequent extension to technical systems where the overall dynamics is significantly influenced by the deformations of single bodies. Since the beginning, models superposing small deflections relatively to the rigid body motion have been used. This intuitive enhancement of the rigid body approach offers a highly structured mathematical model of high computational performance and furthermore good physical interpretability. To capture more details and to allow for the description of material and further geometrical nonlinearities, more sophisticated models were derived partly in co-evolution with modern techniques of nonlinear finite element theory. Nevertheless, flexible MBS should be distinguished from simulations aiming for highly detailed descriptions of local phenomena like it is often the ambition in structural finite element simulations. Due to the desired long-term analysis, flexible MBS must always make a compromise between detailed modeling and the overall performance of the entire simulation even in spite of the continuous growth of computational power.

Since the beginning of multi-body simulation, the description of constraints within the systems' kinematics is a central topic. Constraints can for example trace back to joints between bodies, giving a bilateral connection, or even collision scenarios with attachment and separation. In this context, set-valued descriptions for constraints are of special importance: providing exact kinematic compliance but introducing reaction forces that can not be formulated as explicit functions of the state, they lead to differential algebraic equations probably supplemented by inequality relations. One example can be a revolute joint exchanging arbitrarily high forces between the connected bodies and requesting unitary motion of the joined body axes. This corresponds to the limit case of an infinitely stiff flexibility connecting the bodies. For a closing contact between two bodies, additional considerations are requested to allow for the instantaneous adaption of the relative velocity: this leads to a jump of the system velocities. Due to the high technical relevance, also friction is of immense interest in multi-body simulations. For systems with stick-slip phenomena, the corresponding COULOMB friction is described by inequality conditions for the tangential contact reactions and kinematics depending upon the normal load. The resulting mathematical models must be evaluated considering additional impact conditions for closing contacts. Recently, special methodical and numerical approaches have been developed successfully. However, the contributions to the numerical simulations of multi-body systems with set-valued force laws so far address mainly rigid body systems only.

The formulation of flexible MBS with set-valued force laws including impacts raises additional aspects to concern. Usually MBS model contacts spatially discrete: this has to be captured by the spatial discretization of a flexible body. At the same time, the discretization has influence on the solution of multi-contact situations and the efficiency of the simulation. So far, these points are addressed only insufficiently in literature. Beyond, neither research nor commercial multi-body simulation software include general frameworks for the combination of rigid and flexible MBS with spatial rigid contact situations including dry friction.

1.2 Literature Survey

Speaking of a self-contained research field, multi-body simulation is comparatively new. Nevertheless, the literature is tremendous, though at this point only a small and in no way comprehensive selection can be presented. Aiming for this comprehensive review, SCHIEHLEN [49] provides an encyclopedic article on the roots, progress and perspectives giving about 200 references capturing many of the specialized fields of multi-body simulation.

General Descriptions

Only some prominent contributions to the field of MBS and simulation shall be mentioned. By the way, it is noteworthy that the term “multi-body” is by no means

general in the sense that also the spellings “multibody”, “multi body” are widely used with the same meaning. Still, the central definitions are common.

MAGNUS [40] hosted the first IUTAM symposium on multi-body dynamics in 1977 with many contributions to rotor dynamics. PFEIFFER [44] focuses on theory and application for systems of rigid bodies but also gives extensions to moving frame of reference modeling for flexible bodies. From the broad field of multi-body dynamics, ULBRICH [60] emphasizes machine and rotor dynamics, SCHIEHLEN [49] names vehicle dynamics, robotics and aerospace being most prominent. The definition of MBS given in the introduction of this thesis is according to these authors work.

While giving strong emphasis on flexible sub-systems, the book [56] of SHABANA starts with a profound introduction to rigid body dynamics including various parametrizations for the spatial rotation. Thereafter, the central point is the description of flexible structural elements. This work is continued by his contributions concerning the absolute nodal coordinate formulation. Collecting selected presentations of the ECCOMAS Thematic Conference in Multibody Dynamics 2003, AMBRÓSIO [4] provides an overview on the current research activity.

Flexible Systems

The term flexible MBS refers to systems holding deformable bodies with internal dynamics. Being of prime importance, elastic systems are limited to fully reversible deformation behavior and build their oldest and largest subgroup. A very profound review concerning theory and application of flexible MBS is given by WASFY AND NOOR [62]. Including more than 850 references on the entire field, the authors provide a systematical classification of floating, co-rotational and inertial frame of reference approaches. Naming inputs from other fields of continuum mechanics, especially finite element techniques, important similarities as well as differences between the concepts are described.

Starting in the late 1960s, the moving frame of reference models are the native extension of the rigid body assumptions towards systems with small relative deflections. In their book [10], BREMER AND PFEIFFER concentrate the knowledge in this field: especially the possibility for perfect modal decoupling, the well structured properties of the mass matrices and a sharp frequency range, which is set by the modes used for modeling, are valuable providing high numerical efficiency.

Almost contemporaneously to the moving frame of reference models, co-rotational formulations came up for structural finite element simulations. In 1977, BELYTSCHKO AND SCHWER [7] published a formulation for beams based on specific frames of reference for each element. As mentioned by WASFY AND NOOR, this work is continued up to now: CRISFIELD ET AL. [14] derive a model for geometrical large deformations of spatial beam systems. Similarly being influenced by structural finite element techniques, GÉRADIN AND CARDONA [26] follow the updated LAGRANGIAN approach for the development of finite elements allowing for large rotations on the level of single elements.

SHABANA [54] defines a framework for flexible systems with recursive kinematics and introduces the absolute nodal coordinate formulation (ANCF). The ANCF is among the inertial frame finite element formulations and leads to correct description of large rotations intrinsically. Additionally, his book [56] captures moving frame of reference descriptions. The first ANCF formulation for a planar EULER-BERNOULLI beam is given by SHABANA [55]. Starting with a review on existing ANCF formulations, GERSTMAYR [27] provides extensions towards elasto-plastic material behavior.

Impact and Non-Smooth Dynamics

Among the contributions devoted to impact mechanics, a differentiation is needed whether the description includes jumps in the system velocities induced by rigid contact modeling or a regularization of the contact conditions preserves smoothness of the velocities. While the current work refers to the first definition to characterize non-smooth dynamics, also contributions devoted to flexible contact modeling must be mentioned: both approaches significantly contribute to the overall understanding of contact physics and modeling.

A hybrid approach for the simulation of contact situations is used by EBERHARD [15] switching between multi-body simulation for the long-term investigation and detailed finite element simulation for analyzing contact situations: this embeds local flexibility within the finite element part resolving impact restitutions for the overall behavior. Based on this work, EBRAHIMI [16] describes contacts of complex shaped deformable bodies: he partly resumes rigid contact approaches and also extends the Polygonal Contact Model of HIPPMANN [35, 36] which describes local flexibility for contacting rigid bodies based on a thin layer theory. Utilizing real experiments as well as multi-scale simulations in finite element and multi-body tools, SEIFRIED [53] analyzes a flexible rod with longitudinal impacts to gain interpretations for geometry and material dependency of the contact dynamics in multi-body simulations.

Spanning from the mathematical formulation to real system applications of rigid impact modeling, BROGLIATO ET AL. [11] provide more than 200 references. Also accompanied by many references, the book [12] of BROGLIATO gives a profound introduction to non-smooth multi-body dynamics described by set-valued force laws. A coherent formulation for impacts including planar COULOMB friction is provided by PFEIFFER AND GLOCKER [45] and GLOCKER [29], whereas contact force laws are formulated and evaluated in form of linear complementary problems (LCP).

While the physical interpretation of set-valued force laws is quite clear, the numerical methods for contact treatment and time integration rise additional tasks compared to ordinary differential equations. Lately, ACARY AND BROGLIATO [1] provide an extensive discussion on modern numeric methods for non-smooth systems.

The first time-stepping algorithm was formulated by MOREAU [42] incorporating the equations for planar frictional impacts within the time discretization. Providing formulations on position and on velocity level for the solution of the constraints, STIEGELMAYR [57] also includes spatial friction. The work of JEAN [38] is of special

interest for stiff mechanical problems since an implicit rule of high stability is used for time integration. Very recently, STUDER [58] comprehensively reviews existing integration rules for non-smooth systems. He generalizes the linear time-stepping schemes and constructs rules for time-step adjustment and higher-order integration for impact-free phases.

ALART AND CURNIER [2] introduce a constraint formulation by proximal functions as alternative with better solvability compared to LCPs. On this mathematical basis, FÖRG [19] develops iterative solvers for the constraint problem. For academic and industrial applications he shows the capability for the efficient simulation even of high-dimensional dependent contact situations and spatial friction.

Applications

Applications combining flexible multi-body descriptions with non-smooth dynamical behavior arise from all fields of machine dynamics: embedded in an compact overview, ZANDER ET AL. [66] name academic examples as well as instances of industrial relevance like cam-shaft drives and continuous variable transmissions (CVT).

The behavior of a flexible beam in impact situations is investigated numerically by ZANDER ET AL. [65]. The classic benchmark of a rigid beam rocking on two point obstacles is extended toward structural flexibility. Based on numerical investigation, an interpretation of the restitution coefficient for purely rigid setups is sketched. GINZINGER ET AL. [28] investigate concepts for the control of a rotor mounted eccentrically on a flexible shaft by means of simulation and experiment. Implying a rigid contact between shaft and the actuated auxiliary bearing, the simulation of the system also needs to regard impact dynamical behavior.

Aiming to take advantage of the non-smooth system character, WELGE-LÜSSEN [63] models and controls an under-actuated manipulator. Due to the significant influence on the system dynamics, the flexibility of single components is described within the simulations. Real experiments are used for model validation. BACHMAYER ET AL. [5] develop optimal control trajectories for elastic robots by means of computer simulations. The model for the investigated rack feeder comprises flexible and rigid components connected by bilateral sliding contacts.

ENGELHARDT [17] investigates the dynamics of cam-shaft and timing drives of combustion engines. The deformations of the shafts are of minor magnitude despite of the impacts of rollers, permitting the use of rigid body models. In contrast, the dynamics of the elastic valve-spring with self-contact is of significant influence on the overall behavior. GEIER [25] simulates a push-belt CVT with transient planar motion using large deformation finite elements provided by ZANDER AND ULBRICH [68]. The belt is composed of flexible steel rings guiding rigid elements, whereas the intermediate contacts are modeled rigidly including friction. The work is validated by real system measurements. To allow for the extension of the CVT model towards spatial dynamics, SCHINDLER ET AL. [51] enhances the beam model and additionally regards spatial contact situations.

1.3 Aspects and Outline

The literature provides many contributions to both the description of flexible subsystems and rigid contact treatment in multi-body simulations. Nevertheless, especially the rigid modeling of sliding contacts or impacts on flexible systems is only rarely addressed. The present work discusses aspects of the formulation of flexible MBS in presence of set-valued force laws for discrete contacts: the discretization of the flexible continuum should respect the local character of the contact model. Constraints involving flexible bodies are regarded in two ways: the general description including unilateral contact complements the free body equations of motion by constraint equations. Additionally, strategies for an analytic reduction of the system are regarded for special configurations. The modular concept of multi-body simulations is attended in all steps.

Chapter 2 provides an introduction to the mathematical formulation of systems with non-smooth dynamics. Initially, the HAMILTON principle and the LAGRANGE equations are discussed with constrained and non-smooth systems in mind: energy principles are often used to derive equations for the dynamics of continua. Based on a general interpretation of the contact kinematics, single-valued and set-valued force laws describe contact interactions between the bodies being involved. The chapter closes with a brief overview on numerics for non-smooth MBS.

The derivation of the discrete equations for a flexible system is discussed in chapter 3 with an introduction to the continuous analytic description. Especially the local character of impacts is discussed: the non-continuity of the velocity fields with respect to time also occurs regarding the location. For contact situations, this spatial focus should be preserved by the discretization of the continuum. For the kinematics of a contact, a unitary description of the flexible structure uses the discretization performed for the internal dynamics; independent contour descriptions provide additionally continuous shapes for arbitrary bodies.

Chapter 4 addresses the reduction of bilateral constrained systems using re-parametrizations and projections. A relative kinematic description of tree-structured system is provided giving compact equations of motion. The projection equations describing systems by means of redundant coordinate sets are of similar character: the overall system size and therewith the numerical effort can be reduced.

A numerical framework specialized on the simulation of flexible systems with rigid contacts is shown in chapter 5: concepts and experiences for the time integration, the solution of the constraints and for finding of possible contact points are presented.

Finally, chapter 6 gives examples showing the capabilities of the methodologies. Provided are simple academic setups like the woodpecker toy up to complex multi-contact situations for the simulation of industrial systems, here a push-belt CVT. All simulations are performed within the MBSIM-software¹ package, which holds a module for non-smooth flexible MBS resulting from the present work.

¹ Abbreviation for *Multi-Body Simulation Software*: <http://mbsim.berlios.de>. This was initiated by FÖRG [19] and is developed with colleagues at the Institute of Applied Mechanics.

2 Non-Smooth Multi-Body Systems

Fundamental contributions were made in the past decades to the theoretical and numerical framework for multi-body systems (MBS): descriptions for arbitrary rigid body motion, flexible bodies and all kinds of interactions including kinematic restrictions were developed. One focus of present work is on systems with algebraic constraints including inequalities describing unilateral contacts. It is well known in multi-body dynamics that single-valued approximations for arbitrary contacts preserve the smooth character of the system's velocities, as do all bilateral constraints implying smooth surfaces in case of relative motion. In contrast, set-valued laws for unilateral contacts and friction yield impact behavior leading to jumps within the system's velocities: the resulting dynamics is said to be non-smooth.

The current chapter briefly resumes investigations devoted to the description of non-smooth MBS; for more profound information refer to the cited literature. Even these works mainly address the dynamics of rigid body systems, the general mathematical framework can be applied to all hybrid MBS: all mathematical formulations include differential equations of motion and constraint relations. In section 2.1 the governing equations of motion for constrained systems are developed. An introductory preface is devoted to the principles of analytical mechanics which are often used for the development of the equations for flexible systems. The kinematics of contacts, being a special part of the overall system kinematics, is briefly discussed in section 2.2. Section 2.3 introduces single- and set-valued force laws for contacts also giving a short description of modern formulations based on projection-functions. Finally, section 2.4 provides a brief overview on the numerics for non-smooth MBS.

2.1 Equations of Motion

For developing the differential equations describing the dynamics of a mechanical system, two basically different concepts can be followed: variational methods, based on energy or power considerations, are used in LAGRANGIAN/*analytical mechanics*; dynamical force and momentum equilibrium conditions with additional transformations are referred to as NEWTONIAN/*synthetical methods*. These formulations are equivalent – but not necessarily of the same effort of work for deriving the equations of motion¹ – and can be transferred to another, see MARS DEN AND RATIU [41].

¹ To the belief of the author, non of these formalisms can a-priori be said to be superior compared to the others for all applications. It is a fact that a specific mechanical problem might be easier to describe by one formalism, but this does not yield a general predominance of this formalism in all fields.

Taking the procedural method of FÖRG [19], equations of motion for smooth transition are derived in a first step and extended to non-smoothness subsequently. This can also be seen on the background of the historical development in mechanics, where non-smooth dynamics is an extension to classical smooth dynamics and comparatively new. Amongst others PFEIFFER AND GLOCKER [45] define the characteristic of non-smooth dynamics: jumps occur in the system velocities due to discrete impact events. The equations for smooth dynamics are used as basis for developing equations for the non-smooth behavior represented by measure differential equations, compare for example the work of BROGLIATO [12]. In agreement with others, HUBER AND ULBRICH [37] and ZANDER AND ULBRICH [68] have shown lately in practical applications that this framework is not limited to rigid bodies but can also be used for any hybrid MBS.

2.1.1 Energetic Principles

Within the present work, LAGRANGE equations are used for the development of the equations of motion. Being a classical representative of analytical mechanics, they can be developed from HAMILTON's fundamental considerations of least action, proclaiming an energetic optimality of motion. The HAMILTON principle gives a powerful mathematical basis to a large manifold of dynamic systems not only for flexible solids but also for fluid-dynamics, relativistic extensions and many more. Detailed explanations on the HAMILTON principle and the associated development of the (EULER)-LAGRANGE equations are given by MARSDEN AND RATIU [41]. Less profound concerning the principles of dynamics but more illustrative to read are the books of GÉRADIN AND CARDONA [26] and SHABANA [56], both being devoted mainly to the systematic description of flexible MBS.

The system shall be described by the discrete generalized coordinates $\mathbf{q} = \mathbf{q}(t) \in \mathbb{R}^n$ (generalized positions) and generalized velocities $\mathbf{u} = \frac{d\mathbf{q}}{dt} = \dot{\mathbf{q}}$ both being function of the time t and spanning the n -dimensional configuration space of the system². The dimension n of \mathbf{q} is called the number of degrees of freedom, which will be used even for constraint systems with this meaning. If no constraints are present for the system, \mathbf{q} are minimal coordinates. Using the associated LAGRANGE functional $L = L(\mathbf{q}, \mathbf{u})$, which for mechanical systems is kinetic minus potential energy ($L = T - V$), the HAMILTON-principle utilizes the variation δ on the action integral to claim least action for a change between fixed start- and endpoints $\mathbf{q}_0 = \mathbf{q}(t_0)$ and $\mathbf{q}_1 = \mathbf{q}(t_1)$:

$$\delta \int_{t_0}^{t_1} (L + W) dt = 0 \quad (2.1)$$

The LAGRANGIAN L exclusively depends on the positions and the velocities: this reflects that the dynamics of the systems is uniquely defined by the state $(\mathbf{q}^T, \mathbf{u}^T)^T$. For generalizations to systems with L explicitly being function of time t refer to the

² The more general form $\dot{\mathbf{q}} = \mathbf{T}\mathbf{u}$ with $\mathbf{T} = \mathbf{T}(\mathbf{q})$ can be found in publications (e.g. [19, 22]) but is unusual in flexible MBS. The dot ($\dot{\xi}$) marks the total time derivative of ξ within this work.

literature. The virtual work $\delta W = \delta \mathbf{q}^T \mathbf{Q}$ is performed by the generalized forces \mathbf{Q} due to the variation $\delta \mathbf{q}$ represented in configuration space. This accounts for loads not being included in L , especially dissipations and external loads.

The adaption to fields $\boldsymbol{\varphi} \in \mathcal{F}(\mathbb{R}^3)$ in the linear function space on \mathbb{R}^3 replacing the discrete coordinates \mathbf{q} is straight forward, see MARS DEN AND RATIU [41]. With the associated velocity field $\boldsymbol{\omega} = \dot{\boldsymbol{\varphi}}$, the LAGRANGE density $\mathcal{L}(\boldsymbol{\varphi}, \boldsymbol{\omega})$ is evaluated. While the deformation of flexible bodies is described by fields $\boldsymbol{\varphi}$, usually no exact solution for these can be found. Approximations based on ansatz-functions are used to discretize the field problem to a problem in the finite set \mathbf{q} , which is the central topic of section 3.3. Therefore, the equations discussed at this point are formulated for discrete states only.

Systems in Minimal Coordinate Representation In a first step, only holonomic systems are regarded with all constraints being implicitly fulfilled by the adapted choice of the state variables $(\mathbf{q}^T, \mathbf{u}^T)^T$. Assuming at this point velocities \mathbf{u} being smooth with respect to time, variational calculus yields – in form of a first step of analysis – the (EULER)-LAGRANGE equations of second type

$$\frac{d}{dt} \left(\frac{\partial L}{\partial \mathbf{u}} \right)^T - \left(\frac{\partial L}{\partial \mathbf{q}} \right)^T = \mathbf{Q} \in \mathbb{R}^n \quad (2.2)$$

as equivalent formulation of the optimality stated by equation (2.1); for a detailed derivation see again [41]³. Hence, the requirements concerning continuity of the kinematic quantities \mathbf{q} and \mathbf{u} – the velocities undergo jumps within non-smooth mechanics – are higher in equation (2.2) than for equation (2.1). The HAMILTON-principle therefore might also be used as initial point to contact mechanical problems including non-smooth dynamics intrinsically.

For mechanical systems the kinetic energy $T = T(\mathbf{q}, \mathbf{u})$ is a positive definite quadratic function in the system's velocities \mathbf{u} . The potential $V = V(\mathbf{q})$ does not depend on the velocities \mathbf{u} . With these, equation (2.2) can be rewritten:

$$\begin{aligned} \frac{d}{dt} \left(\frac{\partial T}{\partial \mathbf{u}} \right)^T - \left(\frac{\partial T}{\partial \mathbf{q}} \right)^T + \left(\frac{\partial V}{\partial \mathbf{q}} \right)^T &= \mathbf{Q} \\ \left(\frac{\partial^2 T}{\partial \mathbf{u}^2} \right)^T \frac{d\mathbf{u}}{dt} + \left(\frac{\partial^2 T}{\partial \mathbf{u} \partial \mathbf{q}} \right)^T \mathbf{u} - \left(\frac{\partial T}{\partial \mathbf{q}} \right)^T + \left(\frac{\partial V}{\partial \mathbf{q}} \right)^T &= \mathbf{Q} \\ \mathbf{M} \dot{\mathbf{u}} &= \mathbf{h} \end{aligned} \quad (2.3)$$

Due to the special form of T , the mass matrix $\mathbf{M} = \mathbf{M}(\mathbf{q}) = (\partial^2 T / \partial \mathbf{u}^2)$ is positive definite and symmetric. The generalized force vector $\mathbf{h} = \mathbf{h}(\mathbf{q}, \mathbf{u})$ holds all smooth external, internal and gyroscopic forces. In particular, \mathbf{h} also holds reactions of

³ MARS DEN/RATIU provide an interesting historic detail: in 1834, HAMILTON not LAGRANGE, who worked on variational calculus some years earlier, showed equivalence for (2.1) and (2.2).

contacts described by single-valued force laws representing for example flexible contacts, see section 2.3. The structure of the second order differential equations (2.3), holding linear relations between the accelerations $\dot{\mathbf{u}}$ and the loads through the mass matrix, is the same for all dynamic systems in mechanics; specializations for example for rigid bodies can be given together with interpretations of single terms. When using the LAGRANGE equations for the derivation of the equations of motion, the main tasks are setting up kinematic descriptions, leading to the kinetic energy T , and evaluating the constitutive laws giving rise to the potentials V .

The work δW_i of the generalized force \mathbf{Q}_i with the virtual variation $\delta \mathbf{q}$ corresponds to the force \mathbf{F}_i in physical representation with the compatible virtual variation $\delta \mathbf{r}_i$ of the point of force application:

$$\delta W_i = \mathbf{Q}_i^T \delta \mathbf{q} = \mathbf{F}_i^T \delta \mathbf{r}_i = \mathbf{F}_i^T \frac{\partial \mathbf{r}_i}{\partial \mathbf{q}} \delta \mathbf{q} \quad (2.4)$$

The respective generalized force

$$\mathbf{Q}_i = \left(\frac{\partial \mathbf{r}_i}{\partial \mathbf{q}} \right)^T \mathbf{F}_i = \left(\frac{\partial \dot{\mathbf{r}}_i}{\partial \mathbf{u}} \right)^T \mathbf{F}_i = \mathbf{J}_{T,i}^T \mathbf{F}_i$$

uses the JACOBI-matrix $\mathbf{J}_{T,i}$ of translations representing the linear transformation between physical and generalized translational velocities. Proposing the equality of power committed by a torque \mathbf{R}_i with virtual variation $\delta \boldsymbol{\Omega}$ of angular velocity, the generalized load \mathbf{Q}_i due to a torque is developed analogously⁴:

$$\delta P_i = \mathbf{R}_i^T \delta \boldsymbol{\Omega} = \mathbf{Q}_i^T \delta \mathbf{u} \quad \rightarrow \quad \mathbf{Q}_i = \left(\frac{\partial \boldsymbol{\Omega}_i}{\partial \mathbf{u}} \right)^T \mathbf{R}_i = \mathbf{J}_{R,i}^T \mathbf{R}_i \quad (2.5)$$

Here, $\mathbf{J}_{R,i}$ is the JACOBI-matrix of rotations. The cumulated load vector $\mathbf{Q} = \sum_i \mathbf{Q}_i$ is the sum of all projected loads \mathbf{Q}_i not contributing to the LAGRANGIAN L .

Systems with Holonomic Bilateral Constraints So far, the equations are developed for minimal coordinates \mathbf{q} and velocities \mathbf{u} implicitly fulfilling all system constraints. If the system is limited in a way that no minimal coordinates can or shall be constructed during the model setup, constraint equations need to be included within the system equations. For the extension towards l holonomic bilateral constraints $\mathbf{g}_B = \mathbf{g}_B(\mathbf{q}, t) = \mathbf{0} \in \mathbb{R}^l$, the augmented LAGRANGE functional

$$L = L(\mathbf{q}, \mathbf{u}, \boldsymbol{\lambda}_B) = T - V - \mathbf{g}_B^T \boldsymbol{\lambda}_B \quad (2.6)$$

is used within the HAMILTON principle (2.1). The independent LAGRANGE multipliers $\boldsymbol{\lambda}_B = \boldsymbol{\lambda}_B(t)$ can be seen as extension $(\mathbf{q}^T, \mathbf{u}^T)^T \rightarrow (\mathbf{q}^T, \mathbf{u}^T, \boldsymbol{\lambda}_B^T)^T \in \mathbb{R}^{2n+l}$ of the state ensuring the constraints' validity. The equations of motion again are derived

⁴ Commonly, the symbol “ \mathbf{M} ” is used for torques. This shall be reserved for the mass matrix \mathbf{M} within this work, so \mathbf{R} will be used for torques in physical representation.

by evaluation of the principle (2.1) in analogy to equation (2.2):

$$\frac{d}{dt} \left(\frac{\partial(T-V)}{\partial \mathbf{u}} \right)^T - \left(\frac{\partial(T-V)}{\partial \mathbf{q}} \right)^T - \underbrace{\left(\frac{\partial \mathbf{g}_B}{\partial \mathbf{q}} \right)^T}_{\mathbf{W}_B} \boldsymbol{\lambda}_B = \mathbf{Q} \in \mathbb{R}^n \quad (2.7a)$$

$$\mathbf{g}_B = \mathbf{0} \in \mathbb{R}^l \quad (2.7b)$$

These are n differential equations of system dynamics plus l algebraic equations describing the constraints⁵. The LAGRANGE multipliers $\boldsymbol{\lambda}_B \in \mathbb{R}^l$ are projected into configuration space by the generalized force directions \mathbf{W}_B of bilateral constraints and can take arbitrary values ensuring $\mathbf{g}_B = \mathbf{0}$, see section 2.3.2. Therefore, the formulation of a bilateral constraint is set-valued: only the implicit formulation (2.7) can be given for $\boldsymbol{\lambda}_B$ but no function explicitly depending on the system state.

Systems with Unilateral Constraints and Impacts Within this work, non-smooth dynamics is characterized by jumps within the system velocities due to impacts. This cuts off the general differentiability of \mathbf{u} and therefore effects the variational calculations performed on the kinetic energy T during the evaluation of the HAMILTON principle (2.1). Similarly, the constraint reactions must be adapted to a conforming representation of discrete impact percussions: both is addressed in the following section 2.1.2. In advance, approaches for the evaluation of the principle (2.1) considering non-smoothness and a transfer to the principle of D'ALEMBERT are referred.

Restricted to conservative systems with collisions being perfectly elastic and frictionless, PANAGIOTOPOULOS [43] and BROGLIATO [12] independently give formulations utilizing HAMILTON's principle for the derivation of equations of motion including impacts: an explicit differentiation is introduced between impacts and smooth transitions within the variational framework. The constraint reactions are not included explicitly but accounted for within the impact conditions imposing conservation of tangential momentum and total energy (only perfect elastic and frictionless impacts are regarded). FETECAU ET AL. [18] derive a similar formulation and use it for a time discretization based on the action integral (2.1). Additionally, they sketch the extension to dissipative impacts.

Unilateral inequality constraints $\mathbf{g}_U = \mathbf{g}_U(\mathbf{q}, t) \geq \mathbf{0}$ describing normal contact conditions can be included in the LAGRANGIAN (2.6) like the bilateral relations. Sorting between times of smooth transitions and discrete times of impacts, specific equations describing the system dynamics are derived. The HAMILTON principle (2.1) again

⁵ At this point, a reference and comparison to constrained optimization theory might be useful: The HAMILTON principle (2.1) claims critical work for state changes: in other words optimality. The additional term used for augmentation of the LAGRANGIAN (2.6) is known from optimization with respect to equality constraints. In the following, the equations of motion include inequality constraints and are similar to the KARUSH-KUHN-TUCKER conditions and the LAGRANGE multiplier rule from optimization theory, see e.g. [8, 13] and [29].

is evaluated using LAGRANGE equations:

$$M\dot{\mathbf{u}} = \mathbf{h} + \mathbf{W}\boldsymbol{\lambda} \quad , \quad \mathbf{W} = \left(\left(\frac{\partial \mathbf{g}_B}{\partial \mathbf{q}} \right)^T , \left(\frac{\partial \mathbf{g}_U}{\partial \mathbf{q}} \right)^T \right) \quad (2.8a)$$

$$\mathbf{g}_B = \mathbf{0} \quad (2.8b)$$

$$\mathbf{g}_U \geq \mathbf{0} \quad , \quad \boldsymbol{\lambda}_U \geq \mathbf{0} \quad , \quad \boldsymbol{\lambda}_U^T \mathbf{g}_U = \mathbf{0} \quad (2.8c)$$

These equations with the constraint reactions $\boldsymbol{\lambda} = (\boldsymbol{\lambda}_B^T, \boldsymbol{\lambda}_U^T)^T$ describe smooth parts of motion only. For the times of closing contacts, additional impact laws are needed inducing jumps in the system velocities: these laws must at least ensure post-impact validity of the constraint equations (2.8b) and (2.8c) and are topic of section 2.3.2. The complementarity ($\mathbf{g}_U \geq \mathbf{0}, \boldsymbol{\lambda}_U \geq \mathbf{0}, \boldsymbol{\lambda}_U^T \mathbf{g}_U = \mathbf{0}$) is requested since only active closed contacts imply positive LAGRANGE multipliers $\boldsymbol{\lambda}_U$. For a profound discussion of the theoretical framework including additional references see BROGLIATO [12].

Providing equations similar to (2.2), FUNK [24] develops the LAGRANGE formalism starting from D'ALEMBERT principle of vanishing virtual work in the formulation of LAGRANGE. Right from the start he regards non-smoothness for the generalized velocities and the constraint reactions by introducing the different measures dt , $d\mathbf{u}$ and $d\mathbf{P}$:

$$d \left(\frac{\partial T}{\partial \mathbf{u}} \right)^T - \left(\frac{\partial (T - V)}{\partial \mathbf{q}} \right)^T dt = d\mathbf{P} + \mathbf{Q}dt \quad (2.9)$$

The constraint reactions $d\mathbf{P}$ in the configuration space include discrete percussions of non-smoothness. The following section extends the equations (2.8) of motion towards the measure differential equations (2.9) and gives interpretations.

2.1.2 Measure Differential Equations of Motion

The previous section mainly was formulated for the assumption of the system velocities \mathbf{u} being smooth in time, so the classic acceleration $d\mathbf{u}/dt$ was limited for all times. However, it is the basic characteristic of non-smooth dynamical systems that jumps occur in \mathbf{u} , see amongst others PFEIFFER AND GLOCKER [45]: these can result for example from closing contacts.

As previously mentioned, these effects can be described by the equations (2.8) for smooth transitions while the closing $g_{N,j} = 0$ with $\dot{g}_{N,j} < 0$ of at least one contact j must be formulated separately. Therefore, the set \mathcal{M}_S of times $t_i \in \mathcal{M}_S$ of all non-smooth transitions is defined: for these times, additional impact laws are needed. A more suitable way is the reformulation of the equations of motion in form of measure differential equations, compare MOREAU [42], BROGLIATO [12] and GLOCKER [29]. Besides being more compact, the reading of and calculus with the reformed equations is close to the classic differential equations of motion. Additionally they are well suited for the construction of numerical time integration schemes, see for example the work of FÖRG [19, 22] and STUDER [58].

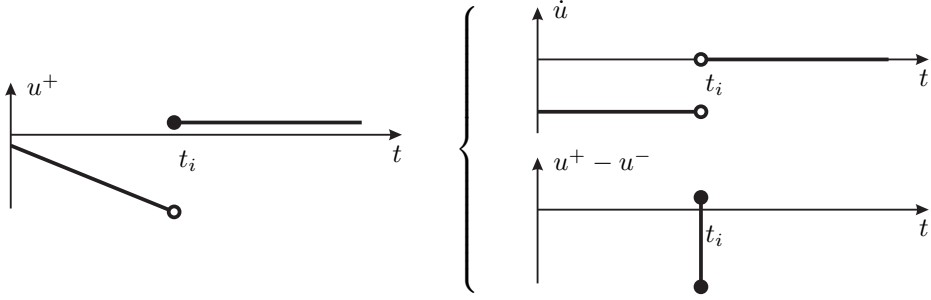


Figure 2.1: Decomposition of the velocity in smooth and non-smooth parts

To allow for non-smoothness in the velocities, the acceleration measure

$$d\mathbf{u} = \dot{\mathbf{u}} dt + (\mathbf{u}^+ - \mathbf{u}^-)d\eta \quad (2.10)$$

is introduced being the sum of the continuous part $\dot{\mathbf{u}} dt$ of smooth dynamics and discrete jumps $(\mathbf{u}^+ - \mathbf{u}^-)d\eta$. The continuous part holds the classic and bounded acceleration $\dot{\mathbf{u}}$ as density with respect to time weighted by the LEBESGUE measure dt . The discontinuous part is the difference of the limits of the velocities,

$$\mathbf{u}^\pm = \lim_{\varepsilon \rightarrow 0^\pm} \mathbf{u}(t + \varepsilon),$$

weighted by the sum of the DIRAC delta distributions $d\delta_i$ at the times of discontinuities $t_i \in \mathcal{M}_S$:

$$d\eta = \sum_i d\delta_i, \quad d\delta_i = d\delta(t - t_i) = \begin{cases} \infty & \text{if } t = t_i \\ 0 & \text{if } t \neq t_i \end{cases}, \quad \int_{-\infty}^{\infty} d\delta_i = 1 \quad (2.11)$$

The integrals over a finite time span $[t_0; t_1]$ and over a discrete point in time $[t_0; t_0]$

$$\int_{t_0}^{t_1} d\mathbf{u} = \mathbf{u}_1^+ - \mathbf{u}_0^-, \quad \int_{t_0}^{t_0} d\mathbf{u} = \mathbf{u}_0^+ - \mathbf{u}_0^- = \begin{cases} \mathbf{0} & \text{if } t_0 \notin \mathcal{M}_S \\ \Delta\mathbf{u} \neq \mathbf{0} & \text{if } t_0 \in \mathcal{M}_S \end{cases} \quad (2.12)$$

can be evaluated without extra regard of non-smooth events within the bounds of integration. Figure 2.1 illustrates this decomposition of the non-smooth velocities into its smooth parts and discrete jumps for a scalar velocity u .

While jumps occur in the velocities at impact times $t_i \in \mathcal{M}_S$, the values \mathbf{u}^+ and \mathbf{u}^- are still bounded. Since the impact time is assumed to be discrete, the systems positions \mathbf{q} remain constant during the impact with infinite length:

$$\int_{t_0}^{t_0} \mathbf{u} dt = \mathbf{q}_0^+ - \mathbf{q}_0^- = \mathbf{0} \quad \forall t_0 \quad (2.13)$$

The generalized coordinates \mathbf{q} are \mathcal{C}^0 smooth with respect to time. The mass matrix $\mathbf{M} = \mathbf{M}(\mathbf{q})$ depends on \mathbf{q} only and therefore is constant during impact. De-

pending on \mathbf{q} and \mathbf{u} , both being of bounded magnitude for all times t , the integral

$$\int_{t_0}^{t_0} \mathbf{h} dt = \mathbf{0} \quad \forall t_0 \quad (2.14)$$

on the generalized forces \mathbf{h} vanishes for all discrete times t_0 including impacts.

The velocities can be discontinuous and so must be the corresponding reactions of constraints introducing these non-continuities. In analogy to the acceleration measure, the LAGRANGE multipliers of the constraints are reformulated:

$$d\mathbf{A} = \boldsymbol{\lambda} dt + \mathbf{A} d\eta \quad (2.15)$$

The constraints imply smooth forces $\boldsymbol{\lambda}$ associated to the persistence and the non-impulsive opening of contacts as well as the discrete impulsive reaction percussions \mathbf{A} due to collisions and discrete excitations at the impact times $t_i \in \mathcal{M}_S$.

The measures of accelerations (2.10) and reactions (2.15) are used to extend the equations of motion (2.8a) of a bi- and unilateral constrained system towards impacts:

$$\mathbf{M} d\mathbf{u} = \mathbf{h} dt + \mathbf{W} d\mathbf{A} \quad (2.16)$$

This result is similar to equation (2.9) using the measures introduced and decomposing the constraint reactions $d\mathbf{P} = \mathbf{W} d\mathbf{A}$ by use of the generalized force directions \mathbf{W} . It is shown in the literature that equation (2.16) formulates the non-smooth dynamics of MBS including holonomic and non-holonomic, bi- and unilateral constraints with friction, see for example again BROGLIATO [12].

Considering the DIRAC delta (2.11) allows for the decomposition of equation (2.16) for interpretation: implicitly formulated are the classical equations of motion

$$\mathbf{M} \dot{\mathbf{u}} = \mathbf{h} + \mathbf{W} \boldsymbol{\lambda} \quad \forall t \notin \mathcal{M}_S \quad (2.17)$$

for a constrained system with smooth dynamics as well as the impact equations

$$\mathbf{M}_i (\mathbf{u}_i^+ - \mathbf{u}_i^-) = \mathbf{W}_i \mathbf{A}_i \quad \forall t_i \in \mathcal{M}_S, \quad (2.18)$$

both with so-far unknown reactions $\boldsymbol{\lambda}$ and \mathbf{A} , respectively. Additional constraint and impact laws connecting feasible reactions and kinematics are necessary for the evaluation of equations (2.17) and (2.18), see section 2.3.2.

2.2 Kinematics of Constraints

In the previous section discrete constraints were introduced restricting the motion of the system by means of limits for kinematic functions. For mechanical systems, these constraints may represent joints or contacts between different bodies. A restriction can be bilateral – a persisting connection which is always active – or unilateral – a contact that may be open or close, active or inactive. The respective force laws are described in the following section 2.3. Regarding point-to-point interactions only exchanging discrete reactions, a unitary framework for the contact kinematics represented by the distance functions \mathbf{g} can be formulated, see for example FÖRG ET AL. [22]. With \mathbf{g} representing relative distances and rotations, the associated constraint reactions $\boldsymbol{\lambda}$ can be interpreted directly as forces or moments, see for example PFEIFFER AND GLOCKER [45].

Within this section, the kinematic functions \mathbf{g} of holonomic and $\boldsymbol{\gamma}$ of non-holonomic constraints are analyzed. For both, the associated generalized force directions \mathbf{W} are developed: these are needed for the formulation of the equations (2.16) of motion. The distance functions of the holonomic bi- and unilateral constraints are collected in the vector $\mathbf{g}_N = (\mathbf{g}_B^T, \mathbf{g}_U^T)^T$ of normal distance functions. In analogy, the velocities $\boldsymbol{\gamma}_N = (\boldsymbol{\gamma}_B^T, \boldsymbol{\gamma}_U^T)^T$ are taken into account for non-holonomic constraints. For a better readability, only one contact with the associated function g_N or γ_N is regarded. Additionally, the relative velocities \dot{g}_N and $\dot{\mathbf{g}}_T$ in normal and tangential directions are analyzed for contacts, whereas the tangential components are provided in advance to impose additional tangential reactions in section 2.3.

The Holonomic Constraint A holonomic constraint restricts directly the positions of the contributing bodies and therefore the generalized coordinates \mathbf{q} . In general the associated kinematic function takes the form

$$g_N = g_N(\mathbf{q}, t) . \quad (2.19)$$

In case of an explicit dependency on the time t , the associated bilateral constraint is called rheonom, else scleronom. This property is taken to the total differential

$$dg_N = \frac{\partial g_N}{\partial \mathbf{q}} d\mathbf{q} + \frac{\partial g_N}{\partial t} dt = \mathbf{W}_N^T d\mathbf{q} + w_N dt \quad (2.20)$$

of the gap function (2.19), where $w_N = w_N(\mathbf{q}, t)$ is equal to zero in case of a scleronomic constraint. The matrix $\mathbf{W}_N = \mathbf{W}_N(\mathbf{q}, t)$ is the column in the matrix of generalized force directions of equation (2.16) associated to the constraint.

The Point-to-Point Contact Within the context of dynamics, constraints may arise of contact situations, for example relative guidance or collision configurations: the contact between two bodies $\mathcal{K}^{(1)}$ and $\mathcal{K}^{(2)}$ restricts their relative motion⁶.

⁶ The number in parentheses put in upper index refers to the body the value is assigned to.

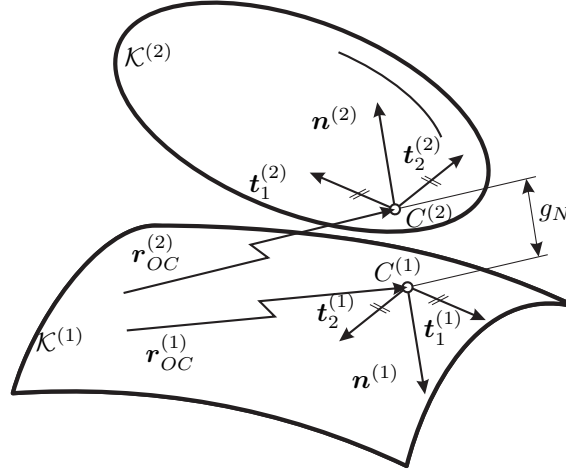


Figure 2.2: Contact kinematics with relative distance g_N of colliding bodies

Thereby, one of the bodies can also be understood as part of the environment not having own degrees of freedom. In case of a relative motion of the contacting bodies, the evaluation of equation (2.19) implies the identification of the points $C^{(i)}$ with positions $\mathbf{r}_{OC}^{(i)} = \mathbf{r}_{OC}^{(i)}(\mathbf{q}^{(i)}, t)$ on each contour that correspond to minimal distance, see figure 2.2. For the points $C^{(i)}$ of minimal distance the necessary conditions

$$\left(\mathbf{T}^{(i)}\right)^T \left(\mathbf{r}_{OC}^{(2)} - \mathbf{r}_{OC}^{(1)}\right) = \mathbf{0} \quad \forall i \in 1, 2 \quad (2.21)$$

need to be fulfilled (see e.g. [45]). For a spatial problem $\mathbf{T}^{(i)} = \mathbf{T}^{(i)}(\mathbf{q}^{(i)}, t) = (\mathbf{t}_1, \mathbf{t}_2)^{(i)}$ holds the tangent directions to the body's contour at the point $C^{(i)}$, respectively. One unique tangential direction is defined for each body in a planar configuration.

Having identified the points $\mathbf{r}_{OC}^{(i)}$, the minimal gap distance is

$$g_N = \left(\mathbf{n}^{(2)}\right)^T \left(\mathbf{r}_{OC}^{(2)} - \mathbf{r}_{OC}^{(1)}\right) \quad \text{with} \quad \left\|\mathbf{n}^{(2)}\right\| = 1. \quad (2.22)$$

The normal $\mathbf{n}^{(2)} = \mathbf{n}^{(2)}(\mathbf{q}, t) = -\mathbf{n}^{(1)}$ on body (2) points in contrary direction to the normal on body (1). In analogy to the bodies' normals the tangents are defined as $\mathbf{T}^{(2)} = -\mathbf{T}^{(1)}$. Positive values of the gap distance g_N denote separation. For an active contact $g_N = 0$, the relative normal and tangential velocities

$$\begin{aligned} \dot{g}_N &= \left(\mathbf{n}^{(2)}\right)^T \left(\mathbf{v}_C^{(2)} - \mathbf{v}_C^{(1)}\right) = \left(\mathbf{n}^T (\mathbf{J}_C \mathbf{u} + \bar{\mathbf{v}})\right)^{(2)} + \left(\mathbf{n}^T (\mathbf{J}_C \mathbf{u} + \bar{\mathbf{v}})\right)^{(1)} \\ \dot{\boldsymbol{\gamma}}_T &= \boldsymbol{\gamma}_T = \left(\mathbf{T}^{(2)}\right)^T \left(\mathbf{v}_C^{(2)} - \mathbf{v}_C^{(1)}\right) = \left(\mathbf{T}^T (\mathbf{J}_C \mathbf{u} + \bar{\mathbf{v}})\right)^{(2)} + \left(\mathbf{T}^T (\mathbf{J}_C \mathbf{u} + \bar{\mathbf{v}})\right)^{(1)} \end{aligned}$$

with the velocity $\mathbf{v}_C^{(i)} = \dot{\mathbf{r}}_C^{(i)} = \mathbf{J}_C^{(i)} \mathbf{u}^{(i)} + \bar{\mathbf{v}}^{(i)}$ of the contact point $C^{(i)}$ are needed for the formulation of the constraints' force laws. Here, $\mathbf{J}_C^{(i)} = \mathbf{J}_C^{(i)}(\mathbf{q}, t) = (\partial \mathbf{r}_C / \partial \mathbf{q})^{(i)}$ is the JACOBI matrix of translations for point $C^{(i)}$ giving linear transformations between physical and configuration space of body (i). A rheonomic dependency is expressed by $\bar{\mathbf{v}}^{(i)} = \bar{\mathbf{v}}^{(i)}(\mathbf{q}, t) \neq \mathbf{0}$ for at least one contact partner. This can be induced by a kinematic excitation of the body explicitly prescribing the motion.

Defining the extended JACOBI matrix $\hat{\mathbf{J}}_C^{(i)} = \partial \mathbf{r}_C^{(i)} / \partial \mathbf{q}$ on the entire configuration space with $\mathbf{q} = (\dots, (\mathbf{q}^{(i)})^T, (\mathbf{q}^{(i+1)})^T, \dots)^T$ allows for a resorting of the equations above and interpretation of the terms of the total differential (2.20):

$$\begin{aligned} \dot{\mathbf{g}}_N &= (\mathbf{n}^{(2)})^T \left(\hat{\mathbf{J}}_C^{(2)} \mathbf{u} + \bar{\mathbf{v}}^{(2)} \right) + (\mathbf{n}^{(1)})^T \left(\hat{\mathbf{J}}_C^{(1)} \mathbf{u} + \bar{\mathbf{v}}^{(1)} \right) \\ &= \left((\mathbf{n}^{(2)})^T \hat{\mathbf{J}}_C^{(2)} + (\mathbf{n}^{(1)})^T \hat{\mathbf{J}}_C^{(1)} \right) \mathbf{u} + (\mathbf{n}^{(2)})^T \bar{\mathbf{v}}^{(2)} + (\mathbf{n}^{(1)})^T \bar{\mathbf{v}}^{(1)} \\ &= \mathbf{W}_N^T \mathbf{u} + w_N \end{aligned} \quad (2.23a)$$

$$\begin{aligned} \dot{\mathbf{g}}_T &= (\mathbf{T}^{(2)})^T \left(\hat{\mathbf{J}}_C^{(2)} \mathbf{u} + \bar{\mathbf{v}}^{(2)} \right) + (\mathbf{T}^{(1)})^T \left(\hat{\mathbf{J}}_C^{(1)} \mathbf{u} + \bar{\mathbf{v}}^{(1)} \right) \\ &= \left((\mathbf{T}^{(2)})^T \hat{\mathbf{J}}_C^{(2)} + (\mathbf{T}^{(1)})^T \hat{\mathbf{J}}_C^{(1)} \right) \mathbf{u} + (\mathbf{T}^{(2)})^T \bar{\mathbf{v}}^{(2)} + (\mathbf{T}^{(1)})^T \bar{\mathbf{v}}^{(1)} \\ &= \mathbf{W}_T^T \mathbf{u} + w_T \end{aligned} \quad (2.23b)$$

For a normal contact with the LAGRANGE multiplier $d\Lambda_N$, the normal $\mathbf{n}^{(1)}$ represents the direction in physical space of the reaction on body (1). Corresponding to NEWTON's third law of reciprocal actions, $\mathbf{n}^{(2)} = -\mathbf{n}^{(1)}$ is the force direction on body (2). This reciprocal interaction is projected to the configuration space by the generalized force directions \mathbf{W}_N via the JACOBI-matrices. The force directions \mathbf{W}_T of the tangential reactions in frictional contacts are composed analogously.

An Example Figure 2.3(a) shows a planar rigid two bar mechanism: each joint C_i is subjected to a unilateral constraint with the ground $y = 0$. The joint positions

$$\mathbf{r}_{OC_1} = l_1 \begin{pmatrix} \cos(\varphi_1) \\ \sin(\varphi_1) \\ 0 \end{pmatrix}, \quad \mathbf{r}_{OC_2} = \mathbf{r}_{OC_1} + l_2 \begin{pmatrix} \cos(\varphi_2) \\ \sin(\varphi_2) \\ 0 \end{pmatrix}$$

in physical space depend on the generalized coordinates $\mathbf{q} = (\varphi_1, \varphi_2)^T$. The ground

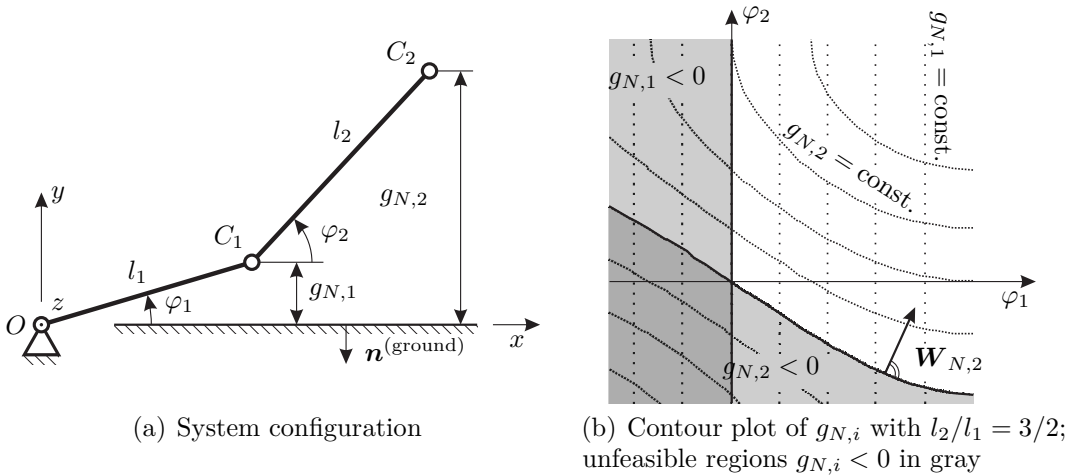


Figure 2.3: Example: two bar link mechanism with unilateral constraints

surface is characterized by the normal $\mathbf{n}^{(\text{ground})} = \mathbf{n} = -(0,1,0)^T$ and an arbitrary point on the x -axis, for simplicity the origin O . Therewith the distances write

$$\mathbf{g}_N = \begin{pmatrix} g_{N,1} \\ g_{N,2} \end{pmatrix} = \begin{pmatrix} -\mathbf{n}^T \mathbf{r}_{OC_1} \\ -\mathbf{n}^T \mathbf{r}_{OC_2} \end{pmatrix} = \begin{pmatrix} l_1 \sin(\varphi_1) \\ l_1 \sin(\varphi_1) + l_2 \sin(\varphi_2) \end{pmatrix}.$$

Figure 2.3(b) shows a contour plot of both constraint functions $g_{N,i}$ for a length ratio $l_2/l_1 = 3/2$ of the rods. Regions $g_{N,i} < 0$ being unfeasible due to the unilateral constraints are marked with gray filling. The normal relative velocities for both contacts are:

$$\dot{\mathbf{g}}_N = \begin{pmatrix} \mathbf{n}^T \dot{\mathbf{r}}_{OC_1} \\ \mathbf{n}^T \dot{\mathbf{r}}_{OC_2} \end{pmatrix} = \begin{pmatrix} l_1 \cos(\varphi_1) & 0 \\ l_1 \cos(\varphi_1) & l_2 \cos(\varphi_2) \end{pmatrix} \mathbf{u} = \mathbf{W}_N^T \mathbf{u}$$

Exemplary, a selected generalized force direction $\mathbf{W}_{N,2}$ of contact 2 implying the point C_2 is depicted in figure 2.3(b) for zero gap distance $g_{N,2} = 0$.

The Non-Holonomic Constraint A non-holonomic constraint imposes a non-integrable restriction on the systems velocities \mathbf{u} that can not be substituted by a corresponding formulation only in \mathbf{q} and t . Since literature does not mention any contrary examples of technical relevance, the associated constraint function

$$\gamma_N = \gamma_N(\mathbf{q}, \mathbf{u}, t) = \mathbf{W}_N^T \mathbf{u} + w_N \quad (2.24)$$

is assumed to be linear in \mathbf{u} . Again, $\mathbf{W}_N = \mathbf{W}_N(\mathbf{q}, t)$ holds columns of the matrix of generalized force directions in equation (2.16). Like for the holonomic case, \mathbf{W}_N is composed of directions of motion in physical space and JACOBI matrices projecting into the configuration space of the associated bodies. A rheonomic constraint implies an explicit time dependency $w_N = w_N(\mathbf{q}, t)$ whereas this term vanishes for a scleronomic constraint. A comparison to the equations (2.23a) and (2.23b) shows that every active holonomic constraint incorporates a hidden but integrable part of the form (2.24). This allows for a unified formulation of all active constraints on velocity level. Thereby the activity, for example of a unilateral holonomic contact, needs to be decided on position level preliminary.

A classic instance implying a bilateral non-holonomic constraint is a wheel rolling ideally on a surface and without slipping: while the position and direction of the wheel on the surface are free (together being the generalized coordinates), the motion is limited to rolling with compatible rotational and translational velocities. FÖRG [19] mentions an one-way overrunning clutch – like it is used in the free-wheel mechanism of a bicycle – as example for a non-holonomic unilateral constraint: the driving velocity of the crank and the rotational velocity of the wheel are bound unilateral in pedaling direction, whereby this one-directional functionality is not influenced by the absolute positions of the crank and the wheel.

2.3 Contact Force Laws

The computation of the accelerations $\dot{\mathbf{u}}$ in equation (2.17) and the post-impact velocities \mathbf{u}_i^+ in equation (2.18) requires the knowledge of the unknown contact reactions $\boldsymbol{\lambda}$ and \mathbf{A}_i , respectively. Therefore, additional laws are needed describing admissible combinations of contact reactions $d\mathbf{A}$ with the kinematics \mathbf{g} of holonomic and $\boldsymbol{\gamma}$ of non-holonomic contacts described in the previous section. Again, only a single contact is discussed for the reason of a better readability.

All contacts between bodies in the system are modeled point-to-point. The kinematic assumptions made during the development of the equations of motion, like the rigid body assumption, are kept unchanged. To give an example, the cross-section of a beam modeled using EULER-BERNOULLI theory remains rigid in the directions normal to the local beam axis. The kinematic relations of section 2.2 are used for the evaluation of both single- and set-valued laws for the contact forces.

Several strategies devoted to contacts can be found within the multi-body literature, whereas two fundamentally different mathematical concepts are used: on the one hand, single-valued force laws formulate the reactions functionally depending upon the contact kinematics. The alternative approach using set-valued laws aims for the exact compliance of the dynamic evolution with the restrictions for both bilateral and unilateral constraints.

In many cases, friction is of high technical relevance for the contact dynamics. Not being a direct result of the kinematic restriction in normal direction, COULOMB friction is introduced additionally for both bilateral and unilateral contacts: depending on the normal reaction, friction reactions are evaluated acting in the tangential directions of the contact.

2.3.1 Single-Valued Force Laws

The reaction force $\boldsymbol{\lambda}$, which may be the normal component of a bilateral or a unilateral contact as well as the tangential component, can be introduced as function

$$\boldsymbol{\lambda} = \boldsymbol{\lambda}(\mathbf{g}, \dot{\mathbf{g}}, t) , \quad \boldsymbol{\lambda} = \boldsymbol{\lambda}(\boldsymbol{\gamma}, t) \quad (2.25)$$

of the respective contact kinematics. The reaction therefore is a function of the state \mathbf{q} and \mathbf{u} . Motivations may arise from opposed intentions:

The stiffness of a specific contact may be relevant for the overall dynamics of the system, raising the necessity to be represented during modeling. For example, a HERTZIAN contact is described by contact reactions being a function of the normal penetration g_N . Contrasting this physical motivation, penalty strategies can be used for the approximation of constraints whereas the restrictions on the kinematic function will not be kept exactly. The systems equations are charged with reactions depending on the violation of the constraint. Therefore, especially for varying loads arbitrary violations may occur within the constrained magnitudes.

To minimize the violation compared to an ideal constraint, high stiffness $\partial \boldsymbol{\lambda} / \partial \mathbf{g}$ and high damping $\partial \boldsymbol{\lambda} / \partial \dot{\mathbf{g}}$ might be necessary, possibly leading to numerical difficulties during time integration⁷. Moreover, the definition and parametrization of relation (2.25) for a specific problem in general is non-trivial and introduces additional modeling coefficients: these might be hard to gain during model build-up and imply additional uncertainties.

For reactions $\boldsymbol{\lambda}$ according to equation (2.25), the forces are limited at times $t_i \in \mathcal{M}_S$ of impacts (compare to generalized forces \mathbf{h} , eqn. (2.14) on page 14) and can be evaluated explicitly. The reaction force

$$\mathbf{Q}_C = \mathbf{W} \boldsymbol{\lambda} \quad (2.26)$$

in configuration space is included as part of the generalized forces \mathbf{h} . Contacts with single-valued formulations do not contribute to the impulsive reactions and therefore do not induce jumps in the velocities. For this reason, after this section λ in all notations will refer exclusively to set-valued force laws assuming that contributions (2.26) to \mathbf{h} are already regarded.

A huge variety of formulations exists, often highly specialized to single problems. Two references shall be named here: to model the distribution of contact reactions, HIPPMANN [35, 36] describes a superposed contact elasticity for colliding rigid bodies using the elastic foundation model for thin layers. GÉRADIN AND CARDONA [26] introduce penalization strategies to impose approximations for constraints. In the following, standard linear formulations for bilateral and unilateral contacts as well as a regularized friction law are briefly presented.

Linear Flexible Bilateral Contact For a bilateral contact, the regularized linear formulation of the contact force uses the stiffness c and the damping d :

$$\lambda_B = -(cg_B + d\dot{g}_B)$$

The resulting force law is displayed for zero relative velocity $\dot{g}_B = 0$ and varying constraint violations g_B in figure 2.4(a).

Linear Flexible Unilateral Contact Like for the bilateral contact, the stiffness c and the damping d are used to formulate the contact force

$$\lambda_U = \begin{cases} 0 & \forall g_U \geq 0 \\ \max(0, -(cg_U + d\dot{g}_U)) & \forall g_U < 0 \end{cases}$$

depending linearly on the kinematic magnitudes g_U and \dot{g}_U . Negative contact forces are prevented in order to avoid adhesion effects for contacts opening fast. Figure 2.4(b) shows the resulting force law for the relative velocity $\dot{g}_U = 0$.

⁷ For numeric algorithms stiffness can be defined as a high gradient of the contact reaction with respect to the state of the system and therefore also includes physical damping.

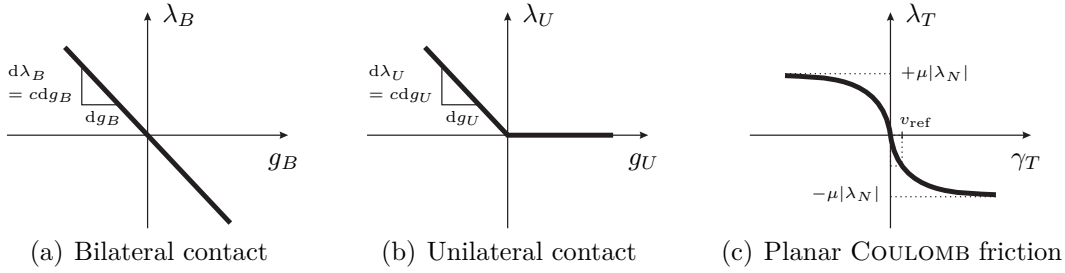


Figure 2.4: Linear force laws for bi- and unilateral contacts and regularized friction

Regularized Coulomb Friction The force of a single frictional contact is decomposed to a normal component $\lambda_N \in \{\lambda_B, \lambda_U\}$ with arbitrary bi- or unilateral contact law and – depending in dimension on planar or spatial character – tangential components λ_T in friction direction. A classic form of regularization for COULOMB friction uses the inverse tangent function, allowing for a functional evaluation:

$$\lambda_T = -\frac{2\mu}{\pi} \operatorname{atan} \left(\frac{\|\gamma_T\|}{v_{\text{ref}}} \right) \frac{\gamma_T}{\|\gamma_T\|} |\lambda_N|$$

The additional regularization parameter v_{ref} can be used to fit the reaction behavior for low tangential velocities γ_T , whereas the tangential reaction always is zero for vanishing relative motion. The coefficient μ represents dry friction at high relative velocities. For the planar case giving one tangential direction, the resulting force depending on the relative tangential velocity γ_T is depicted in figure 2.4(c).

2.3.2 Set-Valued Force Laws

If no discrete flexibility is added between the contacting bodies, a rigid contact corresponds to an algebraic constraint. This implies additional relations to the system, whereas LAGRANGE multipliers are used as new independent variables, see section 2.1. These multipliers $d\mathbf{A}$ take values ensuring the validity of the constraints in combination with the equations of motion. The set \mathcal{N} represents all constraints:

$$(d\mathbf{A}, \mathbf{q}, \mathbf{u}, t) \in \mathcal{N} \quad (2.27)$$

In contrast to regularized contact laws, no additional parameters except restitution coefficients are introduced by modeling exact constraint conditions. For bilateral constraints this formalism is well known: see for example MARSDEN AND RATIU [41] and GÉRARDIN AND CARDONA [26]. Amongst others, PFEIFFER AND GLOCKER [45] extend this concept to unilateral and frictional contacts. LEINE AND GLOCKER [39] and STUDER [58] additionally provide non-standard models for spatial COULOMB-CONTENSOU- and STRIBECK-friction.

Since closing unilateral or frictional contacts in set-valued descriptions induce discontinuities within the velocities, additional impact laws need to be established besides the force laws for persisting or opening contacts. The current section closes with the modern formulation of the force laws for rigid contacts using projection functions.

Force Laws for Smooth Transitions

For the smooth transitions between impacts, set-valued relations connect admissible kinematics g respectively γ to the associated reactions λ in form of equality and inequality expressions. The constraints might influence each other: therefore, the reactions can only be evaluated together with the systems entire set of equations (2.16) including all set-valued restrictions.

Bilateral Constraint A bilateral contact on positions level implies a bilateral holonomic constraint allowing for arbitrary reactions to ensure the kinematic validity:

$$g_B = 0, \quad \lambda_B \in \mathbb{R} \quad (2.28)$$

Figure 2.5(a) visualizes this force law. Similarly, the force law

$$\gamma_B = 0, \quad \lambda_B \in \mathbb{R}$$

represents a non-holonomic bilateral constraint. As stated for equation (2.24), every holonomic bilateral constraint (2.28) implies a constraint on velocity level using the normal velocity $\gamma_B = \dot{g}_B$.

Unilateral Constraint The unilateral contact also allows for detachment leading to in-activity of the kinematic restriction. The associated holonomic unilateral constraint is given by the SIGNORINI-FICHERA-condition

$$g_U \geq 0, \quad \lambda_U \geq 0, \quad g_U \lambda_U = 0. \quad (2.29)$$

The respective force law is shown in figure 2.5(b). In analogy,

$$\gamma_U \geq 0, \quad \lambda_U \geq 0, \quad \gamma_U \lambda_U = 0$$

describes a non-holonomic unilateral constraint. A reformulation of equation (2.29) on velocity level additionally requires the differentiation between closed active contacts $g_U = 0$ and open contacts $g_U > 0$ with $\lambda_U = 0$.

Coulomb Friction For both bi- and unilateral constraints COULOMB friction is considered, capturing most of the dry friction effects of technical relevance, especially stick-slip transitions. Like for the regularized formulation, the contact reaction comprises the normal component $\lambda_N \in \{\lambda_B, \lambda_U\}$ and tangential components λ_T . Using the relative tangential velocity γ_T , COULOMB's friction law is given by

$$\gamma_T = \mathbf{0} \quad \Rightarrow \|\lambda_T\| \leq \mu |\lambda_N| \quad (2.30a)$$

$$\gamma_T \neq \mathbf{0} \quad \Rightarrow \lambda_T = -\mu \frac{\gamma_T}{\|\gamma_T\|} |\lambda_N|. \quad (2.30b)$$

Figure 2.5(c) depicts COULOMB's friction law for the planar case.

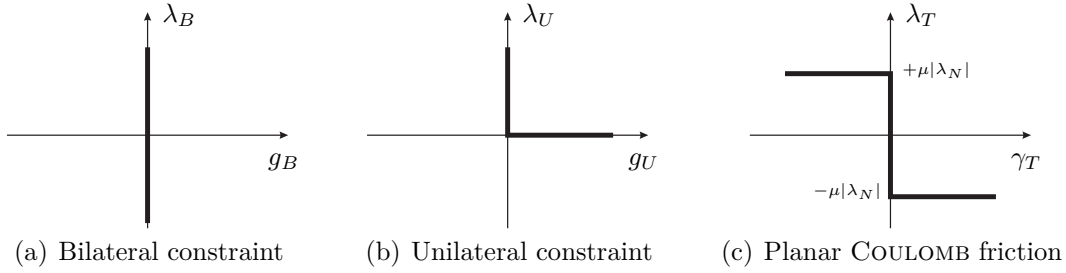


Figure 2.5: Set-valued force laws for bi- and unilateral constraints and friction

Impact Laws

As shown in section 2.1, rigid contacts induce the exchange of discrete impulses Λ_i : a closing contact may imply a discontinuity in the velocities in contrast to persisting and detaching contacts. The impact of a specific contact may effect all other constraints, the bilateral as well as the unilateral ones. The impact laws for times $t_i \in \mathcal{M}_S$ connect the impulsive percussion Λ_i of a single contact with admissible after-impact kinematics \dot{g}^+ or γ^+ . They are formulated on the level of velocities and impulses to supplement the impact equation (2.18), page 14.

Bilateral Constraint The impact law for a bilateral contact is given by

$$\dot{g}_B^+ = 0, \quad \Lambda_B \in \mathbb{R} \quad (2.31)$$

for the holonomic case and ensures that relation (2.28) is not violated after collisions. Analogously, the post-impact validity of a non-holonomic constraint is ensured by

$$\gamma_B^+ = 0, \quad \Lambda_B \in \mathbb{R} .$$

Unilateral Constraint For a unilateral contact on position level, reversibility is considered within the impact. Therefor, the normal relative velocity is interpolated:

$$\dot{g}_U^+ = \varepsilon_U \dot{g}_U^- + \dot{g}_U^+ \quad (2.32)$$

The restitution coefficient $0 \leq \varepsilon_U \leq 1$ allows to choose an impact behavior between fully plastic and fully elastic for the normal direction. With the contact being closed at impact time, NEWTON's impact law can be formulated as

$$\dot{g}_U^+ \geq 0, \quad \Lambda_U \geq 0, \quad \dot{g}_U^+ \Lambda_U = 0 . \quad (2.33)$$

With $\varepsilon_U = 0$, equations (2.32) and (2.33) represent the minimum requirement of non-penetration after impact. They are equivalent to the unilateral constraint (2.29) which is valid for smooth transitions. The impact law

$$\gamma_U^+ \geq 0, \quad \Lambda_U \geq 0, \quad \gamma_U^+ \Lambda_U = 0$$

holds for the non-holonomic unilateral constraint.

Coulomb friction For active normal contacts ($g_N = 0$) with the associated normal reaction $\Lambda_N \in \{\Lambda_B, \Lambda_U\}$, COULOMB's friction law is imposed:

$$\|\mathbf{\Lambda}_T\| \leq \mu |\Lambda_N| \quad \text{if } \boldsymbol{\gamma}_T^+ = \mathbf{0} \quad (2.34a)$$

$$\mathbf{\Lambda}_T = -\frac{\boldsymbol{\gamma}_T^+}{\|\boldsymbol{\gamma}_T^+\|} \mu |\Lambda_N| \quad \text{if } \boldsymbol{\gamma}_T^+ \neq \mathbf{0} \quad (2.34b)$$

PFEIFFER AND GLOCKER [45] also provide extensions to tangential reversibility.

Formulation based on Projection Equations

The set-valued formulation $(d\boldsymbol{\Lambda}, \mathbf{q}, \mathbf{u}, t) \in \mathcal{N}$ of the contact and impact laws (2.28) to (2.34) are self-evident from the mechanical point of view but not suitable for the numerical computation. Convex analysis offers a more appropriate formulation, see ROCKAFELLAR [48] and ALART AND CURNIER [2]: the proximal point

$$\mathbf{prox}_{\mathcal{C}}(\mathbf{x}) = \arg \min_{\mathbf{x}^* \in \mathcal{C}} \|\mathbf{x} - \mathbf{x}^*\|, \quad \mathbf{x} \in \mathbb{R}^n$$

to a convex set \mathcal{C} is the element \mathbf{x}^* of \mathcal{C} that minimizes the norm $\|\mathbf{x} - \mathbf{x}^*\|$ for a given argument \mathbf{x} . Figure 2.6 illustrates the projection using the EUCLIDEAN norm. With the convex sets for bilateral, unilateral and frictional contacts

$$\mathcal{C}_B = \{x ; x \leq 0\}, \quad \mathcal{C}_U = \{x ; x \geq 0\}, \quad \mathcal{C}_T(y) = \{\mathbf{x} ; \|\mathbf{x}\| \leq \mu y\}$$

the relations (2.28) to (2.34) take the fixed-point equation form

$$\lambda_B = \mathbf{prox}_{\mathcal{C}_B}(\lambda_B - r g_B), \quad \Lambda_B = \mathbf{prox}_{\mathcal{C}_B}(\Lambda_B - r \dot{g}_B^+), \quad (2.35a)$$

$$\lambda_U = \mathbf{prox}_{\mathcal{C}_U}(\lambda_U - r g_U), \quad \Lambda_U = \mathbf{prox}_{\mathcal{C}_U}(\Lambda_U - r \dot{g}_U^+), \quad (2.35b)$$

$$\boldsymbol{\lambda}_T = \mathbf{prox}_{\mathcal{C}_T(\Lambda_N)}(\boldsymbol{\lambda}_T - r \boldsymbol{\gamma}_T), \quad \mathbf{\Lambda}_T = \mathbf{prox}_{\mathcal{C}_T(\Lambda_N)}(\mathbf{\Lambda}_T - r \boldsymbol{\gamma}_T^+). \quad (2.35c)$$

The variable $r > 0$ is an independent auxiliary parameter for each contact that does not influence the exact solution. The optimal choice of r with respect to numerical efficiency and stability of the solution scheme is discussed by FÖRG ET AL. [21]. Additionally, FÖRG [19] gives a comprehensive explanation of the formulation (2.35).

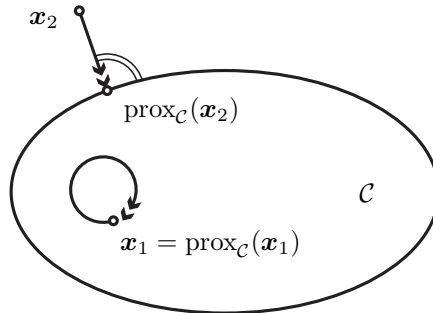


Figure 2.6: Illustration of the proximal function

2.4 Numerical Methods for Non-Smooth Systems

Sophisticated computational methods have been established for non-smooth mechanics opening up a wide range of academic and industrial applications. However, the adaptability of these methods is still limited, raising the need for ongoing research. Recently, ACARY AND BROGLIATO [1] provided a comprehensive overview on modern numerical methods. In order to integrate non-smooth multi-body systems in time, two different approaches for the numerical solution can be distinguished: event-driven and time-stepping schemes.

Event-Driven Integration Schemes Event-driven schemes detect changes of the constraints, for example closing of unilateral contacts or stick-slip transitions, and resolve the exact transition times, see ACARY AND BROGLIATO [1] and PFEIFFER AND GLOCKER [45]. The smooth transitions between the events can be simulated with arbitrary schemes for differential algebraic systems, giving access to higher order time integration. For every event like an impact, the integration is interrupted and additional laws must be evaluated explicitly. While the general procedure of event-driven methods is known, the particular implementation depends on the underlying integrator: the treatment of constraints and the root finding mechanism for event detection play a crucial role within this context. FÖRG ET AL. [20] discuss these topics and provide a comparison to a time-stepping scheme.

Time-Stepping Integration Schemes Time-stepping schemes are based on a time discretization of the system dynamics including all constraints: the concept allows for a unitary treatment of impacts and persisting contacts without an explicit differentiation. After the introduction in the late 1980s by MOREAU [42], subsequent contributions to the algorithms were made by many researchers. Lately, STUDER [58] presented augmented time-stepping methods extending the time discretization from usually constant time step sizes towards step size control. He also provides a broad overview on nowadays wide variety of time-stepping schemes. In the beginning, rigid unilateral constraints were formulated as linear complementarity problems. In modern methods efficient iterative solvers for the proximal point equations (2.35) replaced the direct LCP solvers. Embedded in the semi-explicit time-stepping scheme of FÖRG [19], this is briefly discussed below. Using the same strategies for the constraint solution, section 5.1 presents an A-stable implicit scheme in more detail.

Time-Integration To allow for an unitary treatment, all active constraints are formulated and solved on velocity level: holonomic unilateral contacts need to be sorted by activity $g_i \leq 0$ or inactivity $g_i > 0$. As provided in equations (2.23) and (2.24), pages 17f, the velocities $\boldsymbol{\gamma}_a = (\mathbf{W}_a)^T \mathbf{u} + \mathbf{w}_a$ of all active constraints (index a) are linear combinations of the generalized velocities. The discretization is performed with a constant time step size Δt . A single integration step $l \rightarrow l + 1$ is outlined:

1. Compute the new generalized positions $\mathbf{q}^{l+1} = \mathbf{q}^l + \mathbf{u}^l \Delta t$.

2. Compute the distances $\mathbf{g}_U^{l+1} = \mathbf{g}_U(\mathbf{q}^{l+1}, t^{l+1})$ of all unilateral contacts.
3. Compute the index set $\{i : g_{U,i}^{l+1} \leq 0\}$ of active unilateral contacts, governing the activity of the respective normal and tangential reactions.
4. Compute the generalized velocities by solving the discretized equations of motion considering velocities γ_a of all active holonomic and non-holonomic constraints on velocity level:

$$\mathbf{u}^{l+1} = \mathbf{u}^l + (\mathbf{M}^{l+1})^{-1} (\hat{\mathbf{h}}^{l+1} \Delta t + \mathbf{W}_a^{l+1} \mathbf{\Lambda}_a^{l+1}) , \quad (2.36a)$$

$$\gamma_a^{l+1} = \gamma_a(\mathbf{u}^{l+1}, \mathbf{q}^{l+1}, t^{l+1}) , \quad (2.36b)$$

$$\mathbf{\Lambda}_a^{l+1} = \mathbf{proj}(\gamma_a^{l+1}, \mathbf{\Lambda}_a^{l+1}) . \quad (2.36c)$$

Here, the half-explicit evaluation $\hat{\mathbf{h}}^{l+1} = \mathbf{h}(\mathbf{u}^l, \mathbf{q}^{l+1}, t^{l+1})$ is used to increase numerical stability. The function **proj** comprises the projection functions of equations (2.35) for bilateral and unilateral constraints as well as friction.

The crucial point in solving (2.36) is to find a feasible combination $\mathbf{\Lambda}_a^{l+1}$ and \mathbf{u}^{l+1} .

Solution of Constraint Equations The system (2.36) can be reduced analytically to a relation between the constraint velocities γ_a^{l+1} and the reactions $\mathbf{\Lambda}_a^{l+1}$: inserting equation (2.36a) to a linear expansion of the constraint velocities (2.36b) gives

$$\begin{aligned} \gamma_a^{l+1} &= (\mathbf{W}_a^{l+1})^T (\mathbf{M}^{l+1})^{-1} \mathbf{W}_a^{l+1} \mathbf{\Lambda}_a^{l+1} + (\mathbf{W}_a^{l+1})^T \left[\mathbf{u}^l + (\mathbf{M}^{l+1})^{-1} \hat{\mathbf{h}}^{l+1} \Delta t \right] + \mathbf{w}_a^{l+1} \\ &= \mathbf{G}_a^{l+1} \mathbf{\Lambda}_a^{l+1} + \mathbf{b}_a^{l+1} \end{aligned} \quad (2.37)$$

depending on the known \mathbf{q}^{l+1} , \mathbf{u}^l and t^{l+1} . Using this result again for the projection equation (2.36c) results in a non-smooth nonlinear equation to be solved for the constraint reactions $\mathbf{\Lambda}_a^{l+1}$. The matrix \mathbf{G}_a^{l+1} of projected inertias holds the effective masses in the directions of the set-valued force laws. FÖRG [19] develops various efficient schemes for the solution of this fix-point equation, whereas the properties of \mathbf{G}_a^{l+1} have strong influence on the convergence of the numerical algorithms: fixed-point iteration schemes need a diagonal dominant matrix \mathbf{G}_a^{l+1} reflecting a weak mutual coupling of contacts. Reformulating the fixed-point equation, a numerical root-finding can be utilized, for example a NEWTON-scheme. For overdetermined contact configurations \mathbf{G}_a^{l+1} is not regular; techniques like pseudo-inversion provide solutions but weaken convergence speeds. For flexible multi-body systems practical experience shows root-finding to be most suitable for solving the contact problem.

Comparison While the event-driven integration is very accurate, the detection of events can be time consuming: this approach mainly is used for systems with few transitions in the contact situations. The advantage of the time-stepping approach is that no event detection is necessary. However, common time-discretizations use single step schemes with constant size and only provide first order approximations. Consequently the step size is limited to ensure stability and the required accuracy.

3 Flexible Bodies in Non-Smooth Multi-Body Systems

Within the current chapter, a framework for the derivation of discrete equations of motion for flexible bodies is outlined. While the methods and results presented within this chapter are suitable for arbitrary flexible bodies, a flexible EULER-BERNOULLI beam with small planar deflections and elongations is utilized as an example throughout the chapter. Detailed models for a wide range of structural elements and bodies can be found in the literature. A focus is set on the discretization on the background of constraint dynamics, especially contact and non-smooth impact situations.

In section 3.1, the analytic framework for the description of the dynamics of a flexible body is presented including kinematics and constitutive laws. Section 3.2 discusses the character of non-smooth events within a flexible continuum: in case of an impact, a discontinuity occurs with respect to time – like it is known for rigid body systems – but also with respect to the location within the velocity field of the continuum. Nevertheless, the constitutive laws describing the distributions of internal forces are assumed to remain unchanged within this work: no discontinuities of the displacement field like cracks are regarded. Section 3.3 addresses the spatial discretization of the deformation fields by discrete finite sets. A special focus is set on the influence of the discretization on the approximation of spatially discrete events. Specialties within the contact kinematics of flexible bodies are addressed in section 3.4. Concluding, section 3.5 gives aspects concerning computer implementations. To allow for a better readability, the equations of motion within this chapter will mostly be written for smooth transitions. The generalization including impacts is known from the previous chapter.

3.1 Analytical Framework

The formulation of the equations representing the dynamics of a body, either being rigid or flexible, takes two compulsory steps: kinematics and kinetics, see for example SHABANA [56]. The motion of the continuum is described using kinematic assumptions. Based on these, kinetics states constitutive laws connecting motion and reactions: partial differential equations of motion are formulated describing the dynamics of the system. A wide range of models for flexible continua can be found in literature, see section 1.2. Within the current section, a slender EULER-BERNOULLI beam with elongation is used as an example to discuss the derivation of the describing equations.

3.1.1 Continuum Kinematics

The task of kinematics is to provide a unitary description of the positions, the velocities and the accelerations for all points of the body. This geometric aspect of motion is developed in several steps: a location description is introduced allowing for the unique identification of the points within the continuum. Depending on the geometry and the loads of the body, kinematic assumptions are proclaimed giving restrictions to the modeled deformations. Based on these, fields are introduced describing the motion of all material points.

Location Description

For the description of the location, two fundamentally different concepts can be followed, see figure 3.1 and GROSS ET AL. [31], BATHE [6]: associating the descriptor to a fixed point in space with material moving relatively is known as EULER description. In contrast, the association of an algebraic variable to a moving material element dm leads to LAGRANGE description. Also mixed forms of both are used for special applications. Whereas the EULER description is widely used within fluid dynamic simulations, the LAGRANGIAN parametrization is commonly used for solid mechanics, intrinsically allowing to trace the motion of specific material points.

Euler Description The frame of reference for the EULER description is inertially fixed. The constant coordinate \mathbf{S}_0 therefore describes an spatially fixed reference, depicted as grey slice in figure 3.1(a) using a scalar coordinate S_0 for the beam structure. The mass element dm^* being associated to the position \mathbf{S} is changing with material dm moving through with velocity $\dot{\mathbf{S}} = \dot{\mathbf{S}}(\mathbf{S}, t)$. Thus, the substantial derivative $\frac{d}{dt}$ of a material bound quantity \mathbf{X} , for example representing the position of the mass element, must be built with respect to the material velocity:

$$\mathbf{X} = \mathbf{X}(\mathbf{S}, t) \tag{3.1a}$$

$$\dot{\mathbf{X}} = \frac{d\mathbf{X}}{dt} = \frac{\partial \mathbf{X}}{\partial t} + \frac{\partial \mathbf{X}}{\partial \mathbf{S}} \dot{\mathbf{S}} \tag{3.1b}$$

Figure 3.1(a) decomposes the position $\mathbf{r} = \mathbf{r}_0 + \mathbf{r}_t$ into the constant part $\mathbf{r}_0 = \mathbf{r}_0(S_0)$ and the time variant deflection $\mathbf{r}_t = \mathbf{r}_t(S_0, t)$. Classically the EULER description is used in fluid dynamics referring to inertially fixed control volumes. Using prescribed constant reference paths of motion, this description can also be used successfully for solid mechanical problems with geometrically small deflections. FUNK [24] simulates elastic belt drives with constant transmission ratios based on this approach.

Lagrange Description As depicted in figure 3.1(b), each material element dm is identified by a specific coordinate \mathbf{s} for the LAGRANGE description. For the planar beam example, a scalar value s_0 always refers to the same material point with time-variant position $\mathbf{r} = \mathbf{r}(s_0, t)$. The material bound quantity \mathbf{X} can be expressed in

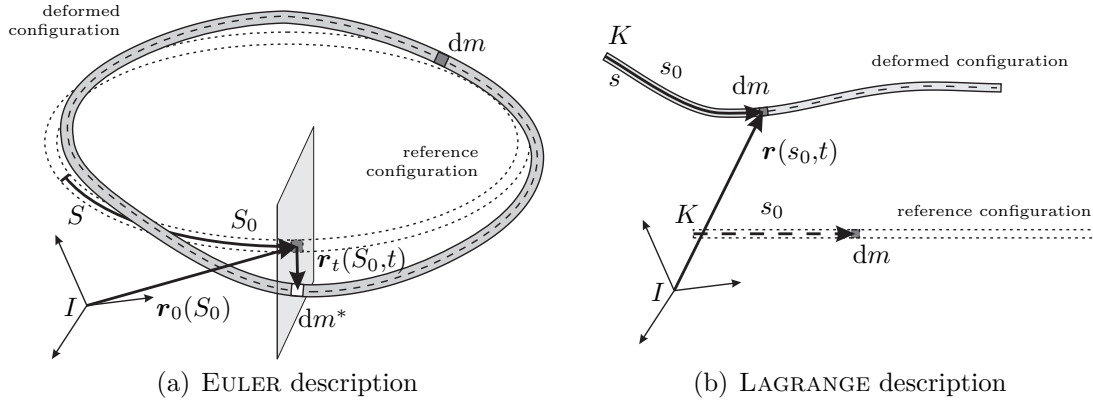


Figure 3.1: Parameterization for descriptions of positions \mathbf{r}

terms of the time t and the constant position \mathbf{s} . The substantial derivative can be evaluated directly:

$$\mathbf{X} = \mathbf{X}(\mathbf{s} = \text{const.}, t) \quad (3.2a)$$

$$\dot{\mathbf{X}} = \frac{d\mathbf{X}}{dt} = \frac{\partial \mathbf{X}}{\partial t} = \dot{\mathbf{X}}(\mathbf{s}, t) \quad (3.2b)$$

The frame of reference for the LAGRANGE coordinate \mathbf{s} with reference point K is moved and deformed with the body. Usually, a coordinate associated to the undeformed length of the body is used. Utilizing the example of the beam of relaxed length l , $s \in [0, l]$ always represents the domain of the body.

Following the LAGRANGE description, the evaluation of kinematic and kinetic quantities is performed in the following sections. This is in analogy to the body-fixed frames used for rigid bodies and floating frame of reference models for flexible bodies. Moreover, systems with large deflections are included.

The kinematic description of a continuum uses fields depending on the time t and the independent algebraic variable \mathbf{s} which is not part of the transient state but used for its description. The dimension of \mathbf{s} correlates with the dimensionality of the body, which is defined by the kinematic assumptions: for one dimensional continua like cables, rods, beams and so on, a material point can be addressed by one scalar position. Plates and shells are described by two coordinates, for spatial models three are needed according to the three spatial directions.

Kinematic Assumptions

The most general kinematic formulation allows for independent motion of all material elements $dm = \rho dV$ of volume dV in all spatial directions. Then, the positions

$$\mathbf{r} = \mathbf{r}(\mathbf{s}, t) \in \mathbb{R}^3 \quad (3.3)$$

are described by field variables $\mathbf{r} \in \mathcal{F}(\mathbb{R}^3)$ originating from the infinite space of functions depending upon the LAGRANGE coordinate \mathbf{s} . Preserving the generality,

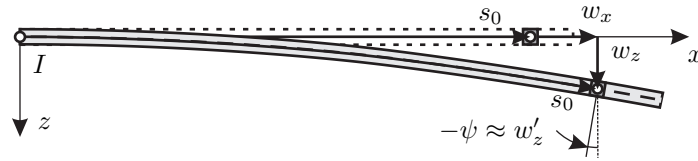


Figure 3.2: Continuum kinematics: flexible beam with small deformations

only the compatibility equations ensuring a unique relation between displacement and strain field are to be fulfilled, compare to standard literature for continuum mechanics. Total derivation with respect to time gives rise to the velocity $\dot{\mathbf{r}} = \frac{d\mathbf{r}}{dt}$ and acceleration $\ddot{\mathbf{r}} = \frac{d^2\mathbf{r}}{dt^2}$ of the mass element.

Depending on the specific problem, assumptions concerning the motion can be introduced to reduce the dimension and complexity of the describing equations. Postulating maximum restrictions in form of constant relative distance of the material points, the rigid body assumption concentrates the kinematic description of the body to a reference point and spatial rotations, see PFEIFFER [44] or SHABANA [56].

To give an example, the EULER-BERNOULLI assumptions for planar slender beams with superposed longitudinal deformations are used within this chapter. For details refer to standard literature of mechanics, for example HIBBELER [34]. A beam is characterized by one dimension – namely the axis defining the local s -direction – being of significantly higher order of magnitude than the two other local dimensions, compare figure 3.2. Usually, a ratio of ten to one between length and cross-sectional dimensions is given as limit for validity. The central assumptions are: the cross-section of the beam remains planar and is always normal on the neutral fiber. All magnitudes depend uniquely on the time and the scalar position s . The shear deformation is negligible small.

The position of the mass element $dm = \rho A ds$ with the cross sectional area $A = A(s)$ and the mass density $\rho = \rho(s)$ is represented by a location on the neutral fiber of the EULER-BERNOULLI beam. For small deflections with respect to the inertial frame I of reference¹ and for linearized deformations, this fiber is described by

$${}_I\mathbf{r} = {}_I\mathbf{r}(\boldsymbol{\varphi}) = (s + w_x, 0, w_z)^T. \quad (3.4)$$

The independent relative displacements $w_x = w_x(s,t)$ and $w_z = w_z(s,t)$ express the longitudinal and transversal deformation and form the vector $\boldsymbol{\varphi} = (s + w_x, w_z)^T$ of position fields, compare to figure 3.2. The derivative $dw_z/ds = w'_z$ approximates the slope $\psi \approx -w'_z$ of the beam². The velocity and acceleration at the position s are

$${}_I\dot{\mathbf{r}} = (\dot{w}_x, 0, \dot{w}_z)^T \quad \text{and} \quad {}_I\ddot{\mathbf{r}} = (\ddot{w}_x, 0, \ddot{w}_z)^T. \quad (3.5)$$

Equation (3.4) describes the spatial position of the mass element with two kinematic degrees of freedom. For the constitution of relations between strain and stress in

¹ The base for the coordinate representation of a vector is marked with a lower left index.

² In this work, $(\xi)'$ marks the total derivative of ξ with respect to the LAGRANGE coordinate s .

the following section, the local deformation measures $\varepsilon = \varepsilon(s,t)$ for strain due to elongation and $\kappa = \kappa(s,t)$ for curvature due to bending are provided:

$$\varepsilon = w'_x \quad , \quad \kappa \approx w''_z \quad (3.6)$$

Thereby, the assumption of small deformations allows for the approximation of the curvature by the second derivative of the bending line w_z .

In section 4.2.3, local moving frames of reference will be used in combination with the EULER-BERNOULLI theory for modeling planar beams undergoing geometrically large deformations. There, further additional kinematic assumptions used for the description are explained in detail.

3.1.2 Constitutive Laws and Kinetics

While the description of the motion can be developed deductively, the coupling of deformations and internal reactions is described by constitutive relations. These are laws of everyday experience but can not be proven. In the same way, NEWTON's second law "forces equal accelerations" is a postulation that properly fits reality.

Constitutive Deformation Laws

The connection between deformations and the internal reactions of the body are proposed by constitutive laws. A classic example is HOOKE's law for linear elastic material: in the spatial case, a linear relation between strains and stresses is declared by the fourth-order tensor of elasticity. For most homogeneous technical materials with elastic behavior, this tensor can be parametrized by two scalars. Standard literature of continuum mechanics comprehensively addresses the topic of elasticity.

The internal stresses and strains need to be analyzed in correspondence to the kinematic assumptions: for the straight EULER-BERNOULLI beam with longitudinal load, the force $N = N(\varepsilon(s)) = \int_A \sigma_s dA$ and the moment $R = R(\kappa(s)) = \int_A \sigma_s z dA$ are the section loads at the position s parametrizing the linear distribution of the normal stress σ_s , see figure 3.3(a). To formulate relations between deformations and section loads based on energy expressions³, the incremental of the work density

$$d\bar{W} = Nd\varepsilon - Rd\kappa \quad (3.7)$$

is associated to the deformation increments $d\varepsilon$ and $d\kappa$ of the element ds . The work

$$\bar{W} = \frac{dW}{ds} = \int_0^\varepsilon Nd\tilde{\varepsilon} - \int_0^\kappa Rd\tilde{\kappa} \quad (3.8)$$

is performed during the deformation of the beam element ds .

³ Since shear deformations are neglected, no work is performed by shear forces.

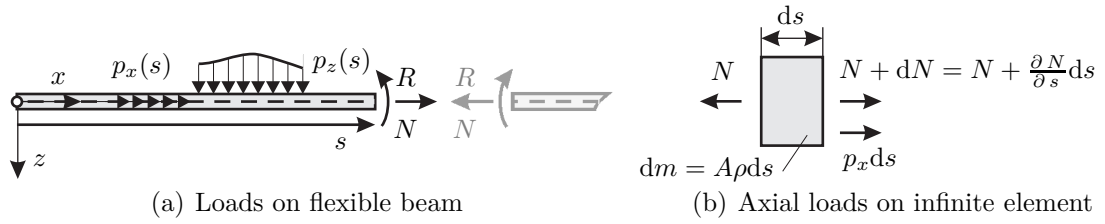


Figure 3.3: Kinetic magnitudes on the beam

Within this thesis, only elastic material behavior is regarded. Amongst others, AMBRÓSIO AND NIKRAVESH [3] and recently GERSTMAYR [27] provide extensions of flexible multi-body systems to irreversible material behavior.

For purely elastic material behavior, \bar{W} necessarily is a function of the state of strain only, expressed by the elongation ε and the curvature κ for the present beam example. This requests independence of the load history and only can be provided if equation (3.7) is the total differential of the work density (3.8). HOOKE'S law of linear elasticity, here formulated for beams, fulfills these criteria:

$$N = EA\varepsilon \quad (3.9a)$$

$$R = -EI\kappa \quad (3.9b)$$

The modulus of elasticity E is a scalar material constant. As a result of the kinematic assumptions, the moment of inertia $I = I(s) = \int_A z^2 d\tilde{A}$ is introduced during integration over the cross sectional area $A = A(s)$. The work density $\bar{W} = \bar{V}_{\text{elast}} = \frac{dV_{\text{elast}}}{ds}$ provides the density function of the elastic deformation potential V_{elast} of the entire beam. Introducing the equations (3.9) in (3.8), the density of the elastic potential takes the form

$$\bar{V}_{\text{elast}} = \int_0^\varepsilon EA\tilde{\varepsilon}d\tilde{\varepsilon} + \int_0^\kappa EI\tilde{\kappa}d\tilde{\kappa} = \frac{1}{2}EA\varepsilon^2 + \frac{1}{2}EI\kappa^2 = \frac{dV_{\text{elast}}}{ds} \quad (3.10)$$

being the positive quadratic potential of the deformation state.

Kinetics

The kinetic considerations for a system connect the kinematics – providing positions, velocities and accelerations – to the internal and external loads. The resulting equations of motion describe the time evolution of the system. As it is discussed in section 2.1, different methodological approaches can be used for the preparation: two of these shall be sketched briefly.

Elementary Equilibrium The constitution of force and momentum equilibria for an infinite mass element dm of the body yields directly the partial differential equations of motion. For initiating the kinematic considerations, especially the D'ALEMBERT

principle in the formulation of LAGRANGE gives a powerful framework projecting the kinematic and constitutive descriptions as well as the external loads into the feasible space of motion, see for example SHABANA [56]. The approach of elementary equilibrium directly instates the dynamic load balance by the evaluation of differential equality based on the kinematic and kinetic assumptions established previously. In addition to the differential equations, boundary conditions for the field variables need to be established. Separate appropriate considerations are needed for every elemental kinematic freedom.

Figure 3.3(b) illustrates exemplary the longitudinal components of the load balance for the element ds of the flexible beam, see for example GROSS ET AL. [31] or SHABANA [56]. The displacements and the section loads at both ends of the beam build the boundary conditions for the partial differential equation.

Variational Formulation In contrast to the elemental equilibrium, the HAMILTON principle (2.1), page 8, can be used in an adaption to fields to formulate equilibrium conditions on the entire body \mathcal{K} , compare to SCHWERTASSEK AND WALLRAPP [52]. For this, the kinetic energy

$$T = \int_{\mathcal{K}} \frac{1}{2} \dot{\mathbf{r}}^T \dot{\mathbf{r}} dm \quad (3.11)$$

of the body \mathcal{K} is introduced. Using integration by parts for the evaluation of the principle (2.1), the integral on the variation of the kinetic energy (3.11) writes

$$\int_{t_0}^{t_1} \delta T dt = - \int_{t_0}^{t_1} \int_{\mathcal{K}} \ddot{\mathbf{r}}^T \delta \mathbf{r} dm dt + \left[\int_{\mathcal{K}} \dot{\mathbf{r}}^T \delta \mathbf{r} dm \right]_{t_0}^{t_1}. \quad (3.12)$$

Due to the invariance of \mathbf{r}_0 and \mathbf{r}_1 , compare page 8f, the second summand vanishes. The first term holds the classic accelerations of the mass element dm and is similar to the results derived utilizing the D'ALEMBERT principle.

For the further evaluation, the elastic EULER-BERNOULLI beam described by the fields $\boldsymbol{\varphi}$ is discussed, see equation (3.4). In accordance with the kinematic assumptions for the beam with endpoints at $s = 0$ and $s = l$, compare to equations (3.5), the kinetic energy and its variation with respect to $\delta \boldsymbol{\varphi} = (\delta w_x, \delta w_z)^T$ write:

$$T = \frac{1}{2} \int_0^l (\rho A \dot{w}_x^2 + \rho A \dot{w}_z^2) ds \quad (3.13a)$$

$$\delta T = - \int_0^l (\rho A \ddot{w}_x \delta w_x + \rho A \ddot{w}_z \delta w_z) ds \quad (3.13b)$$

The elastic potential $V_{\text{elast}} = \int_0^l \bar{V} ds$ of the beam, equation (3.10), is expressed in

terms of the deformations w_x and w_z , see equation (3.6):

$$V_{\text{elast}} = \frac{1}{2} \int_0^l (EA \varepsilon^2 + EI \kappa^2) ds = \frac{1}{2} \int_0^l (EA (w'_x)^2 + EI (w''_z)^2) ds \quad (3.14)$$

Using integration by parts with respect to the position s , the variation δV_{elast} is evaluated with the independent kinematic variations δw_x , δw_z and $\delta w'_z$:

$$\begin{aligned} \delta V_{\text{elast}} &= \int_0^l (EA w'_x \delta w'_x + EI w''_z \delta w''_z) ds \\ &= - \int_0^l ((EA w'_x)' \delta w_x + (EI w''_z)' \delta w'_z) ds \\ &\quad + [(EA w'_x) \delta w_x + (EI w''_z) \delta w'_z]_0^l \\ &= - \int_0^l ((EA w'_x)' \delta w_x - (EI w''_z)'' \delta w_z) ds \\ &\quad + [(EA w'_x) \delta w_x + (EI w''_z) \delta w'_z - (EI w''_z)' \delta w_z]_0^l \end{aligned} \quad (3.15)$$

Whereas the integral part holds terms of the classical beam equations, which are partial differentials of fourth order, the second part of the right hand side contributes to the boundary conditions of the fields and their spatial derivatives.

The variation $\delta W = \delta W_p + \delta W_b$ of the external work accounts for the distributed volume loads $p_x = p_x(s)$ and $p_z = p_z(s)$, compare figure 3.3(a), and the discrete forces $\mathbf{F}_{0,l} = (F_x, 0, F_z)_{0,l}^T$ and torques $\mathbf{R}_{0,l} = (0, R_y, 0)_{0,l}^T$ at the beam's boundaries $s = 0$ and $s = l$. The associated variations

$$\delta_I \mathbf{r} = (\delta w_x, 0, \delta w_z)^T, \quad \delta \boldsymbol{\psi} = (0, -\delta w'_z, 0)^T \quad (3.16)$$

of the translational and angular position are used to formulate the contributions to δW with the separation $\delta W_b = \delta W_F + \delta W_R$:

$$\delta W_p = \int_0^l (p_x \delta w_x + p_z \delta w_z) ds \quad (3.17a)$$

$$\delta W_F = [F_x \delta w_x + F_z \delta w_z]_0^l, \quad \delta W_R = [-R_y \delta w'_z]_0^l \quad (3.17b)$$

To finalize the beam example, equations (3.13b), (3.15) and (3.17) are collected for the evaluation of the HAMILTON principle (2.1) with $L = T - V$. Sorting for different variations δw_x , δw_z and $\delta w'_z$ leads to

$$\int_{t_0}^{t_1} \left(\int_0^l \begin{pmatrix} \rho A \ddot{w}_x - (EA w'_x)' - p_x \\ \rho A \ddot{w}_z + (EI w''_z)'' - p_z \end{pmatrix}^T \begin{pmatrix} \delta w_x \\ \delta w_z \end{pmatrix} ds + \begin{pmatrix} EA w'_x + F_x \\ (EI w''_z)' - F_z \\ EI w''_z - R_y \end{pmatrix}^T \begin{pmatrix} \delta w_x \\ \delta w_z \\ \delta w'_z \end{pmatrix} \Big|_0^l \right) dt = 0.$$

Since the variations are arbitrary but respect the kinematic boundary conditions, the

integral on the body \mathcal{K} with $s \in [0, l]$ and the boundary expressions must vanish independently. The integrand yields one equation of motion for each component of φ :

$$\rho A \ddot{w}_x - (EA w'_x)' - p_x = 0 \quad (3.18a)$$

$$\rho A \ddot{w}_z + (EI w''_z)'' - p_z = 0 \quad (3.18b)$$

The first is the equation of longitudinal waves in a flexible rod, the second equation describes the bending dynamics. The respective boundary conditions, being a mixed form of DIRICHLET and NEUMANN boundary conditions, are:

$$[(EA w'_x + F_x)\delta w_x]_0^l = 0 \quad (3.19a)$$

$$[((EI w''_z)' - F_z)\delta w_z]_0^l = 0 \quad , \quad [(EI w''_z - R_y)\delta w'_z]_0^l = 0 \quad (3.19b)$$

The results are independent of the use of a variational formulation or elementary equilibrium considerations and exactly represent the kinematic assumptions in combination with the constitutive laws. For the general case, they are coupled nonlinear partial differential equations.

3.2 Remarks on Time and Local Continuity

In section 2.1.2, the discrete velocities \mathbf{u} were formulated with respect to non-smooth characteristics allowing for jumps: these non-continuities were caused by discrete percussions Λ_i . For a rigid body, a jump in the velocity parameters \mathbf{u} describes an immediate jump of the velocities for all points of the body.

In contrast, the previous section 3.1 assumed smoothness of all field variables φ including their derivatives with respect to time t and location \mathbf{s} . For an exact description of impacts, this assumption now is contradicted: an impact on a flexible structure at the position \mathbf{s}_i induces a jump within the velocity field $\mathbf{u}(\mathbf{s}, t)$. For a percussion at s_i , this situation is depicted for the transversal velocity u_z of a beam in figure 3.4. Assuming initially zero velocity of the structure at all positions, the post-impact velocity field at impact time $t_i \in \mathcal{M}_S$

$$u_z^+(s) \Big|_{t=t_i} = \begin{cases} u_i & \text{if } s = s_i \\ 0 & \text{everywhere else} \end{cases}$$

can be expressed with a non-zero discrete velocity u_i . The non-continuity with re-

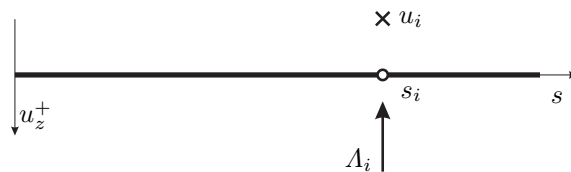


Figure 3.4: Non-smooth velocity field resulting from discrete impact Λ_i

spect to time of the system's velocities, which is known from impacting rigid body systems (compare to literature on non-smooth/impact dynamics and section 2.1), also occurs within the velocity-field of the flexible structure. For the analytic description of flexible bodies, this effect needs to be described within the parametrization of the fields. Discussing a longitudinal percussion on a flexible rod, GLOCKER [30] and WRIGGERS [64] each give physical interpretations without solving the continuous problem analytically: for the exact solution, the contact condition takes the mathematical form of a fully plastic impact. Thereby, perfect reversibility is included by the structural flexibility and a vanishing mass fraction involved in the impact.

In analogy to the invariance (2.13) of the discrete positions \mathbf{q} during impact events for discrete systems, see page 13, the displacement fields of a flexible continuum are continuous with respect to time and location even for discontinuous velocity-fields. Nevertheless, high gradients of deformations can evolve probably overstressing the underlying material laws. A general analytic theory for non-smooth dynamics of flexible bodies must allow for the description of velocity fields being non-continuous with respect to time and location. Thereby, the following points need to be addressed:

- the times of impacts are not known a priori; neither are the locations and the number of discontinuities within the fields
- after an impact, the induced non-continuity travels through the structure as impulsive wave and needs to be described; the wave speed – also known as sound-propagation velocity – is a function of the continuum parameters like modulus of elasticity, mass density or also cross section area and inertia
- in case the constitutive laws include velocity fields, for example to model material damping, the validity may be lost since the velocity fields might become non-differentiable with respect to locations

With numerous references, section 2.1 presented measure differential equations for the description of discrete non-smooth systems. Following BROGLIATO [12], the theory of distributions, which was used successfully for discrete non-smooth systems, might possibly be extended towards the analytic description of non-smooth transitions within flexible structures. FRÉMOND [23] provides a brief theoretical discussion of non-smooth velocity fields. A field formulation of the HAMILTON-principle for non-smooth events is sketched by PANAGIOTOPOULOS [43].

Commonly and within this work, discrete approximations in time and space are used for the simulation of flexible dynamic systems. Mostly based on weak formulation, all these approximations using discrete masses and forces blur discrete events with respect to both time and location via the ansatz-functions used for the discretization. To sharpen the spatial model resolution, refinements are needed especially at positions with high gradients of the discretized fields like positions of impacts, see WRIGGERS [64]. The non-continuity with respect to time can be formulated as described in chapter 2 for the spatially discretized system.

3.3 Discretization of Flexible Bodies with Discontinuities

The partial differential equations together with the boundary conditions presented in section 3.1 exactly describe the dynamics of the flexible structure in the sense of the modeling assumptions. The solution gives the continuous fields $\varphi \in \mathcal{F}(\mathbb{R}^l)$ originating from the infinite linear space of functions for l kinematic freedoms of the differential element. These analytical solutions can be developed only for some very special cases like the vibration of a string or longitudinal elastic waves of a linear rod. In general a discretization is needed to allow for a numerical computation: structural motions are approximated by a finite set of ansatz-functions describing the fields by discrete degrees of freedom \mathbf{q} depending on time only.

After establishing the mathematical methods, common discretization and special demands for rigid contact formulations on flexible structures are discussed in this section. The simulation of multi-body systems usually focuses on long-term dynamics, at least in sense of local structural frequencies. Since the spatial and the frequency resolution of the discretization are closely connected – the finer the discretization the higher the structural frequencies captured, see for example BATHE [6] – a high local resolution increases the frequency range of the overall model but diminishes speeds for numerical time integration. Hence, spatial localized effects like discrete contacts often are discretized comparatively coarse in flexible multi-body systems.

3.3.1 Discretization

Spanning a finite set within the space \mathcal{F} of functions, the discretization approximates the exact solution of infinite dimension by a combination of ansatz-functions, reducing the continuous problem to a set of discrete counterparts. For a general spatial continuum, the field $\mathbf{r} = \mathbf{r}(\mathbf{s}, t) \in \mathcal{F}(\mathbb{R}^3)$ of deformations is described by the postulated ansatz-function $\hat{\mathbf{r}}$:

$$\mathbf{r} \approx \hat{\mathbf{r}}(\mathbf{s}, \mathbf{q}) \in \mathbb{R}^3 \quad (3.20)$$

These are also called shape functions and explicitly depend on the position \mathbf{s} and the discrete degrees of freedom $\mathbf{q} = \mathbf{q}(t) \in \mathbb{R}^n$ implying the implicit time dependency of $\hat{\mathbf{r}}$. To guarantee compatibility with the kinematics of the original field \mathbf{r} , the ansatz-functions need to fulfill at least the kinematic boundary conditions. Differentiation of (3.20) with respect to time leads to the approximation for the velocity field

$$\dot{\mathbf{r}} \approx \frac{d\hat{\mathbf{r}}}{dt} = \frac{\partial \hat{\mathbf{r}}}{\partial \mathbf{q}} \dot{\mathbf{q}} = \hat{\mathbf{J}}_r \mathbf{u} \quad (3.21)$$

with the discrete velocities $\mathbf{u} = \dot{\mathbf{q}}$ and the JACOBI matrix $\hat{\mathbf{J}}_r = \hat{\mathbf{J}}_r(\mathbf{s}, \mathbf{q}) \in \mathbb{R}^{3 \times n}$.

Imposing the discretization on the partial differential equations of motion leads to a set of ordinary differential equations with the dimension n of the generalized

velocities \mathbf{u} . For doing so, two approaches with different basic concepts can be used leading to similar results: the RITZ- and the GALERKIN-method.

Both methods are discussed on the basis of the exemplary EULER-BERNOULLI beam: here, the longitudinal and transversal deformations are approximated by the linear combination

$$\begin{pmatrix} w_x \\ w_z \end{pmatrix} \approx \begin{pmatrix} \hat{w}_x(\mathbf{q}, s) \\ \hat{w}_z(\mathbf{q}, s) \end{pmatrix} = \begin{pmatrix} \bar{\mathbf{w}}_x \\ \bar{\mathbf{w}}_z \end{pmatrix} \mathbf{q} . \quad (3.22)$$

The ansatz respects the kinematic independency of elongation and bending by the special form of the functions

$$\begin{aligned} \bar{\mathbf{w}}_x &= \bar{\mathbf{w}}_x(s) = (\bar{w}_{x1}(s), \bar{w}_{x2}(s), \dots, 0, 0, \dots) \\ \bar{\mathbf{w}}_z &= \bar{\mathbf{w}}_z(s) = (0, 0, \dots, \bar{w}_{z1}(s), \bar{w}_{z2}(s), \dots) \end{aligned}$$

associating each degree of freedom q_i to either elongation or bending deformation. The functions \bar{w}_{ij} incorporate the spatial dependency and therefore need to be compatible with the boundary conditions (3.19). Introducing (3.22) in equation (3.4), page 30, provides the cross-sectional position $\hat{\mathbf{r}}$. Ansatz (3.22) yields the velocities

$$\begin{pmatrix} \dot{w}_x \\ \dot{w}_z \end{pmatrix} \approx \begin{pmatrix} \bar{\mathbf{w}}_x \\ \bar{\mathbf{w}}_z \end{pmatrix} \mathbf{u} = \bar{\mathbf{J}}_T \mathbf{u} \quad (3.23)$$

with the JACOBI matrix $\bar{\mathbf{J}}_T = \bar{\mathbf{J}}_T(s)$ of translations being a function of s only.

The Ritz-Method

The RITZ-method derives the discretized equations of motion by directly utilizing the variational formulation which is equivalent to the partial differential equations. This formulation provided by the HAMILTON principle is solved by the EULER-LAGRANGE equations (2.2), see section 2.1.1. In section 3.1, these equations were evaluated in terms of deformation fields to derive the partial differential equations of motion of the continuum. Now, the functional $L = T - V$ as well as additional loads are expressed by the approximations (3.20) and (3.21). The EULER-LAGRANGE equations then are evaluated in terms of the discrete degrees of freedom \mathbf{q} .

RITZ [47] proposed the method for calculating the deflection w_z of plates. Using the linear form $w_z \approx \bar{\mathbf{w}}_z^T \mathbf{q}$ with $\bar{\mathbf{w}}_z = \bar{\mathbf{w}}_z(s)$ for the approximation of the deformation, he was able to estimate w_z by a finite set of weighted ansatz-functions. RITZ concluded (but did not approve by himself) that the approach provides convergence for increasing numbers of shape functions which means finer discretizations.

Starting with the definition for the exact kinetic energy (3.11), page 33, of an arbitrary system, the introduction of the approximation (3.21) for the velocity yields

$$T = \frac{1}{2} \int_{\mathcal{K}} (\hat{\mathbf{J}}_r \mathbf{u})^T (\hat{\mathbf{J}}_r \mathbf{u}) dm = \frac{1}{2} \mathbf{u}^T \int_{\mathcal{K}} \hat{\mathbf{J}}_r^T \hat{\mathbf{J}}_r dm \mathbf{u} = \frac{1}{2} \mathbf{u}^T \mathbf{M} \mathbf{u} . \quad (3.24)$$

The position dependency in the JACOBI matrix $\hat{\mathbf{J}}_r$ of translations, equation (3.21), is evaluated during integration over the body \mathcal{K} . Hence, the mass matrix $\mathbf{M} = \mathbf{M}(\mathbf{q})$ is function of the generalized positions only.

For the example of the EULER-BERNOULLI beam with ansatz (3.23), the specialized form (3.13a) of the kinetic energy, see page 33, has the discretized approximation

$$\begin{aligned} T &= \frac{1}{2} \int_0^l \left(\rho A (\bar{\mathbf{w}}_x \mathbf{u})^T (\bar{\mathbf{w}}_x \mathbf{u}) + \rho A (\bar{\mathbf{w}}_z \mathbf{u})^T (\bar{\mathbf{w}}_z \mathbf{u}) \right) ds \\ &= \frac{1}{2} \mathbf{u}^T \int_0^l \left(\rho A \bar{\mathbf{w}}_x^T \bar{\mathbf{w}}_x + \rho A \bar{\mathbf{w}}_z^T \bar{\mathbf{w}}_z \right) ds \mathbf{u} = \frac{1}{2} \mathbf{u}^T \mathbf{M} \mathbf{u} \end{aligned} \quad (3.25)$$

with the constant mass matrix \mathbf{M} . In analogy, the deformation potential (3.14), page 34, for the linear elastic behavior of the beam is approximated by

$$\begin{aligned} V &= \frac{1}{2} \int_0^l \left(EA (\bar{\mathbf{w}}'_x \mathbf{q})^T (\bar{\mathbf{w}}'_x \mathbf{q}) + EI (\bar{\mathbf{w}}''_z \mathbf{q})^T (\bar{\mathbf{w}}''_z \mathbf{q}) \right) ds \\ &= \frac{1}{2} \mathbf{q}^T \int_0^l \left(EA (\bar{\mathbf{w}}'_x)^T \bar{\mathbf{w}}'_x + EI (\bar{\mathbf{w}}''_z)^T \bar{\mathbf{w}}''_z \right) ds \mathbf{q} = \frac{1}{2} \mathbf{q}^T \mathbf{K}_R \mathbf{q}. \end{aligned} \quad (3.26)$$

Due to the kinematic assumption of linear deformations, the linear material law and the linear ansatz (3.22), the potential is a quadratic form with the constant symmetric matrix \mathbf{K}_R of stiffness⁴. In general \mathbf{K}_R might depend upon \mathbf{q} .

The variational formulation involving only the LAGRANGIAN L leads to the homogeneous differential equation for a continuum without dissipation or external loads. To include these, the variational work (3.17), page 34, is evaluated with the discretization (3.22). Considering the equivalence of work expressed in terms of configuration or physical space, see page 10, leads to the respective generalized forces:

$$\delta W = \delta W_p + \delta W_F + \delta W_R = \delta \mathbf{q}^T \left(\mathbf{Q}_p + \mathbf{Q}_F + \mathbf{Q}_R \right). \quad (3.27)$$

The variations of the translational position and the rotational velocity

$$\delta \bar{\mathbf{r}} = \delta \begin{pmatrix} \hat{w}_x \\ 0 \\ \hat{w}_z \end{pmatrix} = \begin{pmatrix} \bar{\mathbf{w}}_x \\ 0 \\ \bar{\mathbf{w}}_z \end{pmatrix} \delta \mathbf{q} = \bar{\mathbf{J}}_T \delta \mathbf{q} \quad (3.28a)$$

$$\delta \bar{\boldsymbol{\Omega}} = \delta \begin{pmatrix} 0 \\ -\hat{w}'_z \\ 0 \end{pmatrix} = \begin{pmatrix} 0 \\ -\bar{\mathbf{w}}'_z \\ 0 \end{pmatrix} \delta \mathbf{u} = \bar{\mathbf{J}}_R \delta \mathbf{u} \quad (3.28b)$$

give rise to the JACOBI matrices $\bar{\mathbf{J}}_T = \bar{\mathbf{J}}_T(s)$ and $\bar{\mathbf{J}}_R = \bar{\mathbf{J}}_R(s)$ of translation and rotation (for angular velocity $\delta \Omega_y = -\delta \hat{w}'_z$ see page 30). The generalized force \mathbf{Q}_p

⁴ The indices R and later G denote specific results of RITZ- and GALERKIN-method.

holding the projection of the distributed loads p_x and p_z results from introducing the variation of the deformation field in the variational work (3.17a), page 34:

$$\delta W_p = \int_0^l (\delta \mathbf{q}^T \bar{\mathbf{w}}_x^T p_x + \delta \mathbf{q}^T \bar{\mathbf{w}}_z^T p_z) ds = \delta \mathbf{q}^T \mathbf{Q}_p. \quad (3.29)$$

The virtual work (3.17b) performed by the discrete forces $\mathbf{F}_i = (F_{x,i}, 0, F_{z,i})^T$ and torques $\mathbf{R}_i = (0, R_{y,i}, 0)^T$ is extended from boundary loads to loads applied at arbitrary positions s_i within the body leading to the generalized forces \mathbf{Q}_{F_i} and \mathbf{Q}_{R_i} :

$$\delta W_{F_i} = \delta \mathbf{q}^T \bar{\mathbf{w}}_x^T \Big|_{s_i} F_{x,i} + \delta \mathbf{q}^T \bar{\mathbf{w}}_z^T \Big|_{s_i} F_{z,i} = \delta \mathbf{q}^T \mathbf{Q}_{F_i} \quad (3.30a)$$

$$\delta W_{R_i} = \delta \mathbf{q}^T (-\bar{\mathbf{w}}'_z)^T \Big|_{s_i} R_{y,i} = \delta \mathbf{q}^T \mathbf{Q}_{R_i} \quad (3.30b)$$

Entering the kinetic energy (3.25), the elastic potential (3.26) and the additional loads (3.27) into the EULER-LAGRANGE equation (2.2), page 9, leads to the differential equation describing the beam dynamics by means of the discretization:

$$\begin{aligned} & \int_0^l (\rho A \bar{\mathbf{w}}_x^T \bar{\mathbf{w}}_x + \rho A \bar{\mathbf{w}}_z^T \bar{\mathbf{w}}_z) ds \dot{\mathbf{u}} + \\ & \int_0^l (EA (\bar{\mathbf{w}}'_x)^T \bar{\mathbf{w}}'_x + EI (\bar{\mathbf{w}}''_z)^T \bar{\mathbf{w}}''_z) ds \mathbf{q} = \int_0^l (\bar{\mathbf{w}}_x^T p_x + \bar{\mathbf{w}}_z^T p_z) ds + \\ & \sum_i (\bar{\mathbf{w}}_x^T F_x + \bar{\mathbf{w}}_z^T F_z - (\bar{\mathbf{w}}'_z)^T R_y) \Big|_{s_i} \\ & \mathbf{M} \dot{\mathbf{u}} + \mathbf{K}_R \mathbf{q} = \mathbf{h}_{\text{ext},R} \end{aligned} \quad (3.31)$$

$$\mathbf{M} \dot{\mathbf{u}} + \mathbf{K}_R \mathbf{q} = \mathbf{h}_{\text{ext},R} \quad (3.32)$$

These are equations in the discrete degrees of freedom \mathbf{q} and \mathbf{u} . The vector $\mathbf{h}_{\text{ext},R}$ holds the projection of all loads not contributing to the potential V .

Weighted Residuals and the Galerkin-Method

From the historical perspective, the GALERKIN method can be motivated by the weighted residual techniques, see BATHE [6]: take $\mathbf{D}(\mathbf{s})$ to be the residual expressing the noncompliance of the discretization compared to the exact solution of the partial differential equation. Formulating a general weighted residual technique, the variational integral

$$\int_{\mathcal{K}} \delta \mathbf{y}^T \mathbf{D} ds \stackrel{!}{=} 0 \quad (3.33)$$

with arbitrary test-functions \mathbf{y} is claimed to vanish. This corresponds to a weak formulation and posterior discretization of the partial differential equation. Further-

more it equals the minimization of the mean square error induced by the approximation. The number of independent parameters in the test-function must equal the dimension n of \mathbf{q} used for discretization. The GALERKIN method starts with the weak form of the partial differential equation: introducing the ansatz (3.20), which simultaneously is used as test-function, leads to the discretized equation.

Inserting the ansatz (3.22) with the corresponding velocities (3.23) and accelerations to the exact equation (3.18) of the EULER-BERNOULLI beam yields the residual form

$$\rho A \bar{\mathbf{w}}_x \dot{\mathbf{u}} - (EA \bar{\mathbf{w}}_x')' \mathbf{q} - p_x = D_x \quad (3.34a)$$

$$\rho A \bar{\mathbf{w}}_z \dot{\mathbf{u}} + (EI \bar{\mathbf{w}}_z'')' \mathbf{q} - p_z = D_z \quad (3.34b)$$

of the differential equation. The residual $\mathbf{D} = \mathbf{D}(s) = (D_x, D_z)^T$ comprises the discretization error compared to the original partial differential equation.

To evaluate equation (3.33) of weighted residuals for the beam, the free variation

$$\delta \mathbf{y} = \begin{pmatrix} \bar{\mathbf{w}}_x \\ \bar{\mathbf{w}}_z \end{pmatrix} \delta \mathbf{a} \quad \text{with } \mathbf{a} \in \mathbb{R}^n \quad (3.35)$$

based on the ansatz-functions $\bar{\mathbf{w}}_x$ and $\bar{\mathbf{w}}_z$ but with arbitrary parameters \mathbf{a} is defined. Multiplying the equations (3.34) with $\delta \mathbf{y}$ and integrating over the whole body gives the weighted residual which are required to vanish:

$$\delta \mathbf{a}^T \int_0^l (\bar{\mathbf{w}}_x^T, \bar{\mathbf{w}}_z^T) \begin{pmatrix} \rho A \bar{\mathbf{w}}_x \dot{\mathbf{u}} - (EA \bar{\mathbf{w}}_x')' \mathbf{q} - p_x \\ \rho A \bar{\mathbf{w}}_z \dot{\mathbf{u}} + (EI \bar{\mathbf{w}}_z'')' \mathbf{q} - p_z \end{pmatrix} ds = 0$$

These equations must hold for arbitrary variations $\delta \mathbf{a}$ and lead to the differential equations in the discrete parameters \mathbf{q} and \mathbf{u} :

$$\int_0^l (\rho A \bar{\mathbf{w}}_x^T \bar{\mathbf{w}}_x + \rho A \bar{\mathbf{w}}_z^T \bar{\mathbf{w}}_z) ds \dot{\mathbf{u}} + \int_0^l (-\bar{\mathbf{w}}_x^T (EA \bar{\mathbf{w}}_x')' + \bar{\mathbf{w}}_z^T (EI \bar{\mathbf{w}}_z'')') ds \mathbf{q} = \int_0^l (\bar{\mathbf{w}}_x^T p_x + \bar{\mathbf{w}}_z^T p_z) ds \quad (3.36)$$

$$\mathbf{M} \dot{\mathbf{u}} + \mathbf{K}_G \mathbf{q} = \mathbf{h}_{\text{ext,G}} \quad (3.37)$$

The matrix \mathbf{K}_G is the stiffness matrix, $\mathbf{h}_{\text{ext,G}}$ holds the projection of the volume loads p_x and p_z . Involving higher spatial derivatives, the GALERKIN-method requests ansatz functions being differentiable continuously more often than the RITZ-method. To get optimal results, the ansatz function should fulfill the complete boundary conditions (3.19) also including the kinetic ones, see for example SCHWERTASSEK AND WALLRAPP [52]. Non-compliance can lead to large errors in the internal continuum forces and therefore to large approximation errors. This is addressed briefly in the following comparison.

Equivalence of Ritz- and Galerkin-Method

In the previous two sections, the RITZ- and the GALERKIN-method both were introduced for developing discretized equations of motion: the continuum dynamics is approximated by means of ansatz-functions. For this purpose, both utilize variational forms of vanishing value, either being motivated physically by the HAMILTON principle and solved by EULER-LAGRANGE equations or motivated mathematically by vanishing residuals in weak form.

For the following comparison of the respective equations of motion (3.31) and (3.36) of the EULER-BERNOULLI beam, the same shape functions $\bar{\mathbf{w}}_i$ are assumed for RITZ- and GALERKIN-method. Being requested by the GALERKIN-method, this ansatz needs to fulfill the kinematic and the kinetic boundary conditions. Ad hoc, the compliance of the mass matrices \mathbf{M} and the projections of the volume loads p_x and p_z can be seen. To discuss the remaining terms, the second summand of the left hand side of the GALERKIN equation of motion (3.36) is transformed in analogy to the integration by parts used for the variation (3.15) of the exact analytic elastic potential, compare to page 34:

$$\begin{aligned}
& \int_0^l \left(-\bar{\mathbf{w}}_x^T (EA \bar{\mathbf{w}}_x')' + \bar{\mathbf{w}}_z^T (EI \bar{\mathbf{w}}_z'')'' \right) ds \mathbf{q} \\
&= \int_0^l \left((\bar{\mathbf{w}}_x')^T (EA \bar{\mathbf{w}}_x') + (\bar{\mathbf{w}}_z'')^T (EI \bar{\mathbf{w}}_z'') \right) ds \mathbf{q} - \\
& \quad \left[\bar{\mathbf{w}}_x^T (EA \bar{\mathbf{w}}_x') + (\bar{\mathbf{w}}_z')^T (EI \bar{\mathbf{w}}_z'') - \bar{\mathbf{w}}_z^T (EI \bar{\mathbf{w}}_z'')' \right]_0^l \mathbf{q} \\
&= \int_0^l \left((\bar{\mathbf{w}}_x')^T (EA \bar{\mathbf{w}}_x') + (\bar{\mathbf{w}}_z'')^T (EI \bar{\mathbf{w}}_z'') \right) ds \mathbf{q} - \\
& \quad \left[\bar{\mathbf{w}}_x^T N - (\bar{\mathbf{w}}_z')^T R_y + \bar{\mathbf{w}}_z^T Q \right]_0^l
\end{aligned}$$

Hereby, the constitutive material law (3.9) of the beam, page 32, is used together with the relation for transversal section forces $Q = \frac{dR}{ds} = -(EI w'')$ in slender beams, see for example HIBBELER [34]. According to the kinetic boundary conditions, N , Q and R of both ends are the respective external loads. To minimize the approximation errors these must be captured by the ansatz for the GALERKIN-method and should be regarded as external loads in the RITZ-method pursuant to equation (3.30).

Concluding, the RITZ-method has the advantage that the order of differentiability of the ansatz functions is “half” that required of the GALERKIN-method. Both methods provide equal results when similar ansatz functions and equal levels of information concerning deformation and boundary conditions as well as loads are used. Nevertheless, the definition of the kinetic boundary conditions for general multi-purpose models like finite elements is not trivial. While both kinetic and kinematic boundary conditions need to be fulfilled for the GALERKIN-method, the appropriate form used for RITZ-method need not to satisfy the kinetic ones and so is easier to set up.

3.3.2 Common Formulations

While the previous section provides the formalism for generating discrete equations of motion for known ansatz functions, the crucial point of defining these shape functions for the approximation still must be addressed. It is quite obvious that the quality of the approximation significantly is influenced by the selection of these functions. In case of locally defined constraints and impacts on the continuum – what especially is regarded within this work – special considerations during modeling should aim for preserving the locality of the contact behavior: this is discussed in detail in the following section 3.3.3. The current section briefly introduces the selection of ansatz functions commonly used for flexible multi-body systems. Thereby, solely the longitudinal deformation of the flexible beam according to equation (3.18b), page 35, is used as example with clamping at $s = 0$ and with free end $s = l$, see figure 3.5(a).

Considering flexible multi-body systems, a differentiation must be set whether a standard element of structural mechanics, like beams or shells, or a body of complex geometry shall be described. While a primitive structure can be completely formulated with high efficiency within the MBS itself, the latter usually are discretized by external pre-processes like structural finite element programs. For standard structural elements, the definition of shape functions is discussed in the following. Finally, the use of an external pre-process is briefly addressed.

Modal Discretization Free of excitations, an elastic body performs deformations in its natural modes with associated eigenfrequencies giving steady state dynamics. Commonly known for the clamped-free elastic rod, a separation of variables gives the analytic solution for the modes being the harmonic series

$$\bar{w}_{xi} = \sin\left(i\frac{\pi}{2l}s\right) \quad \text{with } i = 1, 2, \dots, n, \dots, \infty, \quad (3.38)$$

see for example GROSS ET AL. [31]. Using the first n modal deformations as ansatz

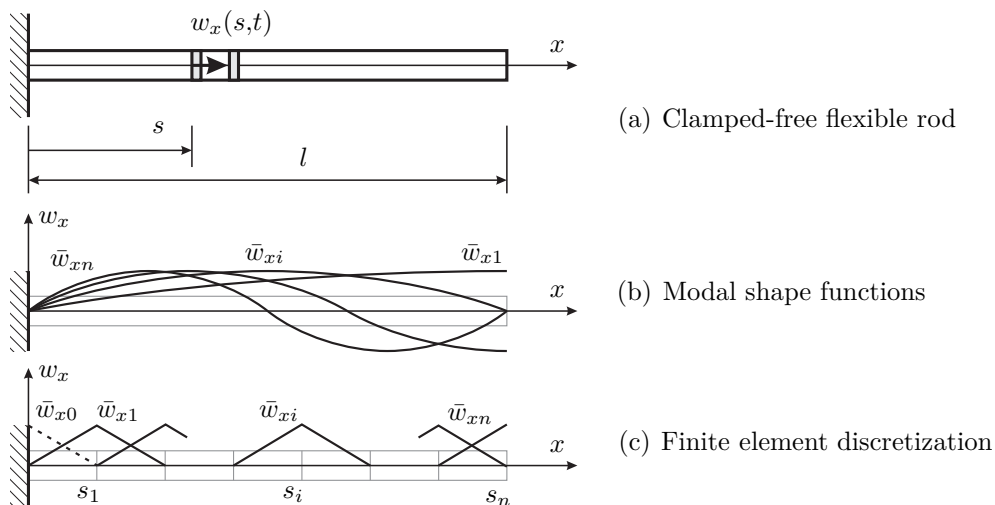


Figure 3.5: Shape functions for the longitudinal deformation of a flexible rod

functions, what implicates the n lower frequency responses, sharply defines the frequency range of the model. Figure 3.5(b) depicts the natural modes for the longitudinal displacement w_x of the clamped-free elastic rod. When no analytic solution for the natural modes can be found, for example for bodies with complex geometry or coupled nonlinear partial differential equations, a finite element pre-process can provide approximative shapes for the use in a modal approach.

The mass matrix and the stiffness matrix of a linear model, which does not account for large rigid body rotations, take diagonal form. Using an infinite number of ansatz functions (3.38), arbitrary excitations including the exact solutions and even singular jumps can be represented, compare to standard mathematical literature. Concurrently spatial smoothness of the shape functions can be guaranteed since the deformation modes are continuously differentiable infinite times.

Since the method is based on an eigenvalue analysis of the system, it is limited to small deflective systems described relatively to one frame of reference for the entire structure. When this frame of reference is moving to account for large rigid body motions, the coupling between rigid body motion and deformations leads to additional non-diagonal entries in the mass matrix. These comprise a dependency on the generalized position \mathbf{q} which can be expressed by rotational transformation matrices. A general presentation of the methodological framework is given by BREMER AND PFEIFFER [10] and SHABANA [56]. Due to the closeness of the modeling to the effects regarded, this method is of very wide propagation especially since often only small deflections are regarded for flexible multi-body systems. A selective modeling, for the present example only of longitudinal deformations, is intrinsically provided and can be used to minimize the model size. Structural elements, mostly beams, are available in modal discretizations in many of the commercial simulation tools. For systems with structural variance like closing unilateral contacts or contacts with relative tangential motion, no constant modes can be identified. A weak approximation may result using non-complying forms for systems with a modified structure.

Finite Element Discretization The finite element method can be motivated by two different intentions leading to the same result. One is to use ansatz functions having values unequal to zero only in a sub-domain $\mathcal{K}_i, i \in \{1, \dots, n\}$ of the entire body $\mathcal{K} = \cup_i \mathcal{K}_i$. At least the smoothness requirements of the RITZ-method must be regarded on \mathcal{K} for all shape functions. The alternative intuition is dividing the entire domain \mathcal{K} into n sub-volumes \mathcal{K}_i of primitive geometry. Approximations then are developed on the level of one uncoupled finite element \mathcal{K}_i . The global solution is gained after reassembling all elements to the overall model. Therefore, compatibility of the displacement fields is required at the finite element boundaries to ensure connectivity and satisfy smoothness requirements.

The more elements are used, the finer a finite element discretization becomes: like for the modal approach, convergence is ensured since the exact solution including non-continuous solutions can be represented using an infinite number of elements. Still, all elements are formulated with the same ansatz functions. Even though only a linear finite element formulation is discussed below, arbitrary mathematical

descriptions including nonlinearity in positions and global coordinates can be defined analogously. For a comprehensive introduction including many specific formulations of elements see BATHE [6].

For the longitudinal deformation of a flexible rod, the element \mathcal{K}_i is defined at positions $s_{i-1} \leq s < s_i$. According to the RITZ-method, at least \mathcal{C}^1 smoothness is required for the shape functions on the entire \mathcal{K} except for singular positions like the element boundaries. This is provided by piecewise linear functions. The element of length $l_i = s_i - s_{i-1}$ implies the nodal displacements $a_{i1} = \hat{w}_x(s_{i-1})$ and $a_{i2} = \hat{w}_x(s_i)$ of the boundary sections. The unified formulation uses the normalized local position $\xi_i = \frac{s-s_{i-1}}{l_i}$ within the element. Constant strain $\varepsilon_i = (\bar{w}_{xi}^*)' = \frac{a_{i2}-a_{i1}}{l_i}$ is assumed leading to the linear deformation field

$$\bar{w}_{xi}^* = \begin{cases} a_{i1}(1 - \xi_i) + a_{i2}\xi_i & \text{for } 0 \leq \xi_i \leq 1 \\ 0 & \text{everywhere else} \end{cases} \quad (3.39)$$

This approximation ensures connectivity since adjacent elements describe equal displacements at their common boundary. Using a mesh of n elements introduces $n+1$ independent nodal displacements $q_i = \hat{w}_x(s_i)$. Sorting for components of the generalized degrees of freedom $\mathbf{q} = (\dots, q_i, \dots)^T$ yields the triangular ansatz functions

$$\bar{w}_{xi} = \begin{cases} 0 & \text{if } s < s_{i-1} \\ \frac{s-s_{i-1}}{l_i} & \text{if } s_{i-1} \leq s < s_i \\ \frac{s_{i+1}-s}{l_{i+1}} & \text{if } s_i \leq s < s_{i+1} \\ 0 & \text{if } s_{i+1} \leq s \end{cases} \quad (3.40)$$

defined globally. These are shown in figure 3.5(c) for equal element sizes l_i . The boundary condition $w_x(s=0)$ due to rigid clamping is regarded by not introducing the ansatz \bar{w}_{x0} and the associated q_0 , what is depicted by a dashed line.

The absolute nodal coordinate formulation (ANCF) of SHABANA [56] is among the nonlinear large deformation finite element approaches. Based on a subdivision of the body's domain, finite elements are formulated with interpolations being nonlinear in the algebraic position variables \mathbf{s} but linear in \mathbf{q} . Strain measures are performed either in moving frames of reference attached to specific elements or referring to the inertial frame. For an overview on ANCF element formulations see GERSTMAYR [27]. Also providing large deflection capabilities, a co-rotational formulation assigning own frames of reference to each finite element is developed within a redundant coordinate formulation in section 4.2. There, one aim is to keep the physical interpretability of the deformation-force-relations at a level of the modal approaches.

Subdividing the domain to finite elements offers the possibility of local mesh refinements. Even though an increased accuracy for example at contact positions can be achieved, no dynamic mesh adaption is regarded within this thesis. For this work, contact situations are regarded with changing positions which are a priori unknown. Dynamic mesh-refinement and reduction back to coarser meshes is topic of active research and offers high theoretical and numerical challenges, see WRIGGERS [64].

External Pre-Processes Aside from developing the mathematical model “by hand” according to section 3.3.1 with specifically designed shape functions, external pre-processes can be used to define the discrete model for a flexible body. Most common is to use structural finite element analyses for example for systems of complex geometry or exceptional parameter distributions: the nontrivial evaluation of the integrals defining the mass matrix and the generalized force vector, compare equations (3.31) and (3.36), is performed by external programs. The result is reduced to an abstract set of coordinates \mathbf{q} , a mass matrix \mathbf{M} and a representation of internal forces \mathbf{h} , which often are described linear in \mathbf{q} using a constant stiffness matrix. See for example SHABANA [56] for a complete presentation of the procedures necessary to embed the models gained in a finite element code within the multi-body simulation including large reference motion. The approach is provided in several commercial tools including the required interfaces: since during the development of a new technical product construction data often is processed in finite element environments for strength analysis this approach offers stringent further data processing as well as high working efficiency.

In contrast to the modal and the finite element approach, discretizations built by external pre-processors usually do not offer continuous geometric shape informations for the body. Interactions then are defined implying special key nodes i with discrete position \mathbf{r}_i and JACOBI matrix \mathbf{J}_i . To allow not only for interactions with these discrete points but for contacts with relative motion on the body, supplementary interpolation rules will be sketched in section 3.4 providing a continuous shape.

3.3.3 Contact and Discontinuity

Of the methods mentioned previously, the modal and the finite element discretization are compared regarding contact situations. At this, the instantaneous reaction of the flexible structure is the central point: rigid contacts are assumed to be point-to-point interactions without spatial expansion. Locally separate contacts to one structure are uncoupled kinematically due to the distributed flexibility in between. The local character of contacts should be preserved by the discretization with respect to the kinematic assumptions and should not be blurred over wide regions; the decoupling of separate contacts should be reflected by the discretization. As will be discussed below, kinematic couplings are introduced by the ansatz functions used. Locality is requested not only for reasons of better numerical performance: a weak coupling of different contacts is displayed by a strong diagonal character of the effective mass matrix $\mathbf{G} = \mathbf{W}^T \mathbf{M}^{-1} \mathbf{W}$ of contacts, equation (2.37) on page 26, what provides better solvability of the contact problem. Moreover, the physical interpretation of the short time reaction corresponds to the disturbance or sound propagation velocity within the continuum, which in reality is of finite value. This transient behavior must be displayed by the internal flexible dynamics.

Regarding the locality of the approximation, two extremal variants of shape function definitions are presented: the modal approach reflects the steady state dynamics of the entire structure with fixed setup whereas the finite element approach allows for a

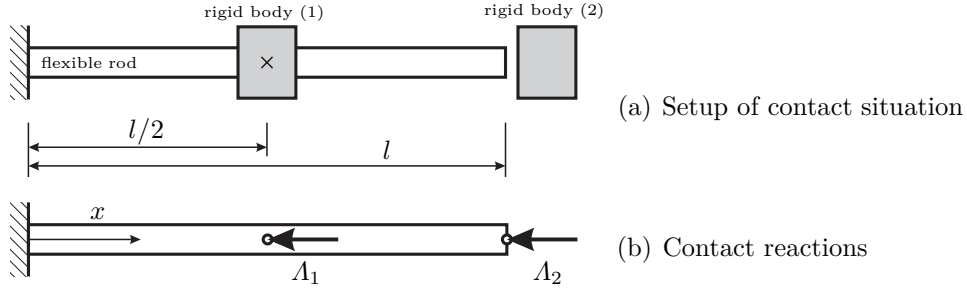


Figure 3.6: Contact situation between rigid bodies and flexible rod

high localization. Models described by external pre-processes will show a behavior in between, depending upon steps of modal reduction and shape interpolations possibly performed during model preparation.

Figure 3.6 depicts the contact situation that is used for the comparison of the discretizations: the rod of figure 3.5(a) with longitudinal flexibility is used with constant cross section A and constant density ρ . It is charged by the reactions $\mathbf{\Lambda} = (\Lambda_1, \Lambda_2)^T$ representing rigid contacts: at $s_1 = \frac{l}{2}$, rigid body (1) is fixated; at $s_2 = l$ rigid body (2) impacts. Since these bodies do not directly influence the internal dynamics of the flexible rod or its discrete approximation, the rigid bodies are entirely represented by their respective contact interactions Λ_i with the rod.

Assuming initial zero velocities for the rod, only the discrete time of impact is regarded. The discrete post-impact velocities of the flexible rod write according to the impact equation (2.18), page 14:

$$\mathbf{u}^+ = \mathbf{M}^{-1} \mathbf{W} \mathbf{\Lambda} \quad (3.41)$$

For the evaluation, the mass matrix \mathbf{M} and the generalized force directions \mathbf{W} are needed depending upon the ansatz functions used. The generalized force vector \mathbf{h} does not influence to instantaneous post-impact behavior. Equation (3.18a), page 35, describes the time and spatial continuous behavior of the rod that needs to be discretized. The contact kinematics of flexible bodies is addressed in detail in the following section 3.4. Here, the generalized force directions associated to the LAGRANGE-multipliers $\mathbf{\Lambda}$ are gained according to equation (2.23a), page 17, using the JACOBI matrices $\bar{\mathbf{J}}_T$, equation (3.23) on page 38, of the contact points s_1 and s_2 with the contact normal $\mathbf{n} = -\mathbf{b}_x = (-1, 0, 0)^T$:

$$\mathbf{W} = (\mathbf{W}^*(s = l/2), \mathbf{W}^*(s = l)) \quad \text{with} \quad \mathbf{W}^* = \bar{\mathbf{J}}_T^T \mathbf{n}$$

Inserting the post-impact velocities (3.41) to the modal and finite element discretizations (3.38) and (3.40) provides the spatial continuous approximations

$$\dot{w}_x^+ = \dot{w}_x^+(s) = \bar{\mathbf{w}}_x \mathbf{u}^+ \quad (3.42)$$

for the velocity field respectively. This function reflects the instantaneous reaction of the discretized model. The idealized percussions $\mathbf{\Lambda}_m = (1, 0)^T$ on the mid-point and $\mathbf{\Lambda}_e = (0, 1)^T$ on the free end are used to investigate the kinematic interference

between the respective post-impact velocity fields \hat{w}_x^+ . When solving the contact problem, the reactions \mathbf{A} are determined in such a way that the kinematic constraints are fulfilled at the discrete points of contact. To allow for the following comparison and discussion, \hat{w}_x^+ are normalized to the amplitude ‘1’ at the contact position.

Modal Discretization A discretization with the n lower frequency modes using the ansatz (3.38) leads to components $M_{ij} = A\rho l \int_0^1 \sin(i\frac{\pi}{2}\xi) \sin(j\frac{\pi}{2}\xi) d\xi$ of the mass matrix. Due to the orthogonality of the ansatz functions, the mass matrix

$$\mathbf{M} = A\rho l \begin{pmatrix} \frac{1}{2} & 0 & \cdots & 0 \\ 0 & \frac{1}{2} & & 0 \\ \vdots & & \ddots & \vdots \\ 0 & 0 & \cdots & \frac{1}{2} \end{pmatrix} \in \mathbb{R}^{n \times n}$$

is diagonal. The matrix of generalized force directions

$$\mathbf{W} = - \begin{pmatrix} \sin(\frac{\pi}{4}) & , \dots , & \sin(i\frac{\pi}{4}) & , \dots \\ \sin(\frac{\pi}{2}) & , \dots , & \sin(i\frac{\pi}{2}) & , \dots \end{pmatrix}^T \in \mathbb{R}^{n \times 2}$$

holds entries alternating with the mode number i and being the modal responses \bar{w}_{xi} at the respective contact positions. For $n = 32$ and $n = 8$ modes, figures 3.7 and 3.8 display in dashed lines the normalized responses to the percussions \mathbf{A}_m (fig. 3.7(a) and 3.8(a)) and \mathbf{A}_e (fig. 3.7(b) and 3.8(b)) according to equations (3.41) to (3.42).

Finite Element Discretization Using n uniform linear finite elements with the ansatz functions (3.40) for n degrees of freedom, whereas $w_x(0) = 0$ is respected by exclusion of q_0 , see equation (3.40) on page 45, yields the tridiagonal mass matrix

$$\mathbf{M} = \frac{A\rho l}{6n} \begin{pmatrix} 4 & 1 & 0 & \cdots & 0 & 0 \\ 1 & 4 & 1 & \cdots & 0 & 0 \\ 0 & 1 & 4 & \cdots & 0 & 0 \\ \vdots & \vdots & \vdots & \ddots & \vdots & \vdots \\ 0 & 0 & 0 & \cdots & 4 & 1 \\ 0 & 0 & 0 & \cdots & 1 & 2 \end{pmatrix} \in \mathbb{R}^{n \times n}$$

commonly known, see BATHE [6]. The generalized force directions depend upon the inner elemental representation ξ of the contact position $s_1 = l/2$ within the element effected by the mid-point contact:

$$\mathbf{W} = - \begin{pmatrix} 0 & \cdots & 0 & 1 - \xi & \xi & 0 & \cdots & 0 & 0 \\ 0 & \cdots & 0 & 0 & 0 & 0 & \cdots & 0 & 1 \end{pmatrix}^T \in \mathbb{R}^{n \times 2} \quad \text{with } \xi \in [0; 1]$$

Having only single entries unequal to zero reflects the spatial subdivision into elements: only degrees of freedom associated to the elements being involved into contact are affected directly. Using $n = 32$ respectively $n = 8$ nodal degrees of

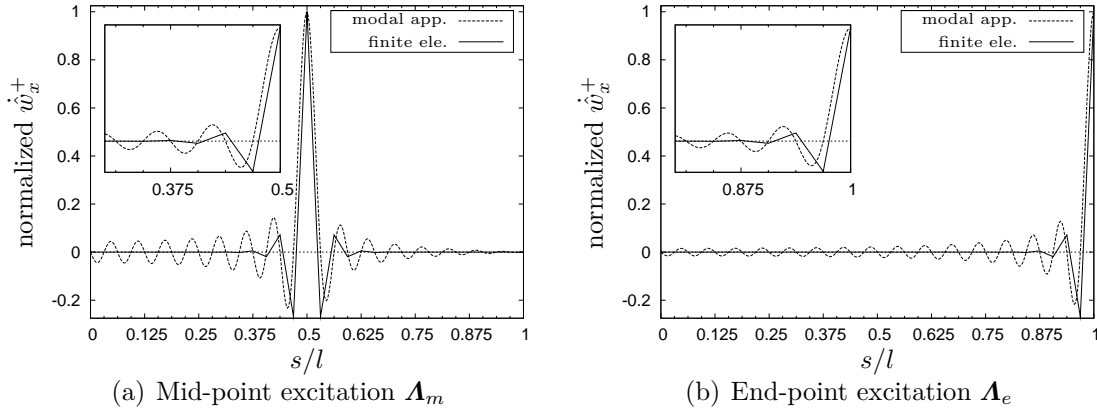


Figure 3.7: Normalized responses for modal and local shape functions with $n = 32$

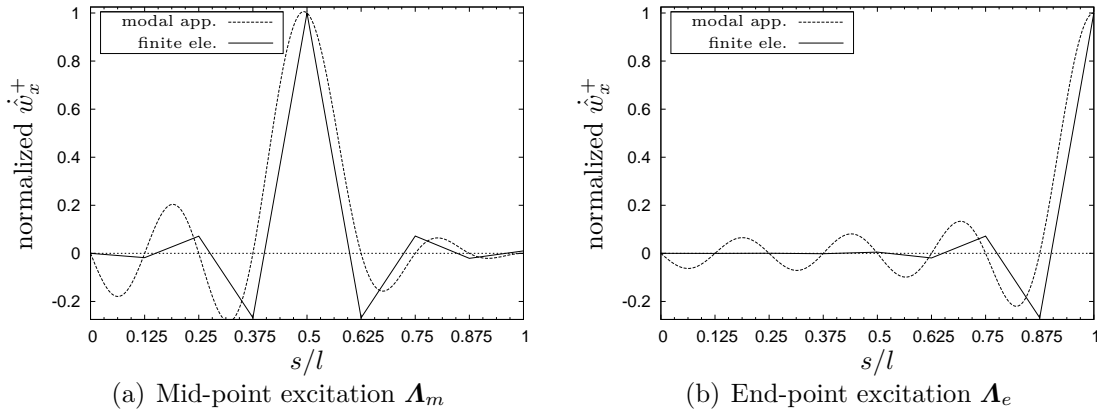


Figure 3.8: Normalized responses for modal and local shape functions with $n = 8$

freedom (for both: $\xi = 1$), figures 3.7 and 3.8 depict in solid lines the responses \dot{w}_x^+ to the percussions \mathbf{A}_m (fig. 3.7(a) and 3.8(a)) and \mathbf{A}_e (fig. 3.7(b) and 3.8(b)).

Comparison Figures 3.7 and 3.8 show the post-impact velocity fields for the modal and the finite element discretization. It is quite obvious that finite elements give the better localization of the spatially discrete contact situation: the mean local decline is stronger. Even though both approaches converge to a spatial discrete response for infinitely fine discretizations, both introduce a kinematic coupling over the entire body \mathcal{K} being an undesired trade-of. The coupling of the contact positions s_1 and s_2 can be seen by non-vanishing amplitudes for excitation of the respective opposite position. Thereby the mean amplitudes using a finite element discretization are lower than for the modal approach. This is taken into the effective mass matrix \mathbf{G} of contacts, equation (2.37) on page 26, in form of a stronger diagonal dominance. For a single finite element of the elastic rod, the kinematic coupling can be seen in a single row $\frac{A\rho l}{6n}(4,1)$ of the mass matrix which directly couples the accelerations of adjacent elemental nodes. The spatial decline in \dot{w}_x^+ is governed by the corresponding entries in the inverse mass matrix and correlates with the number of elements in between the point of reaction application and the point regarded.

Even though this discussion is based on the simple example of longitudinal flexibility, the results are equal for models with more complex internal dynamics: the inherent kinematic coupling of a model is represented by the mass matrix \mathbf{M} and the generalized force directions \mathbf{W} , which both are directly results of the ansatz functions used. For contact simulations, the ansatz functions should emphasize the local aspect to allow for a decoupling of multi-contact situations. Additionally, a mass lumping technique applied on the mass matrix might help in contact simulations providing a diagonal form for finite elements and thereby complete kinematic decoupling.

3.4 Contact Kinematics of Flexible Systems

Flexible bodies are deformable and therefore hold time-variant contours. Based on the kinematic assumptions of section 3.1, a finite dimensional approximation for the dynamics was derived in the previous section. For the description of contact situations, the body's kinematics is needed again, see section 2.2: utilizing the approximation for the shape, positions and velocities of potential contact points need to be evaluated. Establishing the necessary conditions for contact leads to the relative gap distances and velocities of contacts. Some special aspects of contact kinematics, especially the contour definition, are addressed within the current section.

3.4.1 Contour Description

Regarding contact situations with relative motion on the surfaces, additional considerations concerning the smoothness of the approximation for the contours are necessary: GLOCKER [29] mentions impacts without collision when contacting surfaces offer only insufficient local smoothness less \mathcal{C}^2 . Assume a rigid body sliding bilaterally constrained on the shapes depicted in figure 3.9: obviously, an impact occurs when reaching the corner C of shape 3.9(a) being piecewise linear. When sliding through the joining point O of the attached opposed arcs 3.9(b), the instantaneous reverse of the rotation must be interpreted as impact. Therefore, shape functions used for the discretization of undeformed smooth flexible contours should offer sufficiently smooth differentiability also for deformed configurations.

For the derivation of the discretized model, two conceptually different approaches were shown in the previous section: models derived with known shape functions for the kinematic fields and abstract models from other simulation tools like for



Figure 3.9: Examples for planar contours with smoothness less \mathcal{C}^2

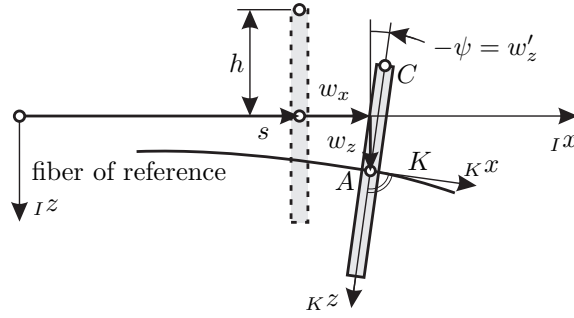


Figure 3.10: Contact kinematics of the EULER-BERNOULLI beam

example finite element programs. While the first hold the shape description for a unitary contact modeling, interactions to models of external pre-processes usually are restricted to discrete points. Based on these points, continuous contours can be modeled subsequently by additional interpolations.

Unitary Shape Functions In section 3.1.1, kinematic assumptions for the continuum were introduced. With respect to the discretization applied in section 3.3, the entire continuous description of the body's surfaces is provided in a unitary way: both inner dynamics and contact description can be evaluated using the same spatial approximations (3.20), page 37.

Figure 3.10 shows the kinematics of a cross section for the EULER-BERNOULLI beam example according to figure 3.2, page 30. Using the kinematic description (3.4), page 30, gives the local tangent direction to the beam

$${}_I \mathbf{t} = {}_I \mathbf{t}(s) = \frac{\partial {}_I \mathbf{r} / \partial s}{|\partial {}_I \mathbf{r} / \partial s|} = {}_I \mathbf{b}_{Kx}$$

defining the local Kx -axis of the coordinate system associated to the cross section at position s . For small deflections this can also be parametrized using the slope ψ , see page 30. The planar system performs motions within a plane parametrized by the binormal ${}_I \mathbf{b}_{Ky} = (0, 1, 0)^T$. Therefore, the contour normal is ${}_I \mathbf{n} = {}_I \mathbf{b}_{Kz} = {}_I \mathbf{b}_{Kx} \times {}_I \mathbf{b}_{Ky}$ leading to the attendant coordinate system K given by the transformation matrix

$$\mathbf{A}_{IK} = \mathbf{A}_{IK}(s, \mathbf{q}) = ({}_I \mathbf{b}_{Kx}, {}_I \mathbf{b}_{Ky}, {}_I \mathbf{b}_{Kz}) \quad (3.43)$$

with respect to the inertial system I .

In spite of starting with the special example, the following derivation is presented in a general form for arbitrary slender structures also undergoing large deflections, whereas special simplifications for the EULER-BERNOULLI beam are not exploited. The position of the surface point C with respect to the cross-sectional system K is ${}_K \mathbf{r}_{AC} = (0, 0, -h)^T = \text{const.}$, see figure 3.10. The inertial position of the point C

$${}_I \mathbf{r}_{OC} = {}_I \mathbf{r}_{OA} + \mathbf{A}_{IK} {}_K \mathbf{r}_{AC} \quad \text{with} \quad {}_I \mathbf{r}_{OA} = {}_I \mathbf{r}_{OA}(s, \mathbf{q}) \quad (3.44)$$

holds the position ${}_I \mathbf{r}_{OA}$ of the neutral fiber and rotations \mathbf{A}_{IK} of the cross section.

Referring to equation (2.20) and the relative velocities (2.23), pages 15 *ff*, the velocities of the contour points are needed for the contact kinematics. Therefore, the rotational velocity of the cross section is derived as screw-symmetric product⁵

$${}_I\tilde{\boldsymbol{\Omega}} = \dot{\mathbf{A}}_{IK} \mathbf{A}_{IK}^T, \quad {}_I\boldsymbol{\Omega} = \mathbf{J}_R \mathbf{u} \quad (3.45)$$

see for example SHABANA [56] or ULBRICH [60], and is a linear combination of the generalized velocities \mathbf{u} and the structure's JACOBI matrix $\mathbf{J}_R = \mathbf{J}_R(s)$ of rotations. Building the total derivative of the position (3.44) gives

$${}_I\mathbf{v}_C = \frac{\partial {}_I\mathbf{r}_{IA}}{\partial \mathbf{q}} \mathbf{u} + \dot{\mathbf{A}}_{IK} {}_K\mathbf{r}_{AC} = \mathbf{J}_T \mathbf{u} + {}_I\tilde{\boldsymbol{\Omega}} \mathbf{A}_{IK} {}_K\mathbf{r}_{AC} = (\mathbf{J}_T - {}_I\tilde{\mathbf{r}}_{AC} \mathbf{J}_R) \mathbf{u} \quad (3.46)$$

with $\mathbf{J}_T = \mathbf{J}_T(s, \mathbf{q})$ being the JACOBI matrix of translations for the neutral fiber and ${}_I\mathbf{r}_{AC} = \mathbf{A}_{IK} {}_K\mathbf{r}_{AC}$ depending on the coordinates \mathbf{q} via the transformation with \mathbf{A}_{IK} . Inserting the velocity (3.46) to the equations leading to the contact velocities (2.23), page 17, yields the generalized force directions \mathbf{W}_N and \mathbf{W}_T based on the approximation (3.20) used for the discretization of the system dynamics. Thereby the shape is described consistently for the entire mechanical model of the flexible structure.

Independent Contour Interpolations When using external pre-processes like finite element codes for the definition of the flexible model, the interactions usually are restricted to discrete points whereas the continuous shape information is lost. With a subsequent interpolation based on the discrete interaction points, shapes can be constructed utilizing arbitrary approaches of computational geometry, see for example the book [46] of PIEGL AND TILLER. Additionally, if the approximation used for the dynamics is known but does not provide contours being sufficiently smooth, a further interpolation for the description of the deformed shape can be used for contact kinematics. The contact formulation based on the discretization of the internal dynamics shown in the previous section is the special case using unitary shape functions.

Every model for the dynamics of a body provides positions and velocities

$${}_I\mathbf{r}_{P_i} = {}_I\mathbf{r}_{P_i}(\mathbf{q}) \quad (3.47a)$$

$${}_I\mathbf{v}_{P_i} = \frac{\partial {}_I\mathbf{r}_{P_i}}{\partial \mathbf{q}} \mathbf{u} = \mathbf{J}_{P_i} \mathbf{u} \quad (3.47b)$$

for discrete points P_i of interactions depending upon the generalized positions \mathbf{q} and velocities \mathbf{u} . The point ${}_I\mathbf{r}_{P_i}$ is the most primitive contour and can be used directly for spatially discrete contact applications. For models with linear dynamics, the JACOBI matrix \mathbf{J}_{P_i} is constant and equation (3.47a) simplifies to ${}_I\mathbf{r}_{P_i} = {}_I\mathbf{r}_{P_{0i}} + \mathbf{J}_{P_i} \mathbf{q}$ with a constant undeformed reference position ${}_I\mathbf{r}_{P_{0i}}$.

Many formulations in computational geometry, for example nonuniform rational B-splines (NURBS), use interpolations which are linear in the positions ${}_I\mathbf{r}_{P_i}$ of the

⁵ The operator $\tilde{\boldsymbol{\xi}}$ gives the antisymmetric matrix so that $\tilde{\boldsymbol{\xi}} \mathbf{a} = \boldsymbol{\xi} \times \mathbf{a}$ equals the cross product.

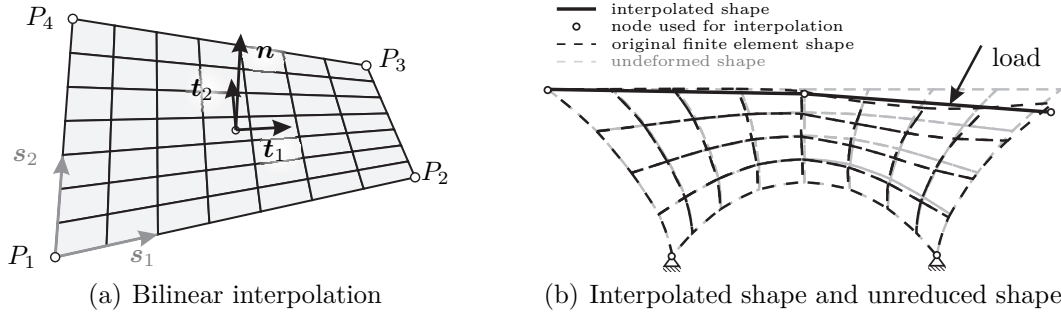


Figure 3.11: Examples for independent contour interpolations

reference points but nonlinear in the contour parameter \mathbf{s} defining the interpolation, see again [46]. The continuous shape is defined by reference points i with the associated weights $N_i = N_i(\mathbf{s})$ only depending on \mathbf{s} :

$${}_I\mathbf{r} = \sum_i N_i {}_I\mathbf{r}_{P_i} \quad (3.48)$$

Derivation with respect to time gives the velocity of the surface points

$${}_I\mathbf{v} = \sum_i N_i {}_I\mathbf{v}_{P_i} = \sum_i (N\mathbf{J}_P)_i \mathbf{u} = \mathbf{J}_C \mathbf{u} \quad (3.49)$$

being linear combinations of the nodal velocities (3.47b) and accordingly of the body's generalized velocities \mathbf{u} . Due to this linearity, which originates from the interpolation (3.48), the JACOBI matrix $\mathbf{J}_C = \mathbf{J}_C(\mathbf{s})$ is the linear combination of the nodal JACOBI matrices using the weights N_i depending on the position \mathbf{s} .

Associated with the position (3.48) are the tangential directions

$${}_I\mathbf{t}_i = \frac{\partial {}_I\mathbf{r} / \partial s_i}{|\partial {}_I\mathbf{r} / \partial s_i|}.$$

In case of a spatial surface, the contour normal $\mathbf{n} = \mathbf{t}_1 \times \mathbf{t}_2$ is the cross product of the tangential directions. For one-dimensional contours the second tangent is substituted by the binormal of the description. Like for every shape description, inserting the velocities (3.49) holding the associated JACOBIAN \mathbf{J}_C into the relative contact velocities (2.23), page 17, yields the force directions for contact description.

Figure 3.11 depicts two examples: the bilinear interpolation 3.11(a) is based on four cornering nodes. Smooth differentiability is provided only within the surface: for a sliding motion to an adjacent bilinear surface, the non-smooth impact situation discussed for figure 3.9(a) may occur at the common edge. Figure 3.11(b) exemplary depicts differences between deformations due to a discrete load for a reduced model with shape interpolation and the original fine finite element mesh.

Applying additional interpolated contours offers the possibility of arbitrary shape descriptions for the contact kinematics. The interpolations do not need to be specialized to demands of the discretization of the equations of motion but can deal

with the requirements of contact problems: these are efficiency and robustness for contact point finding as well as smooth surface description. Thereby, interpolations possibly leading to high oscillations like for example high order polynomials should be avoided. The inconsistency between the discretizations of the equations of motion and the contact surface leads – like every discretization – to approximation errors: these need to be regarded during modeling and can be reduced using fine interpolations and sophisticated techniques of computational geometry.

3.4.2 Contact Conditions

With the continuous shape established in the previous section for all modeling approaches, only some aspects of contact point finding shall be mentioned in addition to section 2.2. Due to the transient shape, a flexible contour can not a priori be known to be convex or concave. Therefore the number of solutions for the contour positions $\mathbf{s}^{(i)}$ of the necessary contact condition (2.21), page 16,

$$\left(\mathbf{T}^{(i)}\right)^T \left(\mathbf{r}_{OC}^{(2)} - \mathbf{r}_{OC}^{(1)}\right) = \mathbf{0} \quad \forall i \in 1,2$$

is in general unknown for a contact situation of the bodies (1) and (2). The contour points $\mathbf{r}_{OC}^{(i)} = \mathbf{r}_{OC}^{(i)}(\mathbf{s}^{(i)}, \mathbf{q}^{(i)})$ as well as the tangent matrices $\mathbf{T}^{(i)} = \mathbf{T}^{(i)}(\mathbf{s}^{(i)}, \mathbf{q}^{(i)})$ are functions of the body's generalized coordinates respectively.

Figure 3.12(a) illustrates condition (2.21) for the example of a planar beam structure (1) with scalar contour parameter s and a point obstacle (2). Configurations leading to different numbers p of solutions for the same deformation state of the beam are depicted in figure 3.12(b). In case of multiple solutions, the solution giving the absolute minimal gap distance g_N , equation (2.22) on page 16, between the obstacle and the corresponding point on the structure has to be chosen. Robust numeric algorithms for finding the corresponding contact points are briefly discussed in section 5.2.

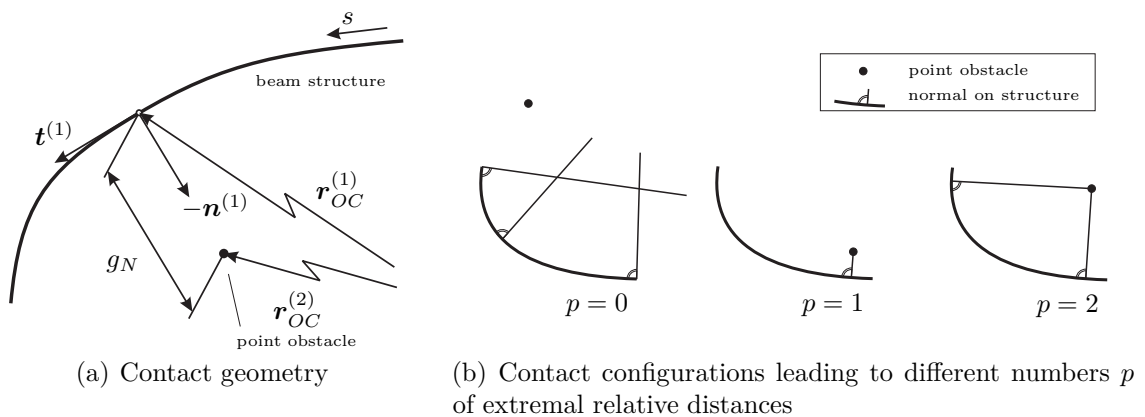


Figure 3.12: Contact situations for beam structure

3.5 Remarks on Implementation

For performing numerical simulations, the models derived according to the current chapter need to be implemented in a software environment. Some concluding remarks aiming for an object-orientation motivated by the physical structure of the systems shall help the readers own work. The remarks refer to the development of the module for flexible bodies in the MBSIM software package written in C++ and especially to the class `BodyFlexible`. This base class provides central functionality for the specific implementation of special models.

As shown in the literature and in the previous sections of this thesis, the dynamics of a single body (i) in a multi-body system can be decomposed into parts of uncoupled internal dynamics and interactions k with the surrounding applied at discrete body points \mathbf{s}_k . Sorting according to this, the equations of motion of the body (i) write

$$\mathbf{M}^{(i)} d\mathbf{u}^{(i)} - \mathbf{h}_{\text{int}}^{(i)} dt = \mathbf{h}_{\text{ext}}^{(i)} dt + \mathbf{W}^{(i)} d\mathbf{\Lambda} = \sum_k \mathbf{J}_k^{(i)} \left[\begin{pmatrix} \mathbf{F} \\ \mathbf{R} \end{pmatrix} dt + \begin{pmatrix} \mathbf{f} \\ \mathbf{m} \end{pmatrix} d\mathbf{\Lambda} \right]_k. \quad (3.50)$$

The terms on the left depend exclusively on the state $\mathbf{q}^{(i)}$ and $\mathbf{u}^{(i)}$ of the body itself. Generalized forces due to the uncoupled dynamics of the body are represented by $\mathbf{h}_{\text{int}}^{(i)}$, single-valued interactions of flexible contacts and applied loads are collected in $\mathbf{h}_{\text{ext}}^{(i)}$. The interactions are projected from physical into configuration space by the JACOBI matrix $\mathbf{J}_k^{(i)} = \mathbf{J}^{(i)}(\mathbf{s}_k) = (\mathbf{J}_{Tk}, \mathbf{J}_{Rk})^{(i)}$ associated to the point \mathbf{s}_k of application. The JACOBIAN exclusively depends on the coordinates $\mathbf{q}^{(i)}$ and the position \mathbf{s}_k and holds translational and rotational parts. The evaluation of interactions including additional loads can be separated from the body implementation: forces \mathbf{F} and torques \mathbf{R} with single-valued force laws as well as the normalized direction matrices \mathbf{f} and \mathbf{m} of translational and rotational set-valued interactions are provided by modules evaluating the kinematics of the interaction points. Thereby, a set-valued interaction k imposes the LAGRANGE multipliers $d\mathbf{\Lambda}_k$ to the MBS.

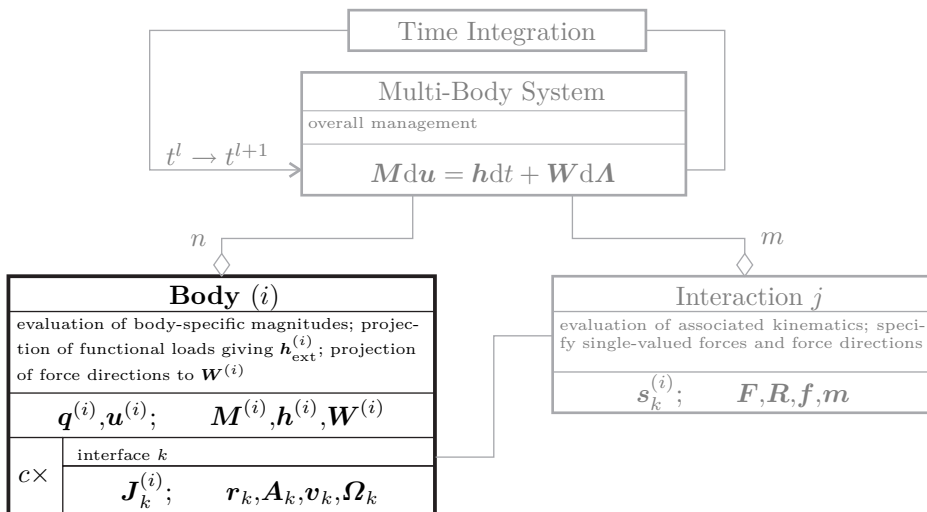


Figure 3.13: Diagram of the object structure according to equation (3.50)

Figure 3.13 illustrates the responsibilities within a multi-body system as realized in MBSIM. Components which can be encapsulated apart from modeling and software realization for the specific body are shaded in gray: the overall MBS comprehends all bodies and interactions and is connected to the time integration algorithm. This includes the solution of constrained systems. Not depicted are further MBS elements like for example control devices.

During evaluation of the current state, the body (i) provides the mass matrix $\mathbf{M}^{(i)}$, the generalized force vector $\mathbf{h}^{(i)}$ and the generalized reaction directions $\mathbf{W}^{(i)}$. For a flexible body, the model-specific implementation for the mass matrix $\mathbf{M}^{(i)}$, the vector $\mathbf{h}_{\text{int}}^{(i)}$ and the JACOBI matrices $\mathbf{J}_k^{(i)}$ are evaluated. Centrally implemented for all flexible bodies in the class `BodyFlexible`, the generalized forces and directions

$$\mathbf{h}^{(i)} = \mathbf{h}_{\text{int}}^{(i)} + \sum_k \left[\mathbf{J}^{(i)} \begin{pmatrix} \mathbf{F} \\ \mathbf{R} \end{pmatrix} \right]_k \quad \text{and} \quad \mathbf{W}^{(i)} = \sum_k \left[\mathbf{J}^{(i)} \begin{pmatrix} \mathbf{f} \\ \mathbf{m} \end{pmatrix} \right]_k$$

are synthesized.

The inertial loads \mathbf{F}_k and \mathbf{R}_k and the directions \mathbf{f}_k and \mathbf{m}_k are defined by separate modules accounting for the interaction k specifically. These evaluate the respective body kinematics which is specific to single models: for the material point \mathbf{s}_k , the inertial position ${}_I\mathbf{r}_k^{(i)} = {}_I\mathbf{r}_k^{(i)}(\mathbf{s}_k)$ and orientation $(\mathbf{A}_{IC})_k^{(i)} = (\mathbf{A}_{IC})_k^{(i)}(\mathbf{s}_k)$ need to be provided by the body. In case of relative motion of contacting surfaces, the position is processed during the search of the contact points $\mathbf{s}_k^{(i)}$ on both bodies and calculation of the distance g_N . The velocities ${}_I\mathbf{v}_k^{(i)} = \mathbf{J}_{T_k}^{(i)}\mathbf{u}^{(i)}$ and ${}_I\boldsymbol{\Omega}_k^{(i)} = \mathbf{J}_{R_k}^{(i)}\mathbf{u}^{(i)}$ are linear projections of the generalized velocities $\mathbf{u}^{(i)}$ by the JACOBI matrices of translation and rotation.

4 Analytic System Reduction

The previous chapters provide methods for the description of dynamic systems with constraints. Among these, the holonomic bilateral contact takes a special role of high technical relevance: it restricts the positions and motions of the associated bodies relative to each other for all states. As previously discussed, bilateral constraints can be imposed by associated constraint functions and LAGRANGE multipliers. Alternatively, a specialized parametrization of the kinematics might be used implicitly fulfilling restrictions and resulting in equations of motion free of these constraints. This can be achieved either by an adopted choice of the generalized coordinates during model formulation or by a subsequent transformation of the free-body equations of motion to a reduced coordinate set. The resulting equations use less degrees of freedom than for the equivalent bilateral constrained system.

A relative parametrization of the kinematic values often gives an intuitive way to unconstrained dynamics. In section 4.1, an abstract general formulation for a relative kinematic description is set up for tree-structured systems. The free-body equations are transformed to minimal coordinate representations with analytic evaluation of the constraint equations. The framework afterwards is applied to the description of rigid bodies on a preceding flexible structure. For modeling a single body in redundant coordinate sets, section 4.2 provides the adequate formulation along with two attendant examples. Being necessarily constraint to provide a unitary description of the system, the redundant modeling leads to similar structures of the equations as for relative kinematics. For a single finite element the easy access to the equations of motion in one coordinate set and the coupling to adjacent elements provided intrinsically for a second parametrization can be a motivation for this approach.

4.1 Relative Kinematics

In the previous chapter the kinematic parametrization referred directly to an inertial system. For bodies moving relatively constrained to each other, a redundancy in the kinematic description can be avoided by referring to the preceding bodies: for tree structured systems, the joint coordinates provide an intuitive success to realize this relative kinematic approach. Taking advantage of the tree structure provides minimal dimension for the vector of generalized coordinates and can be used to construct recursive algorithms of high efficiency for the solution of the system equations. Initially developed for rigid body systems, especially robots, see VERESHCHAGIN [61] and BRANDL ET AL. [9], BREMER AND PFEIFFER [10] and SHABANA [54] extend the joint coordinate approach to flexible multi-body systems. FÖRG [19] also gives formulations for non-smooth dynamics of rigid tree-structured systems.

In a first step, known equations of motion are assumed for the two bodies of relative kinematics. Using a re-parametrization of one body that implicitly fulfills the constraint equations, the equations of motion are projected to a representation free of the specific constraint. The framework is applied to the relative kinematic description of rigid bodies on flexible structures.

4.1.1 General System Description

The uncoupled dynamics of the two bodies (i), $i = 1, 2$ with relative motion is described in terms of own independent sets of coordinates $\mathbf{p}^{(i)} \in \mathbb{R}^{v^{(i)}}$ and velocities $\dot{\mathbf{p}}^{(i)}$ used for the kinematic parametrization, forming $v^{(i)}$ degrees of freedom for each body. For a rigid body, a native form of kinematic parametrization would for example be the three spatial translations and three KARDAN-angles. For the following derivation, the equations of motion with the common form

$$\mathbf{M}^{(1)}\ddot{\mathbf{p}}^{(1)} = \mathbf{h}^{(1)} + \mathbf{W}^{(1)}\boldsymbol{\lambda}^{(1)} \in \mathbb{R}^{v^{(1)}} \quad (4.1a)$$

$$\mathbf{M}^{(2)}\ddot{\mathbf{p}}^{(2)} = \mathbf{h}^{(2)} + \mathbf{W}^{(2)}\boldsymbol{\lambda}^{(2)} \in \mathbb{R}^{v^{(2)}} \quad (4.1b)$$

are assumed to be known. The mass matrices $\mathbf{M}^{(i)} = \mathbf{M}^{(i)}(\mathbf{p}^{(i)})$, the generalized forces $\mathbf{h}^{(i)} = \mathbf{h}^{(i)}(\mathbf{p}^{(i)}, \dot{\mathbf{p}}^{(i)}, t)$ and the generalized force directions $\mathbf{W}^{(i)} = \mathbf{W}^{(i)}(\mathbf{p}^{(i)})$ depend on the respective body-parameters $\mathbf{p}^{(i)}$ and $\dot{\mathbf{p}}^{(i)}$ exclusively.

For a tree structured system, exactly one predecessor can be identified for each body. The inertial system is the reference for the first body called root. Opening a chain that forms a closed loop at one connection and describing the removed kinematic relation as bilateral constraint releases the remaining system tree-structured. Assuming body (1) to be the root, the original parametrization $\mathbf{p}^{(1)}$ provides a set of minimal coordinates $\mathbf{q}^{(1)}$ with $n^{(1)} = v^{(1)}$ degrees of freedom:

$$\mathbf{p}^{(1)} = \mathbf{q}^{(1)} \in \mathbb{R}^{n^{(1)}} \quad (4.2)$$

In contrast, the kinematic parameters of the subsequent body (2) need to be expressed involving the generalized coordinates $\mathbf{q}^{(1)}$ of body (1) and own coordinates $\mathbf{q}^{(2)} \in \mathbb{R}^{n^{(2)}}$ describing the relative motion. Therewith, the positions

$$\mathbf{p}^{(2)} = \mathbf{p}^{(2)}(\mathbf{q}^{(1)}, \mathbf{q}^{(2)}) = \mathbf{p}^{(2)}(\mathbf{q}) \in \mathbb{R}^{v^{(2)}} \quad (4.3)$$

of equation (4.1b) depend on all generalized coordinates $\mathbf{q} = ((\mathbf{q}^{(1)})^T, (\mathbf{q}^{(2)})^T)^T$.

The velocities $\dot{\mathbf{p}}^{(i)}$ and accelerations $\ddot{\mathbf{p}}^{(i)}$ in equations (4.1) are gained by derivation of the equations (4.2) and (4.3) with respect to time. Expressed in terms of the generalized coordinates \mathbf{q} , velocities \mathbf{u} and accelerations $\dot{\mathbf{u}}$ these are:

$$\dot{\mathbf{p}}^{(1)} = \frac{\partial \mathbf{p}^{(1)}}{\partial \mathbf{q}^{(1)}} \mathbf{u}^{(1)} + \frac{\partial \mathbf{p}^{(1)}}{\partial \mathbf{q}^{(2)}} \mathbf{u}^{(2)} = (\mathbf{J}_{11}, \mathbf{J}_{12}) \mathbf{u} = (\mathbf{E}, \mathbf{0}) \mathbf{u} \quad (4.4a)$$

$$\ddot{\mathbf{p}}^{(1)} = (\mathbf{J}_{11}, \mathbf{J}_{12}) \dot{\mathbf{u}} + (\dot{\mathbf{J}}_{11}, \dot{\mathbf{J}}_{12}) \mathbf{u} = (\mathbf{E}, \mathbf{0}) \dot{\mathbf{u}} \quad (4.4b)$$

$$\dot{\mathbf{p}}^{(2)} = \frac{\partial \mathbf{p}^{(2)}}{\partial \mathbf{q}^{(1)}} \mathbf{u}^{(1)} + \frac{\partial \mathbf{p}^{(2)}}{\partial \mathbf{q}^{(2)}} \mathbf{u}^{(2)} = (\mathbf{J}_{21}, \mathbf{J}_{22}) \mathbf{u} \quad (4.4c)$$

$$\ddot{\mathbf{p}}^{(2)} = (\mathbf{J}_{21}, \mathbf{J}_{22}) \dot{\mathbf{u}} + (\dot{\mathbf{J}}_{21}, \dot{\mathbf{J}}_{22}) \mathbf{u} \quad (4.4d)$$

The matrix \mathbf{E} is the identity, $\mathbf{J}_{ij} = \mathbf{J}_{ij}(\mathbf{q})$ are JACOBI matrices transforming from the configuration space of body (j) to the space of the parameters $\mathbf{p}^{(i)}$ of body (i).

Implicitly fulfilling the kinematic restrictions between the bodies (1) and (2), the relative description provides validity of the respective bilateral constraint. Corresponding to the JOURDAIN principle, see PFEIFFER [44], the mutual reactions related to this constraint do not contribute to the overall balance of virtual power: the reactions do not occur when projecting into minimal configuration space. Inserting the relations (4.4) to the original equations of motion (4.1) yields the equations of the coupled system. The over-all JACOBI matrix \mathbf{J} is used to define the resulting generalized mass matrix, the vector of generalized forces and the generalized force directions of the entire system:

$$\mathbf{J} = \begin{pmatrix} \mathbf{J}_{11} & \mathbf{J}_{12} \\ \mathbf{J}_{21} & \mathbf{J}_{22} \end{pmatrix} = \begin{pmatrix} \mathbf{E} & \mathbf{0} \\ \mathbf{J}_{21} & \mathbf{J}_{22} \end{pmatrix} \in \mathbb{R}^{(v_1+v_2) \times (n_1+n_2)} \quad (4.5)$$

$$\mathbf{M} = \mathbf{J}^T \begin{pmatrix} \mathbf{M}^{(1)} & \mathbf{0} \\ \mathbf{0} & \mathbf{M}^{(2)} \end{pmatrix} \mathbf{J}$$

$$\mathbf{h} = \mathbf{J}^T \left[\begin{pmatrix} \mathbf{h}^{(1)} \\ \mathbf{h}^{(2)} \end{pmatrix} - \begin{pmatrix} \mathbf{M}^{(1)} & \mathbf{0} \\ \mathbf{0} & \mathbf{M}^{(2)} \end{pmatrix} \mathbf{J} \mathbf{u} \right], \quad \mathbf{W} = \mathbf{J}^T \begin{pmatrix} \mathbf{W}^{(1)} \\ \mathbf{W}^{(2)} \end{pmatrix}$$

The generalized force vector \mathbf{h} comprises projections of gyroscopic terms $\mathbf{M}^{(i)} \dot{\mathbf{J}}_{ij} \mathbf{u}^{(j)}$ due to the relative kinematic formulation. The entire system equations are

$$\mathbf{M} \ddot{\mathbf{q}} = \mathbf{h} + \mathbf{W} \boldsymbol{\lambda} \quad (4.6)$$

with the reactions $\boldsymbol{\lambda} = ((\boldsymbol{\lambda}^{(1)})^T, (\boldsymbol{\lambda}^{(2)})^T)^T$. In consequence of the system's tree-structure, the JACOBI matrix (4.5) is lower block-triangular. This reflects the forward kinematic property: the motion of a body depends upon own parameters as well as the state of the predecessors. The resulting equations of motion are:

$$\begin{pmatrix} \mathbf{M}^{(1)} + \mathbf{J}_{21}^T \mathbf{M}^{(2)} \mathbf{J}_{21} & \mathbf{J}_{21}^T \mathbf{M}^{(2)} \mathbf{J}_{22} \\ \mathbf{J}_{22}^T \mathbf{M}^{(2)} \mathbf{J}_{21} & \mathbf{J}_{22}^T \mathbf{M}^{(2)} \mathbf{J}_{22} \end{pmatrix} \begin{pmatrix} \dot{\mathbf{u}}^{(1)} \\ \dot{\mathbf{u}}^{(2)} \end{pmatrix} =$$

$$\begin{pmatrix} \mathbf{h}^{(1)} + \mathbf{W}^{(1)} \boldsymbol{\lambda}^{(1)} + \mathbf{J}_{21}^T \left(\mathbf{h}^{(2)} - \mathbf{M}^{(2)} (\dot{\mathbf{J}}_{21} \mathbf{u}^{(1)} + \dot{\mathbf{J}}_{22} \mathbf{u}^{(2)}) + \mathbf{W}^{(2)} \boldsymbol{\lambda}^{(2)} \right) \\ \mathbf{J}_{22}^T \left(\mathbf{h}^{(2)} - \mathbf{M}^{(2)} (\dot{\mathbf{J}}_{21} \mathbf{u}^{(1)} + \dot{\mathbf{J}}_{22} \mathbf{u}^{(2)}) + \mathbf{W}^{(2)} \boldsymbol{\lambda}^{(2)} \right) \end{pmatrix} \quad (4.7)$$

Due to the reduction to smaller parameter-sets and the kinematic structure, the mass matrix \mathbf{M} and the generalized force directions \mathbf{W} are of dense structure. Interpreting (4.7) as equation of motion of a new root in sense of equation (4.1a), multi-body trees can be build recursively. The projective NEWTON-EULER method for rigid body systems is included in equation (4.7), compare to ULBRICH [60].

Applying specific models to the equations (4.1), the recursive algorithms of BRANDL ET AL. [9] and SHABANA [54] can be used for the solution of the system equations also with extension to non-smooth dynamics provided by FÖRG [19]. Thereby, $\mathcal{O}(n)$ -methods with computational effort proportional to the number n of bodies can be constructed exploiting the kinematic forward property that occurs in the triangular structure of the JACOBI matrix (4.5). The present work does not aim to reformulate these recursive algorithms which can be taken from the referred literature.

4.1.2 Rigid Bodies on Flexible Structures

Being of high technical relevance, the kinematics of a rigid body (2) moving relatively to a flexible parent body (1) is investigated. Examples can be a mass sliding on a cable or the rigid elements of a push-belt CVT, which is studied in section 6.5.

Methods for deriving the equations of motion for a flexible body are provided in chapter 3: the equations (4.1a) are assumed to be known. The NEWTON-EULER equations describe spatial dynamics of the rigid body (2), see ULBRICH [60]. Referring to an arbitrary body-fixed reference point C , in general not being identical to the center S of mass with relative position \mathbf{r}_{CS} , the equations of motion are:

$$\begin{pmatrix} m\mathbf{E} & m\tilde{\mathbf{r}}_{SC} \\ m\tilde{\mathbf{r}}_{CS} & \boldsymbol{\Theta}_C \end{pmatrix}^{(2)} \begin{pmatrix} \mathbf{a}_C \\ \boldsymbol{\Psi} \end{pmatrix}^{(2)} = \begin{pmatrix} -m\tilde{\boldsymbol{\Omega}}^2 \mathbf{r}_{CS} + \mathbf{F}_C \\ -\tilde{\boldsymbol{\Omega}}\boldsymbol{\Theta}_C\tilde{\boldsymbol{\Omega}} + \mathbf{R}_C \end{pmatrix}^{(2)} + \mathbf{W}^{(2)}\boldsymbol{\lambda} \quad (4.8a)$$

$$\mathbf{M}^{(2)}\ddot{\mathbf{p}}^{(2)} = \mathbf{h}^{(2)} + \mathbf{W}^{(2)}\boldsymbol{\lambda} \quad (4.8b)$$

The force \mathbf{F}_C and the moment \mathbf{R}_C are the resulting external loads with respect to C , $\mathbf{a}_C^{(2)} \in \mathbb{R}^3$ and $\boldsymbol{\Psi}^{(2)} = \tilde{\boldsymbol{\Omega}}^{(2)} \in \mathbb{R}^3$ are the translational and rotational accelerations. In order to gain constancy of the inertia tensor $\boldsymbol{\Theta}_C$ and therewith of the mass matrix $\mathbf{M}^{(2)}$, the equations (4.8) usually refer to a moving frame K fixed to body (2).

Kinematics

To evaluate equation (4.8), the translational and rotational accelerations $\mathbf{a}_C^{(2)}$ and $\boldsymbol{\Psi}^{(2)}$ need to be parametrized. Therefore, also the position $\mathbf{r}_{IC}^{(2)}$ and the orientation matrix $\mathbf{A}_{IK}^{(2)}$ must be developed leading to translational and rotational velocities $\mathbf{v}_C^{(2)}$ and $\boldsymbol{\Omega}^{(2)}$. Since mainly terms related to body (2) are discussed in the following paragraphs, the index $^{(2)}$ marking this relation will mostly be dropped except for the minimal state variables $\mathbf{q}^{(2)}$ and $\mathbf{u}^{(2)}$ and JACOBI matrices $\mathbf{J}_T^{(2)}$ and $\mathbf{J}_R^{(2)}$.

Adapting the classical approach of using joint coordinates for the relative kinematic description, the material position \mathbf{s} of the reference point C on the flexible body is used as translational parameter of the rigid body¹, compare to figure 4.1(a):

$$\mathbf{s} = \mathbf{s}_0 + \mathbf{J}_T^{(2)}\mathbf{q}^{(2)}, \quad \dot{\mathbf{s}} = \mathbf{J}_T^{(2)}\mathbf{u}^{(2)} \quad (4.9)$$

¹ Section 3.1.1 introduced the material coordinate \mathbf{s} as an algebraic variable; therefore no time derivatives occurred. Here, $\dot{\mathbf{s}}$ are rigid body velocities measured on the deformed reference.

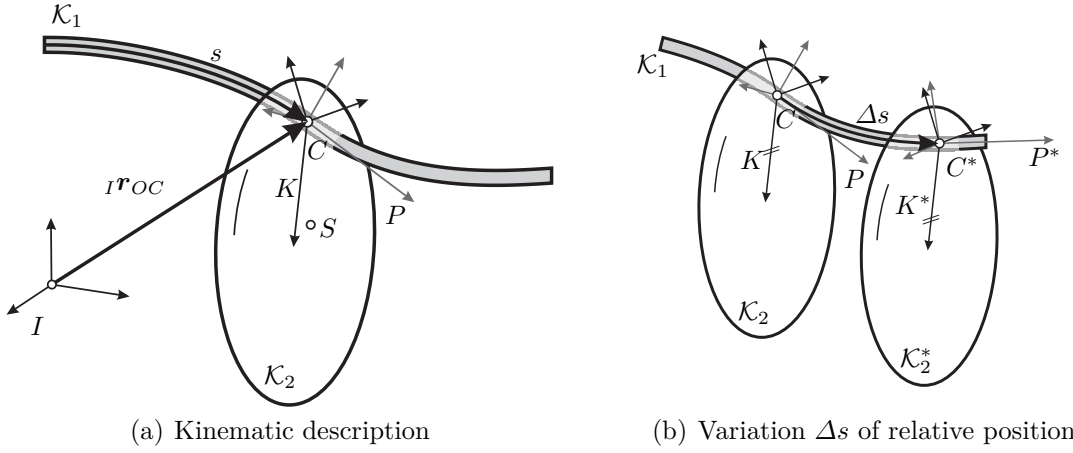


Figure 4.1: Relative kinematics of rigid body on a beam structure

The JACOBI-matrix $\mathbf{J}_T^{(2)} = \text{const.}$ of translations refers to the structural directions of the flexible body. The number of rows of $\mathbf{J}_T^{(2)}$ is limited by the dimensionality of the flexible structure, see section 3.1.1, whereas zero rows correspond to a constant position \mathbf{s}_0 . The coordinate \mathbf{s} coevally marks the time-varying contact position that would be used for a bilateral description. Figure 4.1(a) depicts exemplary a flexible beam structure with scalar relative position s . With the parametrization (4.9), the minimal coordinates $\mathbf{q}^{(2)} = ((\mathbf{q}_T^T, \mathbf{q}_R^T)^T)^{(2)}$ and velocities $\mathbf{u}^{(2)} = ((\mathbf{u}_T^T, \mathbf{u}_R^T)^T)^{(2)}$ are build by parts of translation and rotation with respective JACOBI-matrices. The matrix of relative rotation $\mathbf{A}_{PK} = \mathbf{A}_{PK}(\mathbf{q}^{(2)})$ refers to the coordinate system P of the preceding body: arbitrary descriptions including redundant parametrizations can be used, see for example GERADIN AND CARDONA [26].

Angular Position and Velocity The angular position of the rigid body is described with respect to the coordinate system P provided by the predecessor at the joined point C , see equation (3.43), page 51, with P replacing K . At the position \mathbf{s} the attendant system P is described by the transformation matrix $\mathbf{A}_{IP} = \mathbf{A}_{IP}(\mathbf{s}, \mathbf{q}^{(1)})$ holding tangential and normal directions on the structure. Using the matrix \mathbf{A}_{PK} of relative rotation, the absolute rotational position of body (2) is

$$\mathbf{A}_{IK} = \mathbf{A}_{IP}\mathbf{A}_{PK} . \quad (4.10)$$

The rotational velocity is derived as screw-symmetric product implying these transformation matrices, see PFEIFFER [44] and SHABANA [56]:

$$\begin{aligned} {}_I\tilde{\boldsymbol{\Omega}} &= \dot{\mathbf{A}}_{IK}\mathbf{A}_{IK}^T = [\dot{\mathbf{A}}_{IP}\mathbf{A}_{PK} & + \mathbf{A}_{IP}\dot{\mathbf{A}}_{PK} &]\mathbf{A}_{IK}^T \\ &= [\dot{\mathbf{A}}_{IP}\mathbf{A}_{PK}\mathbf{A}_{KP}\mathbf{A}_{PI} + \mathbf{A}_{IP}\dot{\mathbf{A}}_{PK}\mathbf{A}_{KP}\mathbf{A}_{PI}] \\ &= {}_I\tilde{\boldsymbol{\Omega}}_{IP} & + {}_I\tilde{\boldsymbol{\Omega}}_{PK} \end{aligned}$$

The component ${}_I\tilde{\boldsymbol{\Omega}}_{IP}$ describes the absolute motion of the moving frame P of reference, ${}_I\tilde{\boldsymbol{\Omega}}_{PK}$ is the relative rotational velocity of body (2) referring to P . According to classic rigid body formalisms, the latter is parametrized with respect to the body

fixed frame K by the matrix ${}_K\mathbf{J}_R^{(2)} = \text{const.}$ of rotation directions, see FÖRG [19]:

$${}_K\boldsymbol{\Omega}_{PK} = {}_K\mathbf{J}_R^{(2)} \mathbf{u}^{(2)}, \quad {}_I\boldsymbol{\Omega}_{PK} = \mathbf{A}_{IK} {}_K\boldsymbol{\Omega}_{PK}$$

Due to the total differentiation $\dot{\mathbf{A}}_{IP}$, the reference velocity ${}_I\tilde{\boldsymbol{\Omega}}_{IP} = \dot{\mathbf{A}}_{IP}\mathbf{A}_{IP}^T$ holds contributions with rates $\mathbf{u}^{(1)}$ of changes in $\mathbf{q}^{(1)}$ and parts with rates $\dot{\mathbf{s}}$: decomposition of these gives ${}_I\boldsymbol{\Omega}_{IP} = {}_I\boldsymbol{\Omega}_C + {}_I\boldsymbol{\Omega}_\kappa$. The rotational velocity of the flexible body uses the JACOBI matrix $\mathbf{J}_R^{(1)} = \mathbf{J}_R^{(1)}(\mathbf{q}^{(1)}, \mathbf{s})$ of rotations, see equation (3.45) on page 52:

$${}_I\boldsymbol{\Omega}_C = \mathbf{J}_R^{(1)} \mathbf{u}^{(1)}$$

The component ${}_I\boldsymbol{\Omega}_\kappa = {}_I\boldsymbol{\Omega}_\kappa(\mathbf{q}^{(1)}, \mathbf{s}, \dot{\mathbf{s}})$ holds rotations of the frame P due to translations of the rigid on the parent body: since \mathbf{A}_{IP} depends on the position \mathbf{s} , a variation $\Delta\mathbf{s}$ of the relative position induces a variation $\Delta\mathbf{A}_{IP}$. Figure 4.1(b) illustrates the variation $\mathcal{K}_2 \rightarrow \mathcal{K}_2^*$ on a beam structure: the rotational velocities induced by translations can be decomposed by single components s_i of the relative position and are defined in analogy to the rotational velocity as screw product:

$${}_I\tilde{\boldsymbol{\Omega}}_{\kappa,i} = \frac{\partial \mathbf{A}_{IP}}{\partial s_i} \dot{s}_i \mathbf{A}_{IP}^T = {}_I\tilde{\boldsymbol{\kappa}}_i \dot{s}_i \quad \text{with} \quad {}_I\tilde{\boldsymbol{\kappa}}_i = \frac{\partial \mathbf{A}_{IP}}{\partial s_i} \mathbf{A}_{IP}^T$$

Summing up the components i , the rotational velocity induced by $\dot{\mathbf{s}}$ is

$${}_I\boldsymbol{\Omega}_\kappa = \sum_i {}_I\boldsymbol{\Omega}_{\kappa,i} = {}_I\mathbf{K} \dot{\mathbf{s}} \quad \text{with} \quad {}_I\mathbf{K} = (\dots, {}_I\boldsymbol{\kappa}_i, \dots),$$

whereas the matrix ${}_I\mathbf{K} = {}_I\mathbf{K}(\mathbf{q}^{(1)}, \mathbf{s})$ holds the spatial curvatures of body (1).

Using the relations above, the rotational velocity of body (2) is:

$${}_I\boldsymbol{\Omega} = {}_I\boldsymbol{\Omega}_C + {}_I\boldsymbol{\Omega}_\kappa + {}_I\boldsymbol{\Omega}_{PK} = \mathbf{J}_R^{(1)} \mathbf{u}^{(1)} + ({}_I\mathbf{K} \mathbf{J}_T^{(2)} + \mathbf{A}_{IK} {}_K\mathbf{J}_R^{(2)}) \mathbf{u}^{(2)} \quad (4.11a)$$

$${}_K\boldsymbol{\Omega} = \mathbf{A}_{KI} {}_I\boldsymbol{\Omega} = \mathbf{A}_{IK}^T \mathbf{J}_R^{(1)} \mathbf{u}^{(1)} + (\mathbf{A}_{IK}^T {}_I\mathbf{K} \mathbf{J}_T^{(2)} + {}_K\mathbf{J}_R^{(2)}) \mathbf{u}^{(2)} \quad (4.11b)$$

Translational Position and Velocity The point of reference C of the rigid body is identical to the structural point described by \mathbf{s} , compare figure 4.1:

$${}_I\mathbf{r}_{OC} = {}_I\mathbf{r}_{OC}^{(1)} = {}_I\mathbf{r}_{OC}^{(1)}(\mathbf{q}^{(1)}, \mathbf{s}) \quad (4.12)$$

The translational velocity is the total derivative with respect to time:

$${}_I\mathbf{v}_C = \frac{\partial {}_I\mathbf{r}_{OC}}{\partial \mathbf{q}^{(1)}} \mathbf{u}^{(1)} + \frac{\partial {}_I\mathbf{r}_{OC}}{\partial \mathbf{s}} \dot{\mathbf{s}} = \mathbf{J}_T^{(1)} \mathbf{u}^{(1)} + {}_I\mathbf{S} \mathbf{J}_T^{(2)} \mathbf{u}^{(2)} \quad (4.13a)$$

$${}_K\mathbf{v}_C = \mathbf{A}_{KI} {}_I\mathbf{v}_C \quad (4.13b)$$

The matrix ${}_I\mathbf{S} = {}_I\mathbf{S}(\mathbf{q}^{(1)}, \mathbf{s}) = \partial {}_I\mathbf{r}_{OC} / \partial \mathbf{s}$ holds the tangential directions on the structure at \mathbf{s} . Due to the deformations of the flexible structure in general these are not of unit length. The columns of ${}_I\mathbf{S}$ align with columns of \mathbf{A}_{IP} .

Accelerations Using the rotational velocity (4.11a) referring to the inertial system I , the angular acceleration is the total derivative with respect to time:

$${}_I\dot{\Psi} = \mathbf{J}_R^{(1)} \dot{\mathbf{u}}^{(1)} + \dot{\mathbf{J}}_R^{(1)} \mathbf{u}^{(1)} + \left({}_I\dot{\mathbf{K}} \mathbf{J}_T^{(2)} + \mathbf{A}_{IK} \dot{\mathbf{K}} \mathbf{J}_R^{(2)} \right) \dot{\mathbf{u}}^{(2)} + \left({}_I\dot{\mathbf{K}} \mathbf{J}_T^{(2)} + \dot{\mathbf{A}}_{IK} \mathbf{K} \mathbf{J}_R^{(2)} \right) \mathbf{u}^{(2)}$$

The transformation to the system K utilizes $\mathbf{A}_{KI} \dot{\mathbf{A}}_{IK} = \mathbf{A}_{KI} \dot{\mathbf{I}} \tilde{\mathbf{\Omega}} \mathbf{A}_{IK} = {}_K \tilde{\mathbf{\Omega}}$:

$${}_K\dot{\Psi} = \mathbf{A}_{KI} \mathbf{J}_R^{(1)} \dot{\mathbf{u}}^{(1)} + \mathbf{A}_{KI} \dot{\mathbf{J}}_R^{(1)} \mathbf{u}^{(1)} + \left(\mathbf{A}_{KI} \dot{\mathbf{K}} \mathbf{J}_T^{(2)} + {}_K \mathbf{J}_R^{(2)} \right) \dot{\mathbf{u}}^{(2)} + \left(\mathbf{A}_{KI} \dot{\mathbf{K}} \mathbf{J}_T^{(2)} + {}_K \tilde{\mathbf{\Omega}}^{(2)} \mathbf{K} \mathbf{J}_R^{(2)} \right) \mathbf{u}^{(2)} \quad (4.14)$$

Analogously, the translational acceleration is the derivate of equation (4.13a):

$$\begin{aligned} {}_I\mathbf{a}_C &= \mathbf{J}_T^{(1)} \dot{\mathbf{u}}^{(1)} + \dot{\mathbf{J}}_T^{(1)} \mathbf{u}^{(1)} + {}_I\dot{\mathbf{S}} \mathbf{J}_T^{(2)} \dot{\mathbf{u}}^{(2)} + {}_I\dot{\mathbf{S}} \mathbf{J}_T^{(2)} \mathbf{u}^{(2)} \\ {}_K\mathbf{a}_C &= \mathbf{A}_{KI} {}_I\mathbf{a}_C \end{aligned} \quad (4.15)$$

Assuming at least \mathcal{C}^2 smoothness of the flexible body shape, the time derivative of ${}_I\dot{\mathbf{S}}$ can be computed by permutation of the order of differentiation:

$${}_I\dot{\mathbf{S}} = \frac{\partial^2 {}_I\mathbf{r}_{OC}}{\partial \mathbf{q}^{(1)} \partial \mathbf{s}} \mathbf{u}^{(1)} + \frac{\partial^2 {}_I\mathbf{r}_{OC}}{\partial \mathbf{s}^2} \dot{\mathbf{s}} = \frac{\partial {}_I\mathbf{v}_C}{\partial \mathbf{s}}$$

The velocity ${}_I\mathbf{v}_C$ of the reference point, equation (4.13a), accounts for $\dot{\mathbf{s}}$.

Projection

To evaluate the equations for the rigid body on its flexible predecessor, the framework developed in section 4.1.1 is employed. Due to the tree structure, the flexible body is parametrized by own independent coordinates: equations (4.4) hold with $\mathbf{J}_{11} = \mathbf{E}$ and $\mathbf{J}_{12} = \mathbf{0}$. Based on the positions (4.10) and (4.12), velocities (4.11b) and (4.13b) and accelerations (4.14) and (4.15), all depending on the cumulative generalized coordinates $\mathbf{q} = ((\mathbf{q}^{(1)})^T, (\mathbf{q}^{(2)})^T)^T$ and velocities $\mathbf{u} = ((\mathbf{u}^{(1)})^T, (\mathbf{u}^{(2)})^T)^T$, the JACOBI matrices

$$\begin{aligned} \mathbf{J}_{21} &= \begin{pmatrix} \mathbf{A}_{KI} \mathbf{J}_T^{(1)} \\ \mathbf{A}_{KI} \mathbf{J}_R^{(1)} \end{pmatrix}, & \dot{\mathbf{J}}_{21} &= \begin{pmatrix} \mathbf{A}_{KI} \dot{\mathbf{J}}_T^{(1)} \\ \mathbf{A}_{KI} \dot{\mathbf{J}}_R^{(1)} \end{pmatrix} \\ \mathbf{J}_{22} &= \begin{pmatrix} \mathbf{A}_{KI} \dot{\mathbf{S}} \mathbf{J}_T^{(2)} \\ \mathbf{A}_{KI} \dot{\mathbf{K}} \mathbf{J}_T^{(2)} + {}_K \mathbf{J}_R^{(2)} \end{pmatrix}, & \dot{\mathbf{J}}_{22} &= \begin{pmatrix} \mathbf{A}_{KI} \dot{\mathbf{S}} \dot{\mathbf{J}}_T^{(2)} \\ \mathbf{A}_{KI} \dot{\mathbf{K}} \mathbf{J}_T^{(2)} + {}_K \tilde{\mathbf{\Omega}} \mathbf{K} \mathbf{J}_R^{(2)} \end{pmatrix} \end{aligned}$$

project between physical and configuration space of the rigid body (2). Using the mass matrix $\mathbf{M}^{(2)}$, the force vector $\mathbf{h}^{(2)}$ and the generalized force directions $\mathbf{W}^{(2)}$ of the equations (4.8) with reference to a body-fixed frame K , the over-all equations of motion (4.7) of the bodies (1) and (2) can be assembled.

4.2 The Redundant Coordinate Method

The selective modeling of different physical effects with an associated parametrization, for example of transversal and longitudinal dynamics of slender structures, is one advantage of the classic floating frame of reference formulations. These advantages are related to the describing set of minimal coordinates which provide equations of motion in a structured and compact form. As a drawback, these coordinates in general can not be used for coupling different finite elements to represent one discretized structure without imposing equality constraints by LAGRANGE-multipliers. Instead, a redundant coordinate set incorporating nodal degrees of freedom can be introduced: the nodes are part of adjacent elements and therefore provide connectivity. Since the overall description must be unique, both sets are coupled by equality conditions. The redundant coordinate method (RCM) uses transformations similar to the analytic reduction of bilateral constraints by utilizing relative kinematic descriptions. The advantages of both parametrizations can be preserved when developing the equations of motion for a single finite element².

In a first step, the mathematical formulation is prepared connecting two coordinate sets used for one single element. Thereafter, two examples demonstrate the methodical concept: a one-dimensional bar element is shown to describe the selection of coordinates and the development of the equations of motion. Secondly, a finite element for free planar motion of elastic beams is developed: through this model the RCM was introduced by ZANDER AND ULBRICH [68]. Even though only a bar and a beam are discussed at this point, the proposed formalism is not restricted to one dimensional structures.

4.2.1 Transformations between Coordinate Sets

Single Finite Element Using different redundant coordinate sets \mathbf{q}_i and \mathbf{q}_g for the description of one element, both sets have to consistently describe all modeled physical effects. In anticipation of the physical interpretation the indices i and g denote sets used for internal dynamics and global couplings. The equation

$$\mathbf{0} = \mathbf{f}(\mathbf{q}_i, \mathbf{q}_g) \in \mathbb{R}^n \quad (4.16)$$

states the interactive restriction incorporating the sets $\mathbf{q}_i, \mathbf{q}_g \in \mathbb{R}^n$ of n degrees of freedom. Total derivation with respect to time yields relations for the velocities:

$$\mathbf{0} = \frac{\partial \mathbf{f}}{\partial \mathbf{q}_i} \mathbf{u}_i + \frac{\partial \mathbf{f}}{\partial \mathbf{q}_g} \mathbf{u}_g = \mathbf{D}_i \mathbf{u}_i + \mathbf{D}_g \mathbf{u}_g \quad (4.17)$$

Uniqueness and integrity of the description by the redundant sets is guaranteed if the JACOBI matrices $\mathbf{D}_i = \mathbf{D}_i(\mathbf{q}_i, \mathbf{q}_g)$ and $\mathbf{D}_g = \mathbf{D}_g(\mathbf{q}_i, \mathbf{q}_g)$ are regular for all \mathbf{q}_i

² Even though the same name is used here, the intension is different for classic finite element formulations: starting from a segmentation of the body domain, local ansatz-functions define approximations for the primitive parts called the finite elements, see page 44 ff.

and \mathbf{q}_g . Then equation (4.16) is bijective and an explicit form $\mathbf{q}_i = \tilde{\mathbf{f}}(\mathbf{q}_g)$ exists. If found analytically, this explicit form should be used for implementation to avoid the necessity of numerical root finding for the solution of the transformation (4.16).

With \mathbf{D}_i being regular, equation (4.17) is solved for the internal velocities

$$\mathbf{u}_i = \mathbf{J}_{ig} \mathbf{u}_g \quad \text{with} \quad \mathbf{J}_{ig} = -(\mathbf{D}_i^{-1} \mathbf{D}_g) = \frac{\partial \mathbf{q}_i}{\partial \mathbf{q}_g} = \frac{\partial \mathbf{u}_i}{\partial \mathbf{u}_g} . \quad (4.18)$$

The JACOBI matrix \mathbf{J}_{ig} describes the linear dependency between \mathbf{u}_i and \mathbf{u}_g common for all relations between velocity representations. Further derivation yields

$$\dot{\mathbf{u}}_i = \mathbf{J}_{ig} \dot{\mathbf{u}}_g + \dot{\mathbf{J}}_{ig} \mathbf{u}_g . \quad (4.19)$$

The accelerations $\dot{\mathbf{u}}_i$ hold linear projections of the accelerations $\dot{\mathbf{u}}_g$ and gyroscopic terms $\dot{\mathbf{J}}_{ig} \mathbf{u}_g$, compare to the relative kinematic equation (4.4), page 58. These redundant kinematic values are needed for the evaluation of the equations of motion.

In terms of the internal coordinate set \mathbf{q}_i the equations of motion

$$\mathbf{M}_i \dot{\mathbf{u}}_i = \mathbf{h}_i + \mathbf{W}_i \boldsymbol{\lambda} \quad (4.20)$$

of a single finite element are derived with the mass matrix $\mathbf{M}_i = \mathbf{M}_i(\mathbf{q}_i)$, the vector of smooth forces $\mathbf{h}_i(\mathbf{q}_i, \mathbf{u}_i, t)$ and the force directions $\mathbf{W}_i = \mathbf{W}_i(\mathbf{q}_i)$. Like for the relative kinematic description, the contact forces $\boldsymbol{\lambda}$ only include constraints between different physical bodies but no forces resulting from the coupling of adjacent finite elements, see JOURDAIN-principle on page 59. Using equation (4.19), the equations of motion (4.20) are transferred to the global coordinate set \mathbf{q}_g :

$$\underbrace{\mathbf{J}_{ig}^T \mathbf{M}_i \mathbf{J}_{ig}}_{\mathbf{M}_g} \dot{\mathbf{u}}_g = \underbrace{\mathbf{J}_{ig}^T (\mathbf{h}_i - \mathbf{M}_i \dot{\mathbf{J}}_{ig} \mathbf{u}_g)}_{\mathbf{h}_g} + \underbrace{\mathbf{J}_{ig}^T \mathbf{W}_i}_{\mathbf{W}_g} \boldsymbol{\lambda} . \quad (4.21)$$

This matches the projection (4.6), page 59, for a re-parametrization $\mathbf{p} = \mathbf{p}(\mathbf{q})$ of a single body. In order to evaluate the equations of motion, \mathbf{q}_i and \mathbf{u}_i are calculated depending on \mathbf{q}_g and \mathbf{u}_g using equations (4.16) and (4.18). Knowing \mathbf{M}_i , \mathbf{h}_i and \mathbf{W}_i of equation (4.20), the global accelerations $\dot{\mathbf{u}}_g$ result of equation (4.21).

Finite Element Assembly For a structure discretized by finite elements, the global coordinate set $\mathbf{q}_g^{(j)}$ of a single element j is a subset of all coordinates $\mathbf{q}_s \in \mathbb{R}^m$:

$$\mathbf{q}_g^{(j)} = \mathbf{B}^{(j)} \mathbf{q}_s \quad \text{with} \quad \mathbf{B}^{(j)} \in \mathbb{R}^{n \times m} \quad (4.22)$$

The selection matrix $\mathbf{B}^{(j)}$ of full row rank holds ‘0’ and a single ‘1’ entry per row; the most simple structure is $\mathbf{B}^{(j)} = (\mathbf{0}, \dots, \mathbf{E}, \dots, \mathbf{0})$ representing local incremental order of the elemental coordinates. One node may be associated to different elements leading to overlapping of different $\mathbf{q}_g^{(j)}$, compare to finite element discretization page 44*f*. Processing the structure’s coordinates \mathbf{q}_s in relations (4.16) and (4.18)

of the element j equals the selection of the associated parameters $\mathbf{q}_g^{(j)}$ and the subsequent transformation. The constraint relations are:

$$\mathbf{0} = \hat{\mathbf{f}}(\mathbf{q}_i^{(j)}, \mathbf{q}_s) = \mathbf{f}^{(j)}(\mathbf{q}_i^{(j)}, \mathbf{B}^{(j)} \mathbf{q}_s^{(j)})$$

$$\mathbf{u}_i^{(j)} = \mathbf{J}_{\text{is}}^{(j)} \mathbf{u}_s \quad \text{with} \quad \mathbf{J}_{\text{is}}^{(j)} = \frac{\partial \mathbf{q}_i^{(j)}}{\partial \mathbf{q}_s} = \mathbf{J}_{\text{ig}}^{(j)} \mathbf{B}^{(j)}$$

The JACOBI-matrix \mathbf{J}_{is} holds structured zero entries according to $\mathbf{B}^{(j)}$, $\mathbf{J}_{\text{ig}}^{(j)}$ is the JACOBIAN for the single finite element according to equation (4.18)

According to section 3.3.2, the equations of motion for the entire structure discretized by finite elements is gained by summation of the contributions of all elements:

$$\underbrace{\sum_j \left(\mathbf{J}_{\text{is}}^T \mathbf{M}_i \mathbf{J}_{\text{is}} \right)^{(j)}}_{\mathbf{M}_s} \dot{\mathbf{u}}_s = \underbrace{\sum_j \left(\mathbf{J}_{\text{is}}^T \left(\mathbf{h}_i - \mathbf{M}_i \dot{\mathbf{J}}_{\text{is}} \mathbf{u}_s \right) \right)^{(j)}}_{\mathbf{h}_s} + \underbrace{\sum_j \left(\mathbf{J}_{\text{is}}^T \mathbf{W}_i \right)^{(j)}}_{\mathbf{W}_s} \boldsymbol{\lambda} \quad (4.23)$$

To minimize the computational effort, the implementation should use index-scanning in the JACOBI matrices $\mathbf{J}_{\text{is}}^{(j)}$ to utilize the sparse structure induced by $\mathbf{B}^{(j)}$: operations on zero-entries can be avoided efficiently. Due to the structure of the JACOBI-matrices, the mass matrix \mathbf{M}_s always has a band diagonal structure.

4.2.2 A One-Dimensional Example

A bar element with constant cross-sectional properties, as it was instantiated in section 3.3.2, page 43, is studied to demonstrate the advances of the proclaimed method. The element is formulated assuming homogeneous strain parametrized by two internal and two global degrees of freedom which are illustrated in figure 4.2.

The global position x_s of the center of mass and the elastic strain ε are chosen as internal coordinates $\mathbf{q}_i = (x_s, \varepsilon)^T$. In difference to classic finite element approaches for small deformations – where usually nodal displacements are used as discrete degrees of freedom – the global positions x_1 and x_2 form the global coordinates $\mathbf{q}_g = (x_1, x_2)^T$. According to figure 4.2, the equality constraint (4.16) takes the form

$$\mathbf{0} = \begin{pmatrix} x_s - \frac{1}{2}(x_2 + x_1) \\ l_0(1 + \varepsilon) - (x_2 - x_1) \end{pmatrix}$$

An explicit expression for \mathbf{q}_i can be given, leading to the JACOBIAN (4.18):

$$\mathbf{q}_i = \begin{pmatrix} \frac{1}{2}(x_1 + x_2) \\ \frac{1}{l_0}(x_2 - x_1) - 1 \end{pmatrix}, \quad \mathbf{J}_{\text{ig}} = \begin{pmatrix} \frac{1}{2} & \frac{1}{2} \\ -\frac{1}{l_0} & \frac{1}{l_0} \end{pmatrix}$$

Since \mathbf{J}_{ig} is constant, $\dot{\mathbf{J}}_{\text{ig}}$ is zero.

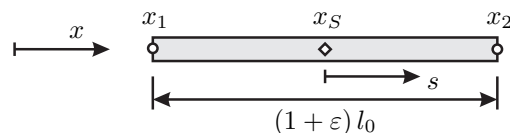


Figure 4.2: One-dimensional example with redundant coordinates

Depending on \mathbf{q}_i and \mathbf{u}_i , the position $w_x(\mathbf{q}_i, s)$ and velocity $\dot{w}_x(\mathbf{q}_i, \mathbf{u}_i, s)$ of a cross section at the position $s \in [-\frac{l_0}{2}, \frac{l_0}{2}]$ within the element are formulated:

$$w_x = x_S + (1 + \varepsilon) s, \quad \dot{w}_x = \dot{x}_S + \dot{\varepsilon} s$$

Therewith, the kinetic and potential energies of the element are

$$T = \frac{1}{2} \rho A \int_{-l_0/2}^{l_0/2} (\dot{w}_x(s))^2 ds \quad \text{and} \quad V = \frac{1}{2} EA \int_{-l_0/2}^{l_0/2} \varepsilon^2 ds .$$

Here, A is the area of the cross section, ρ gives the density of the material and E the modulus of elasticity. Evaluating the LAGRANGE equations (2.2), page 9, yields the mass matrix and the generalized force vector for the internal coordinates:

$$\mathbf{M}_i = \begin{pmatrix} m & 0 \\ 0 & \frac{m l_0^2}{12} \end{pmatrix}, \quad \mathbf{h}_i = \begin{pmatrix} 0 \\ -EA l_0 \varepsilon \end{pmatrix}$$

Evaluating the transformation (4.21) with the specified terms leads to the global forms of the mass matrix and the force vector for a single finite element:

$$\mathbf{M}_g = m \begin{pmatrix} \frac{1}{3} & \frac{1}{6} \\ \frac{1}{6} & \frac{1}{3} \end{pmatrix}, \quad \mathbf{h}_g = \frac{EA}{l_0} \begin{pmatrix} (x_2 - x_1 - l_0) \\ -(x_2 - x_1 - l_0) \end{pmatrix}$$

Except for using global positions instead of displacements, these are the well-known results for the bar element, see BATHE [6]. Even though this is a linear problem, the internal forms of the mass matrix and the force vector are more compact than the global equivalents. If nonlinearities occur for example due to large deformations, gyroscopic effects or the coupling of longitudinal and transversal deformations of a beam, the difference in complexity between an internal and a global formulation increases rapidly. Using the proclaimed method especially the multiple occurrence of equal terms like $(x_2 - x_1 - l_0)$ can be reduced leading to less computational effort.

4.2.3 A Formulation for Planar Slender Beams

The formulation of beam finite elements with own floating frames of reference leads to a co-rotational formulation and allows for geometrical large deformations of the discretized structure. To gain compact forms of the equations of motion and to keep the parametrization close to the described physical effects, a redundant coordinate formulation is used: the internal coordinates describe the element dynamics in a compact form of rigid body movement and superposed elastic deformations; the global

coordinates hold the positions of both nodes at the element endpoints and selected bending deflections. The planar element is based on the BERNOLLI-hypothesis for slender beams and includes longitudinal strain. The focus of the approximation is set on the bending what prevails the deformation behavior.

This RCM formulation for planar slender beams was introduced by ZANDER AND ULBRICH in [68] and proofed to provide high computational performance in [67]. Exact rigid body motion and geometrical large deformations are captured. SCHINDLER ET AL. [51] extend the planar beam model to full spatial motion.

Shape Functions and Elemental Coordinate Sets The element of undeformed length l_0 is described in two intervals I and II , see figure 4.3(a). For each interval a specific coordinate system is used originated at the mid-point and aligned tangential to the beams neutral fiber at the end nodes. The LAGRANGE coordinate s runs along the local x_I - and x_{II} -axis and refers to positions within the element whereas $s = 0$ marks the mid-point. The ansatz for the deformation is described in the two intervals: two polynomials $w_I = w_I(\mathbf{q}_i, s)$ and $w_{II} = w_{II}(\mathbf{q}_i, s)$ are used as bending shape functions of the element. Homogeneous strain is assumed within the element. The internal degrees of freedom (DOF) \mathbf{q}_i are closely related to physical effects like rigid body movement or bending:

$$\mathbf{q}_i = \left(\underbrace{x_S, y_S, \varphi_S}_{\text{rigid body DOFs}}, \underbrace{\tilde{\varepsilon}, a_I, \beta_I, a_{II}, \beta_{II}}_{\text{elastic DOFs}} \right)^T \quad (4.24)$$

Apart from the directional strain $\tilde{\varepsilon}$, these coordinates are illustrated in figure 4.3(a): the vector $\mathbf{r}_S = (x_S, y_S)^T$ parametrizes the translations of the center of mass and φ_S is the angle of rotation in case of an undeformed shape. The directional strain $\tilde{\varepsilon}$ is related to the node displacements in direction of the bases $\mathbf{b}_{x,i} = \mathbf{b}_{x,i}(\mathbf{q}_i)$, $i \in \{I, II\}$. The relative deflections and slopes at the nodes are described by a_I , β_I , a_{II} and β_{II} and refer to the floating frames I and II of reference respectively.

The position $\mathbf{r} = \mathbf{r}(\mathbf{q}_i, s)$ of the neutral fiber is described by

$$\mathbf{r} = \mathbf{r}_S + \begin{cases} \mathbf{b}_{x,I}(1 + \tilde{\varepsilon})s + \mathbf{b}_{y,I}w_I & \text{for } -\frac{l_0}{2} \leq s < 0 \\ \mathbf{b}_{x,II}(1 + \tilde{\varepsilon})s + \mathbf{b}_{y,II}w_{II} & \text{for } 0 \leq s \leq \frac{l_0}{2} \end{cases} \quad (4.25)$$

To approximately ensure \mathcal{C}^2 -smoothness within the element, both shape functions w_I and w_{II} are defined at $s = 0$ with equal radius of curvature R_C and the reciprocal R'_C of the curvatures derivative with respect to s :

$$R_C = \frac{2l_0^2}{(-8a_I - 8a_{II} + 3(\beta_I + \beta_{II})l_0)}$$

$$R'_C = \frac{l_0^3}{2(8a_I - 8a_{II} + 3(\beta_{II} - \beta_I)l_0)}$$

Therewith, the bending shape function w of the entire element is defined piecewise

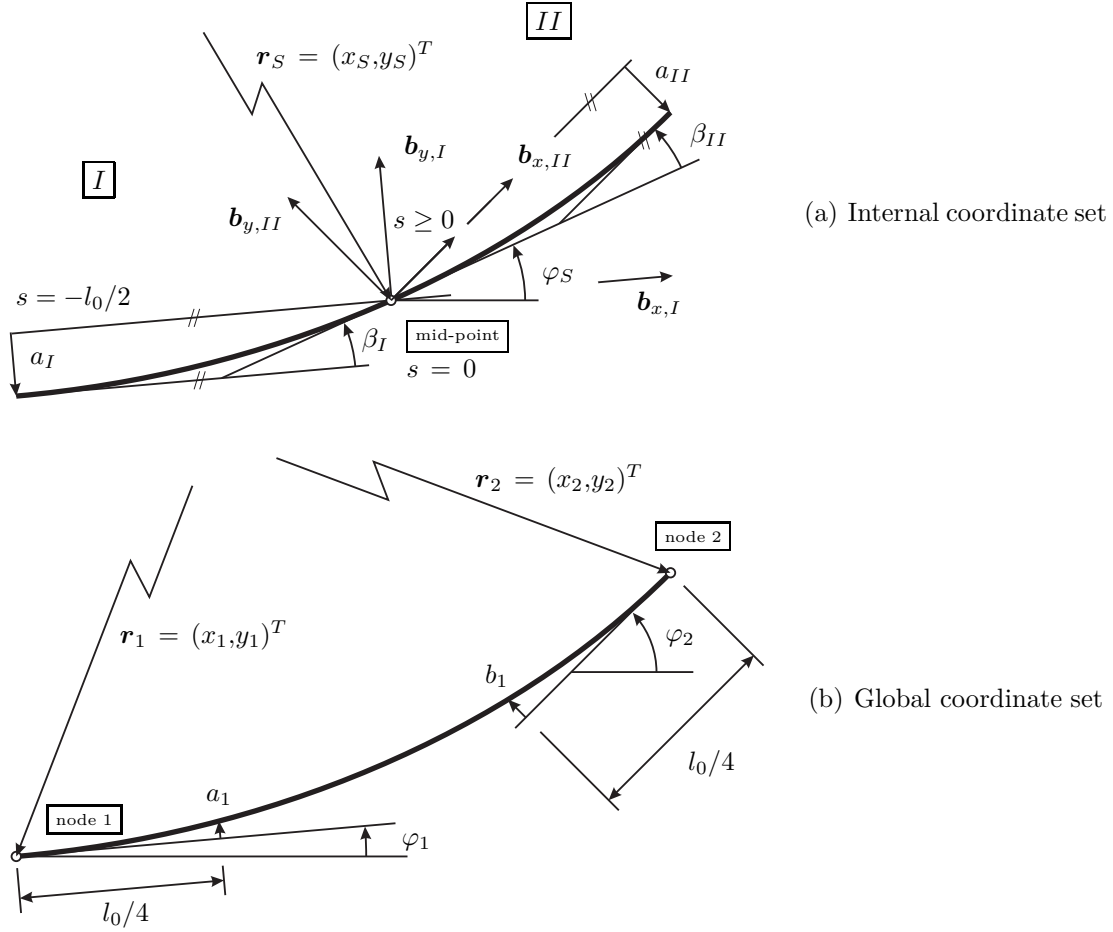


Figure 4.3: Redundant coordinate sets of a single beam element

using the polynomials w_I and w_{II} of fourth order:

$$w = \begin{cases} w_I = \frac{2(16a_I - 8a_{II} - 5\beta_I l_0 + 3\beta_{II} l_0)}{l_0^4} s^4 + \frac{1}{R'_c} s^3 + \frac{1}{R_c} s^2 + \beta_I s & \text{for } s < 0 \\ w_{II} = \frac{2(-8a_I + 16a_{II} + 3\beta_I l_0 - 5\beta_{II} l_0)}{l_0^4} s^4 + \frac{1}{R'_c} s^3 + \frac{1}{R_c} s^2 - \beta_{II} s & \text{for } s \geq 0 \end{cases} \quad (4.26)$$

Due to the planar character of the model, the rotation matrix \mathbf{A}_{IK} of a cross section, which is defined in analogy to equation (3.43), page 51, can be described by one angle φ referring to the tangent on the deformed shape, compare to figure 4.3:

$$\mathbf{A}_{IK} = \mathbf{A}_{IK}(\varphi) \quad \text{with} \quad \varphi = \varphi(\mathbf{q}_i, s) = \begin{cases} \varphi_s - \beta_I + w'_I & \text{for } s < 0 \\ \varphi_s + \beta_{II} + w'_{II} & \text{for } s \geq 0 \end{cases} \quad (4.27)$$

With equations (4.25) and (4.27), the JACOBI-matrices of translation and rotation

$$\mathbf{J}_{T,i} = \frac{\partial \mathbf{r}}{\partial \mathbf{q}_i} \quad \text{and} \quad \mathbf{J}_{R,i} = \frac{\partial \varphi}{\partial \mathbf{q}_i}, \quad (4.28)$$

are evaluated in terms of the internal coordinates for further development of the equations of motion as well as for the projection of external loads and reactions.

The global coordinate set

$$\mathbf{q}_g = \left(\underbrace{x_1, y_1, \varphi_1}_{\text{node 1}}, \underbrace{a_1, b_1}_{\substack{\text{element} \\ \text{internal DOFs}}}, \underbrace{x_2, y_2, \varphi_2}_{\text{node 2}} \right)^T \quad (4.29)$$

holds the nodal coordinates of the element, both the positions and the angles. These can be part of different adjacent elements and hence can be used for coupling of different elements. Since the internal and the global coordinates have to be unique and bijective, the global coordinate set is supplemented by two internal degrees of freedom a_1 and b_1 . These denote the relative beam deflection at the distance $l_0/4$ from the nodes. Figure 4.3(b) illustrates the global coordinates.

The equality restriction (4.16) is set by eight independent equations for positions and tangential angles connecting \mathbf{q}_i and \mathbf{q}_g and can be solved analytically. Using the following abbreviations for sums and differences of coordinates

$$\begin{aligned} S_x &= x_1 + x_2, & S_y &= y_1 + y_2, & S_\varphi &= \varphi_1 + \varphi_2, & S_a &= a_1 + b_1 \\ D_x &= x_1 - x_2, & D_y &= y_1 - y_2, & D_\varphi &= \varphi_1 - \varphi_2, & D_a &= a_1 - b_1, \end{aligned}$$

the explicit transformation generated by a computer algebra system reads:

$$\mathbf{q}_i = (x_s, y_s, \varphi_s, \tilde{\varepsilon}, a_I, \beta_I, a_{II}, \beta_{II})^T = \tilde{\mathbf{f}}(\mathbf{q}_g) = \begin{pmatrix} \frac{1}{72} \left((64S_a - 5l_0D_\varphi) \sin\left(\frac{S_\varphi}{2}\right) \sec\left(\frac{D_\varphi}{2}\right) + 36 \left(S_x + D_y \tan\left(\frac{D_\varphi}{2}\right) \right) \right) \\ \frac{1}{72} \left((64S_a - 5l_0D_\varphi) \cos\left(\frac{S_\varphi}{2}\right) \sec\left(\frac{D_\varphi}{2}\right) + 36 \left(S_y - D_x \tan\left(\frac{D_\varphi}{2}\right) \right) \right) \\ \frac{2(-8D_a + l_0S_\varphi) + 11 \sec\left(\frac{D_\varphi}{2}\right) \left(D_x \sin\left(\frac{S_\varphi}{2}\right) - D_y \cos\left(\frac{S_\varphi}{2}\right) \right)}{4l_0} \\ 1 - \frac{36 \sec\left(\frac{D_\varphi}{2}\right) \left(D_x \cos\left(\frac{S_\varphi}{2}\right) + D_y \sin\left(\frac{S_\varphi}{2}\right) \right) - (64S_a - 5D_\varphi l_0) \tan\left(\frac{D_\varphi}{2}\right)}{36l_0} \\ \frac{1}{72} \left(64S_a - 5D_\varphi l_0 + 36 \sec\left(\frac{D_\varphi}{2}\right) \left(D_x \sin\left(\frac{S_\varphi}{2}\right) - D_y \cos\left(\frac{S_\varphi}{2}\right) \right) \right) \\ \frac{-2(8D_a + D_\varphi l_0) + 11 \sec\left(\frac{D_\varphi}{2}\right) \left(D_x \sin\left(\frac{S_\varphi}{2}\right) - D_y \cos\left(\frac{S_\varphi}{2}\right) \right)}{4l_0} \\ \frac{1}{72} \left(64S_a - 5D_\varphi l_0 + 36 \sec\left(\frac{D_\varphi}{2}\right) \left(D_y \cos\left(\frac{S_\varphi}{2}\right) - D_x \sin\left(\frac{S_\varphi}{2}\right) \right) \right) \\ \frac{2(8D_a - D_\varphi l_0) - 11 \sec\left(\frac{D_\varphi}{2}\right) \left(D_x \sin\left(\frac{S_\varphi}{2}\right) - D_y \cos\left(\frac{S_\varphi}{2}\right) \right)}{4l_0} \end{pmatrix}$$

The unusual way to introduce two different coordinate systems, one at each end of the element, provides this explicit instead of an implicit form.

Equations of Motion The equations of motion are derived using the LAGRANGE formalism for a constrained system, equation (2.6), page 10. Therefore, the kinetic energy T and the cumulative potential V need to be developed in terms of the parameters \mathbf{q}_i . The slender beam is characterized by the cross section area A , the moment of inertia I , the modulus of elasticity E and the density ρ .

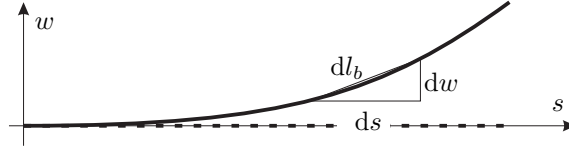


Figure 4.4: Length calculus for a curve

The kinetic energy of the EULER-BERNOULLI beam only accounts for the translation of the cross section; the rotational inertia of the differential elements is neglected for slender structures. The kinetic energy (3.24), page 38, is evaluated under consideration of the JACOBI-matrix $\mathbf{J}_{T,i}$ of translations according to equation (4.28) and leads to the mass matrix $\mathbf{M}_i = \mathbf{M}_i(\mathbf{q}_i)$ related to the internal coordinates \mathbf{q}_i .

The potential $V = V_{\text{elast}} + V_{\text{grav}}$ holds the elastic potential of deformations and the gravitational potential. The physical strain ε and the curvatures κ are needed for the constitutive laws of elasticity, see equation (3.9) on page 32. The strain measure provided by $\tilde{\varepsilon}$ is incorrect for large bending deformations since it is based on the nodal displacements in the directions $\mathbf{b}_{x,I}$ and $\mathbf{b}_{x,II}$ of the local coordinate systems. For large deflections, the shape function w , equation (4.26), describes shapes with lengths $l_b = l_b(\mathbf{q}_i)$ significantly larger than for the unbended structure. Figure 4.4 illustrates the length calculation for a curve commonly known for sagging cables:

$$l_b = \int_{-l_0/2}^{l_0/2} \sqrt{1 + (w')^2} ds \approx \int_{-l_0/2}^{l_0/2} \left(1 + \frac{(w')^2}{2} \right) ds \geq l_0$$

The TAYLOR-expansion of the square-root is used to approximate the exact form since an analytic integration can be given using the derivatives w' of the shape function. Comparing the length $(1 + \tilde{\varepsilon})l_b$ described by the parametrization to the deformed length $(1 + \varepsilon)l_0$ of the element yields the physical strain ε :

$$(1 + \varepsilon)l_0 = (1 + \tilde{\varepsilon})l_b \quad \Rightarrow \quad \varepsilon = \frac{l_b}{l_0}(1 + \tilde{\varepsilon}) - 1$$

The potential of elastic deformations accounts for elongation and bending, whereas $\kappa \approx w''$ approximates the curvature of the deformed beam:

$$V_{\text{elast}} = \frac{1}{2} \int_{-l_0/2}^{l_0/2} (EA\varepsilon^2 + EI(w'')^2) ds$$

A homogeneous acceleration field \mathbf{g} is accounted for by the gravitational potential

$$V_{\text{grav}} = -\rho A \int_{-l_0/2}^{l_0/2} (\mathbf{g}^T \mathbf{r}) ds .$$

To project loads and constraint reactions, the generalized force directions \mathbf{W}_i result

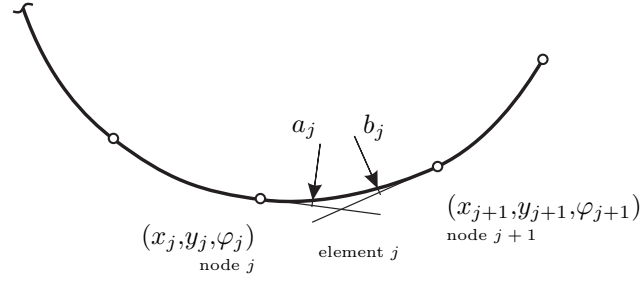


Figure 4.5: Element j with part of the surrounding structure

of the JACOBI-matrix $\mathbf{J}_{T,i}$, equation (4.28), and the respective contact kinematics according to section 2.2.

Assembly of Elements to a Discretized Structure Figure 4.5 shows the j -th finite element and parts of the surrounding structure: the global coordinates $\mathbf{q}_g^{(j)}$ of the single element are part of the coordinates

$$\mathbf{q}_s = \left(\dots \overbrace{x_j, y_j, \varphi_j, a_j, b_j, x_{j+1}, y_{j+1}, \varphi_{j+1}}^{\text{coordinates } \mathbf{q}_g^{(j)} \text{ of the } j\text{-th element}} \dots \right)^T$$

of the whole discretized body, see equation (4.22). Associating the nodal coordinates (x_j, y_j, φ_j) to adjacent elements provides structural connectivity.

5 Numerical Aspects

Even though this work is not devoted to the numerics of multi-body systems, a numeric environment is needed to simulate the nonlinear and non-smooth systems. The current chapter discusses briefly important aspects, giving a rough knowledge of the numerical methods that are essential for setting up simulations for discontinuous flexible MBS with contacts. Section 5.1 is devoted to implicit time-stepping: a scaled linear implicit integration scheme offering A-stability is set up to complement the semi-explicit scheme cited in section 2.4. Section 5.2 addresses the numerical part of the contact kinematics evaluation: schemes are sketched for the search of contact point pairs by means of pre-selection and numerical root-finding; thereby the global validity of the numeric solution must be ensured.

5.1 Time Integration

For the simulation of a non-smooth dynamic system, the velocity-position relation and the measure differential equation of motion (2.16), page 14,

$$\begin{pmatrix} d\mathbf{q} \\ M d\mathbf{u} \end{pmatrix} = \begin{pmatrix} \mathbf{u} dt \\ \mathbf{h} dt + \mathbf{W} d\mathbf{\Lambda} \end{pmatrix} \quad (5.1a)$$

need to be integrated under consideration of the constraints (2.27), page 21,

$$(d\mathbf{\Lambda}, \mathbf{q}, \mathbf{u}, t) \in \mathcal{N}. \quad (5.1b)$$

A numeric integration substitutes the time-continuous values by corresponding discrete sets at the points $\{t^0, \dots, t^l, t^{l+1}, \dots\}$ of evaluation¹. Due to the good feasibility for numerical algorithms, equality formulations by proximal functions nowadays are used widely for the constraints (2.27)/(5.1b), see page 24 of section 2.3.2.

Event-driven and time-stepping schemes are mentioned in section 2.4 with references to ACARY AND BROGLIATO [1] and STUDER [58] for integrating the non-smooth system (5.1). The efficient semi-explicit time-stepping scheme of FÖRG [21, 19] was presented: performing a successive update, no time consuming solution of implicit equations is needed. The evaluation $\hat{\mathbf{h}}^{l+1} = \mathbf{h}(\mathbf{q}^{l+1}, \mathbf{u}^l, t^{l+1})$ of the generalized forces increases the stability of the scheme. Still the step-size Δt used for integration is limited by the maximum local eigenvalue of equation (5.1a). This reflects the physical stiffness of the system by means of the spatial discretization: fine local

¹ The upper index marks the time of evaluation.

resolutions for flexible bodies decrease the critical step-sizes Δt_{max} needed for stable time integration with explicit integration schemes.

When using A-stable time discretizations, the time step sizes are not limited by the spatial discretization to ensure stability for the simulation of flexible MBS. Together with the semi-explicit time stepping scheme of section 2.4, the following A-stable modified θ -method is used for the simulation of the examples in chapter 6.

Modified θ -Method Implicit formulations provide stable numerical integration. Among these schemes, the θ -method with constant step size Δt approves to be robust and simple in implementation, see for example HAIRER ET AL. [32, 33]. For the ordinary differential problem $\dot{x} = f(x)$, $x(0) = x_0$, the method uses

$$\int_{t^l}^{t^{l+1}} \dot{x} dt \approx x^{l+1} - x^l = \Delta t(1 - \theta)f(x^l, t^l) + \Delta t \theta f(x^{l+1}, t^{l+1}) \quad (5.2)$$

with $\theta \in [0, 1]$ for the discrete step $l \rightarrow l + 1$. Note that the evaluation is implicit in the new x^{l+1} for $\theta \neq 0$; explicit and implicit EULER-schemes are described by $\theta = 0$ and $\theta = 1$. The trapezoidal rule with $\theta = 0.5$ achieves second order accuracy. Applied to linear systems, the scheme is A-stable for $\theta \geq 0.5$ (e.g. [33]).

The non-smooth contact dynamics method of JEAN [38] is a linear adaption of the θ -method (5.2) to the solution of the non-smooth system (5.1). A linear TAYLOR-expansion is used to approximate the implicit evaluation of \mathbf{h}^{l+1} . FUNK [24] gives a detailed derivation and discussion including a stability analysis for the time integration. The scheme is modified to solve constraints on velocity level corresponding to the time-stepping scheme in section 2.4: FÖRG [19] discusses the increased stability of the constraint solution compared to methods on position level. The integrals of the terms in equation (5.1a) are approximated as follows:

$$\begin{aligned} \int_{t^l}^{t^{l+1}} d\mathbf{q} &\approx \Delta \mathbf{q}^l &&= \mathbf{q}^{l+1} - \mathbf{q}^l \\ \int_{t^l}^{t^{l+1}} \mathbf{u} dt &\approx ((1 - \theta)\mathbf{u}^l + \theta\mathbf{u}^{l+1}) \Delta t = (\mathbf{u}^l + \theta\Delta\mathbf{u}^l) \Delta t \\ \int_{t^l}^{t^{l+1}} \mathbf{M} d\mathbf{u} &\approx \mathbf{M}^l \Delta\mathbf{u}^l &&= \mathbf{M}^l(\mathbf{u}^{l+1} - \mathbf{u}^l) \\ \int_{t^l}^{t^{l+1}} \mathbf{h} dt &\approx ((1 - \theta)\mathbf{h}^l + \theta\mathbf{h}^{l+1}) \Delta t \approx \\ &&&\left(\mathbf{h}^l + \theta \left. \frac{\partial \mathbf{h}}{\partial \mathbf{q}} \right|_l \Delta \mathbf{q}^l + \theta \left. \frac{\partial \mathbf{h}}{\partial \mathbf{u}} \right|_l \Delta \mathbf{u}^l + \theta \left. \frac{\partial \mathbf{h}}{\partial t} \right|_l \Delta t \right) \Delta t \\ \int_{t^l}^{t^{l+1}} \mathbf{W} d\Lambda &\approx \mathbf{W}_a^l \Lambda_a^{l+1} \end{aligned}$$

Only contacts being active at the beginning t^l of the time-step are taken into account, denoted by the index a . Using $\Delta \mathbf{q}^l = (\mathbf{u}^l + \theta\Delta\mathbf{u}^l) \Delta t$, the continuous equation of

motion is approximated by the discrete evolution

$$\begin{aligned}\Delta \mathbf{u}^l &= \left(\tilde{\mathbf{M}}^l\right)^{-1} \left(\tilde{\mathbf{h}}^l \Delta t + \mathbf{W}^l \boldsymbol{\Lambda}^{l+1}\right), \\ \mathbf{q}^{l+1} &= \mathbf{q}^l + \left(\mathbf{u}^l + \theta \Delta \mathbf{u}^l\right) \Delta t, \quad \mathbf{u}^{l+1} = \mathbf{u}^l + \Delta \mathbf{u}^l\end{aligned}$$

with the following abbreviations:

$$\tilde{\mathbf{M}}^l = \mathbf{M}^l - \theta \left. \frac{\partial \mathbf{h}}{\partial \mathbf{u}} \right|_l \Delta t - \theta^2 \left. \frac{\partial \mathbf{h}}{\partial \mathbf{q}} \right|_l \Delta t^2, \quad \tilde{\mathbf{h}}^l = \mathbf{h}^l + \theta \left. \frac{\partial \mathbf{h}}{\partial \mathbf{q}} \right|_l \mathbf{u}^l \Delta t + \theta \left. \frac{\partial \mathbf{h}}{\partial t} \right|_l \Delta t$$

In analogy to section 2.4, a single integration step of the θ -method is outlined:

1. Compute the distances $\mathbf{g}_U^l = \mathbf{g}_U(\mathbf{q}^l, t^l)$ of all unilateral contacts.
2. Compute the index set $\{i : g_{U,i}^l \leq 0\}$ of active unilateral contacts governing the activity of the respective normal and tangential reactions. Note that a bilateral constraint per definition is always active.
3. Compute the generalized velocities by solving the discretized equations of motion considering the velocities $\boldsymbol{\gamma}_a$ of all active constraints:

$$\Delta \mathbf{u}^l = \left(\tilde{\mathbf{M}}^l\right)^{-1} \left(\tilde{\mathbf{h}}^l \Delta t + \mathbf{W}^l \boldsymbol{\Lambda}^{l+1}\right), \quad (5.3a)$$

$$\boldsymbol{\gamma}_a^{l+1} = \boldsymbol{\gamma}_a(\mathbf{u}^{l+1}, \mathbf{q}^l, t^{l+1}), \quad (5.3b)$$

$$\boldsymbol{\Lambda}_a^{l+1} = \mathbf{proj}(\boldsymbol{\gamma}_a^{l+1}, \boldsymbol{\Lambda}_a^{l+1}) \quad (5.3c)$$

The function **proj** comprises the projection functions of equations (2.35), page 24, claiming compatibility $(\boldsymbol{\Lambda}_a^{l+1}, \mathbf{q}^l, \mathbf{u}^{l+1}, t^{l+1}) \in \mathcal{N}$ for the active constraints at the end of the time-step.

4. Compute the new generalized positions $\mathbf{q}^{l+1} = \mathbf{q}^l + (\mathbf{u}^l + \theta \Delta \mathbf{u}^l) \Delta t$ and the new velocities $\mathbf{u}^{l+1} = \mathbf{u}^l + \Delta \mathbf{u}^l$.

Again the crucial point is to find compatible reactions $\boldsymbol{\Lambda}_a^{l+1}$ and velocities \mathbf{u}^{l+1} . The algorithms of FÖRG [21, 19] are used: these form the numeric kernel of the MB-SIM software package which is used as simulation platform for the present work.

Solution of Constraint Equations The discretization of the constraints (5.3c) with (5.3b) is implicit in the velocities \mathbf{u}^{l+1} and explicit in the positions \mathbf{q}^l . Using the equations (5.3a) and (2.24), page 18, the constraint velocities

$$\begin{aligned}\boldsymbol{\gamma}_a^{l+1} &= \left(\mathbf{W}_a^l\right)^T \mathbf{u}^{l+1} + \mathbf{w}_a^{l+1} \\ &= \left(\mathbf{W}_a^l\right)^T \left(\tilde{\mathbf{M}}^l\right)^{-1} \mathbf{W}_a^l \boldsymbol{\Lambda}_a^{l+1} + \left(\mathbf{W}_a^l\right)^T \left(\mathbf{u}^l + \left(\tilde{\mathbf{M}}^l\right)^{-1} \tilde{\mathbf{h}}^l \Delta t\right) + \mathbf{w}_a^{l+1} \\ &= \mathbf{G}_a^l \boldsymbol{\Lambda}_a^{l+1} + \mathbf{b}_a^{l+1}\end{aligned} \quad (5.4)$$

are gained by linear expansion as linear combination of the unknown constraint

reactions Λ_a^{l+1} . The solution of the system (5.3) for the particular reactions is reduced analytically to the solution of the non-smooth nonlinear equation

$$\Lambda_a^{l+1} = \mathbf{proj} \left(\mathbf{G}_a^l \Lambda_a^{l+1} + \mathbf{b}_a^{l+1}, \Lambda_a^{l+1} \right). \quad (5.5)$$

Unlike for the semi-explicit formulation (2.36) with (2.37), page 26, the matrix \mathbf{G}_a^l in (5.5) not only holds projections of the inertias \mathbf{M}^l but also includes scaled contributions of the derivatives $\partial \mathbf{h} / \partial \mathbf{u} |_l$ and $\partial \mathbf{h} / \partial \mathbf{q} |_l$. These influence the solution behavior of the iterative algorithms of FÖRG [21, 19]: neither symmetry nor diagonal dominance of \mathbf{G}_a^l can be guaranteed; a possible kinematic decoupling of contacts may be lost since kinetic couplings by single-valued force laws occur in \mathbf{G}_a^l due to in general outer-diagonal entries of $\partial \mathbf{h} / \partial \mathbf{u} |_l$ and $\partial \mathbf{h} / \partial \mathbf{q} |_l$ in $\tilde{\mathbf{M}}^l$. The convergence of fixed-point iterations is not ensured but in practical application usually regarded. Like for the semi-explicit time-stepping formulation, root-finding schemes usually provide the faster solution than fixed-point algorithms if convergence is achieved.

5.2 Contact Point Search

Evaluating the kinematics of a unilateral or a sliding bilateral contact implies the detection of the points of minimal distance on the contacting surfaces, compare to section 2.2. The solution of the condition (2.21), page 16,

$$\left(\mathbf{T}^{(i)} \right)^T \left(\mathbf{r}_{OC}^{(2)} - \mathbf{r}_{OC}^{(1)} \right) = \mathbf{0} \quad \forall i \in 1, 2$$

gives the contour points associated to extremal distance between colliding bodies and is illustrated in the figures 2.2 and 3.12, pages 16 and 54. The solution is not necessarily unique, compare to figure 3.12(b), especially since for flexible bodies the contour can not be said a priori to be convex or concave. If solutions of equation (2.21) exist, the solution associated with the absolute minimal distance g_N is included and must be identified by comparisons.

Only in cases of primitive contour pairings like sphere to cone and mostly limited to rigid bodies, the points of contact can be determined analytically what is most efficient. Contrasting, for complex geometries including deformable bodies, the contact points need to be determined numerically. Therefor, a hierarchical approach is sketched: a bounding volume test for coarse pre-selection of possible regions of contact and a subsequent root finding concerning the extremal condition above.

Bounding Volume Hierarchies Collision detection between bodies with large relative motion and complex geometries is subject of ongoing research. TESCHNER ET AL. [59] give a profound overview on bounding volume methods in the context of textile modeling: a hierarchy of primitive bounding volumes encloses the contacting surfaces. Instead of testing the exact condition (2.21) directly, these bounding volumes are analyzed for intersection analytically. Figure 5.1 shows a planar example

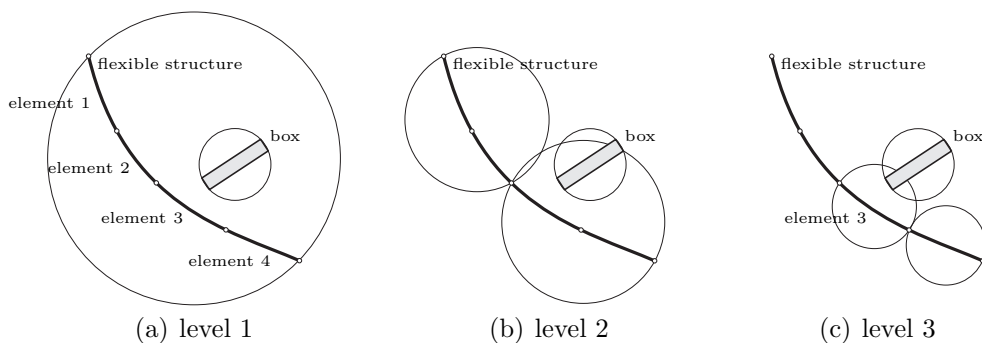


Figure 5.1: Example for a bounding volume hierarchy

using bounding circles: the box is enclosed by one circle without refinement, the finite element discretization of the beam is used as intrinsic access to a three-level hierarchy for the detection of the closest element 3. Starting at level 1, tests are performed for refined hierarchy only in case of intersection. The algorithm identifies all intersecting sub-volumes of the bounding volume hierarchy. Depending on the required accuracy, these volumes with intersection directly represent the positions of contact or are used to set up starting values for local numerical root-finding.

HIPPMANN [35, 36] provides the Polygonal Contact Model with collision detection by hierarchical bounding volumes for rigid bodies of complex geometry. Using a hierarchy of inertially aligned rectangles, he decreases computation times for contact detection by magnitudes compared to the triangulation of all possible polygonal pairings. This strategy is extended to flexible multi-body systems by EBRAHIMI [16]. Also for shapes compound of several primitive elements for a single body, bounding volume strategies can help to reduce significantly the computation times for the evaluation of the contact kinematics.

Root-Finding Arbitrary numerical root-finding algorithms can be used for local detection of the exact contact points. Special care is needed for configurations that allow for singular situations and for jumps of the contour points of minimal distance: two concentric circles are the classic example for a configuration with an infinite set of solutions for condition (2.21). Figure 5.2 additionally illustrates the instantaneous jump of the contact point $C_i^{(2)}$ on the contour for a point moving from $\mathbf{r}_1^{(1)}$ via $\mathbf{r}_2^{(1)}$ to $\mathbf{r}_3^{(1)}$. This must be regarded by the numerical algorithms.

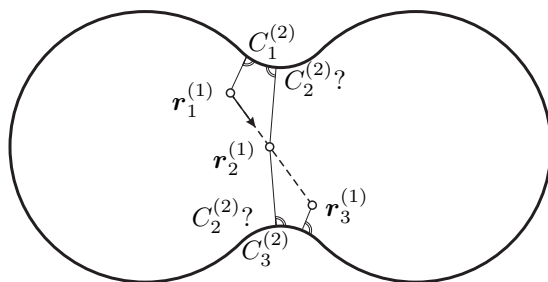


Figure 5.2: Singular point $\mathbf{r}_2^{(1)}$ and jump in contact position $C_i^{(2)}$

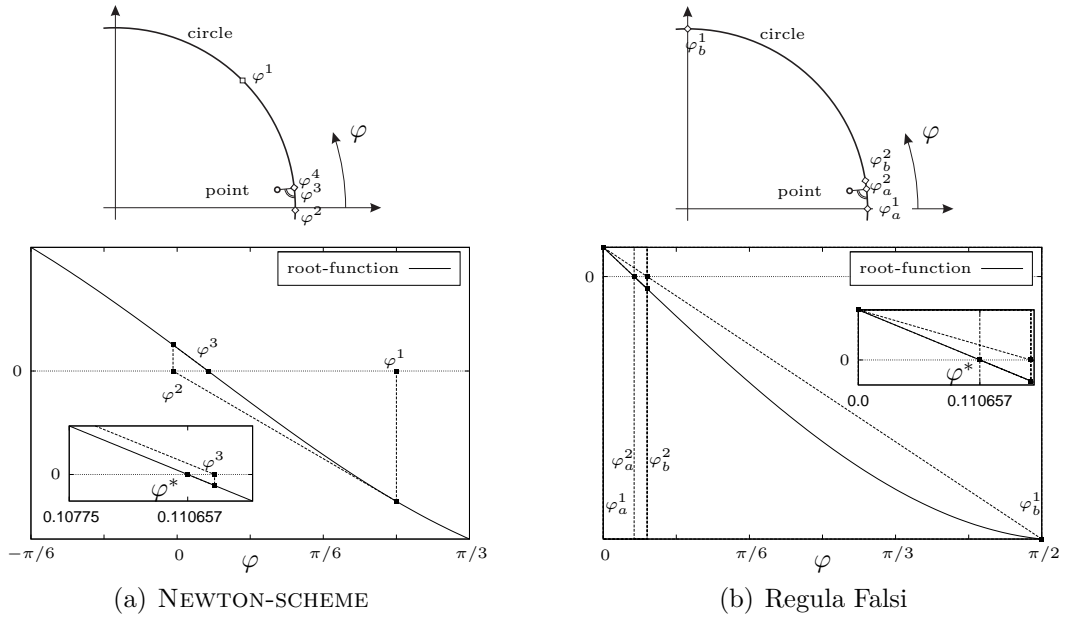


Figure 5.3: Schemes for numerical root-finding

Since classic root-finding schemes only test for a local solution, supplemental tests are needed to ensure global validity: initial values for numeric schemes can originate for example from bounding volume intersections or the solution of the last time-step evaluation. Due to the smooth position evolution and small changes between the steps of time integration, for bilateral contacts the last value suits best after a compatible initialization at the beginning of the simulation. Figure 5.3 exemplarily illustrates a NEWTON-scheme and a regula falsi: for a circle and an eccentric point, a local solution φ^* of condition (2.21) is generated giving minimal distance.

The evaluation of tangents $\mathbf{T}^{(i)}$ can cause high computational effort. A projection to the moving undeformed frame of reference with the tangents $\tilde{\mathbf{T}}^{(i)}$ and the normal $\tilde{\mathbf{n}}$ can be used for a fast computation on bodies with small deflections. Figure 5.4 depicts this for a beam and different points P_i : the approximated potential contact points $\tilde{C}_i^{(1)}$ in general do not coincide with the exact points $C_i^{(1)}$. Thus, the projection $\tilde{g}_{N,i} = \tilde{\mathbf{n}}^T(\mathbf{r}_{OC_i^{(1)}} - \mathbf{r}_{OP_i})$ usually does not equal the minimal distance $g_{N,i}$. Nevertheless, a closed contact is indicated by $g_{N,i} = \tilde{g}_{N,i} = 0$ with coinciding points $\tilde{C}_i^{(1)}$ and $C_i^{(1)}$ for the same $s_{C,i}$. Only for closed contacts the correct distance g_N , normals and tangents are needed to evaluate the force directions $\mathbf{W}^{(i)}$ and the force laws.

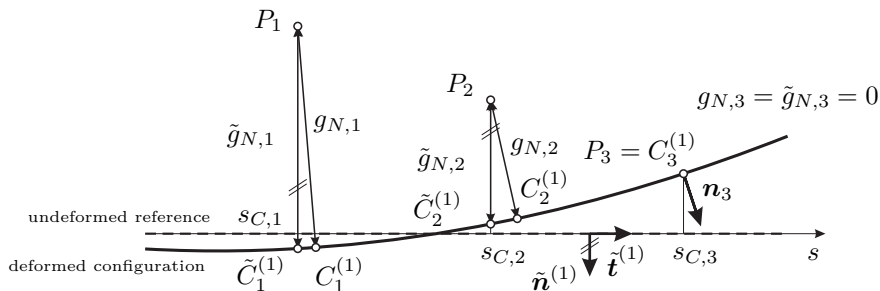


Figure 5.4: Projections to undeformed reference

6 Examples

The models and concepts of the previous chapters are tested by means of numerical simulations. Starting with simple setups, which partly are inspired by classic examples for non-smooth rigid multi-body systems like the rocking rod, key-points of the dynamic behavior of the systems are surveyed with a focus on contacts to flexible bodies. Closing up, a continuous variable transmission forms a complex multi-contact problem of industrial relevance. Animations for some examples can be found at the homepage of the Institute of Applied Mechanics¹.

All simulations are performed using MBSIM: this multi-body simulation software was initiated by FÖRG, see [19], and is complemented during the present work by elements of flexible multi-body systems with rigid contact descriptions in mind. The software accounts for classic rigid multi-body systems and formulates and solves systems with set-valued and single-valued force laws.

6.1 Cantilever Beam with Impacts

The first example is a cantilever beam excited by a discrete impulse Λ_{ex} , see figure 6.1. Due to the strong excitation, the beam bends with large deflections. The amplitudes are limited on one side by an inertially fixed point obstacle.

Mechanical Setup Table 6.1 specifies the parameters of the planar gravity-free system. The beam is discretized by eight redundant coordinate finite elements, see section 4.2.3. Bilateral constraints regarding the translations $\mathbf{r}(s=0) = \text{const.}$ and the rotation $\varphi(s=0) = \text{const.}$ describe the inertial clamping of the left beam end. Set-valued force laws model the frictionless rigid impacts and contacts between the point obstacle and the beam at varying positions within the elements. The magnitude Λ_{ex} of the impulse is chosen so that large bending deformations occur after the initial excitation. The θ -time-stepping algorithm is used for time integration.

¹ Institute of Applied Mechanics: <http://www.amm.mw.tum.de/static/animations>

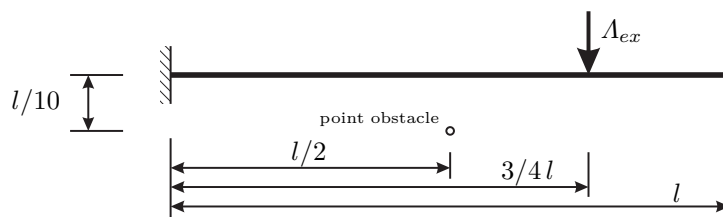
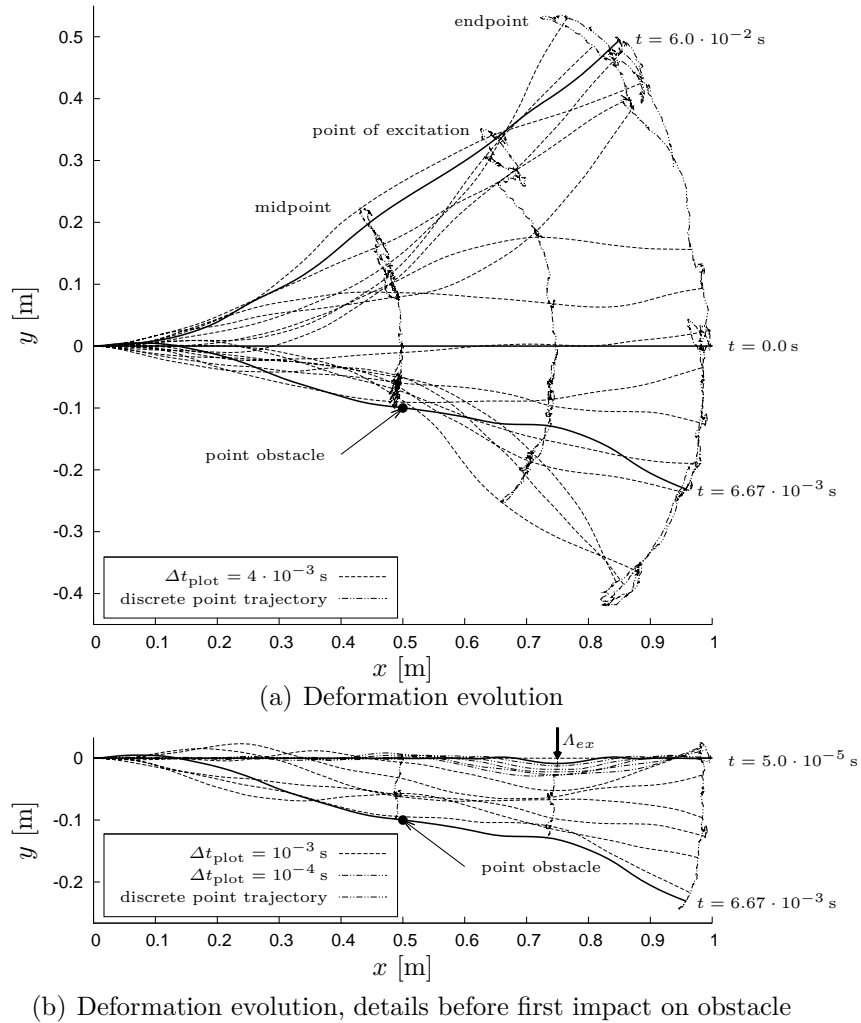


Figure 6.1: Impact excited cantilever beam with point obstacle

Table 6.1: Parameters of the cantilever beam

| specification | symbol | value |
|--------------------------------------|--------------------|------------------------------------|
| modulus of elasticity | E | $2.2 \cdot 10^{11} \text{ N/m}^2$ |
| mass density | ρ | $7.8 \cdot 10^3 \text{ kg/m}^3$ |
| rod length | l | 1.0 m |
| cross sectional area | A | $100.0 \cdot 10^{-6} \text{ m}^2$ |
| cross sectional moment of inertia | I | $8.333 \cdot 10^{-12} \text{ m}^4$ |
| excitation impulse | Λ_{ex} | 10.0 kg m/s |
| parameters of θ -time-stepper | $\Delta t, \theta$ | $5 \cdot 10^{-7} \text{ s}, 0.5$ |

**Figure 6.2:** Cantilever beam with point obstacle

Simulation Results The figures 6.2 plot the deformation history in form of deformed states at specific time intervals Δt_{plot} and selected point paths. Especially the detail plot 6.2(b) captures the wave propagation after the initial impact at $t = 0 \text{ s}$ and further dynamics up to the first impact at the obstacle at $t \approx 6.67 \cdot 10^{-3} \text{ s}$. Due to the impact, the entire frequency range of the beam model is excited leading to high frequent oscillations of the normal distance g_N between beam and obstacle, see figure 6.3. Due to these vibration, the contact closes and re-attaches several times.

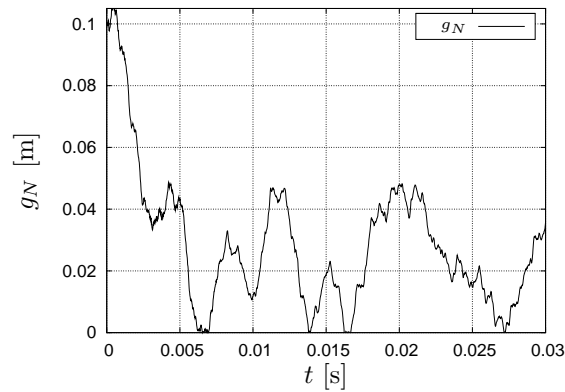
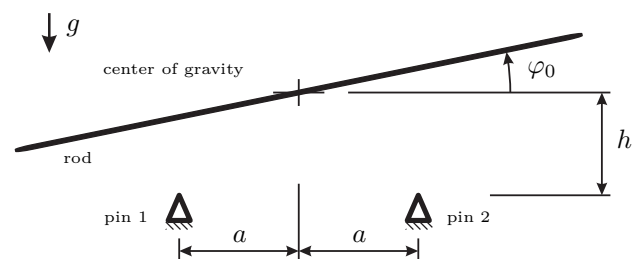


Figure 6.3: Normal distance g_N between beam and point obstacle

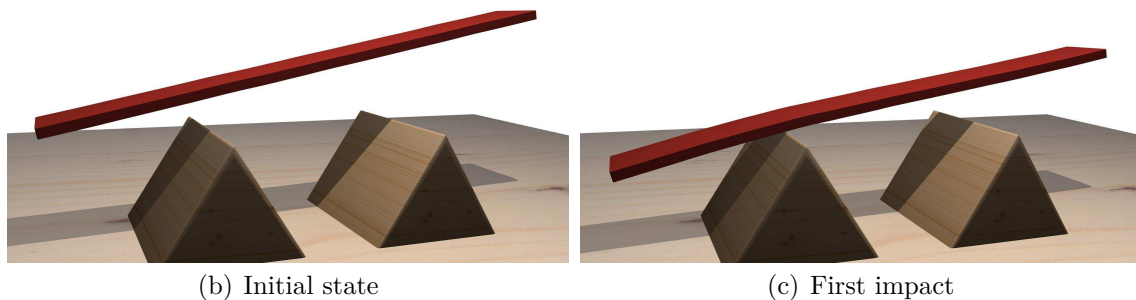
6.2 The Elastic Rocking Rod

The rocking rod displayed in figure 6.4 is a classic example for non-smooth rigid body dynamics, see amongst others PFEIFFER AND GLOCKER [45] and FÖRG [19]: falling on two inertially fixed discrete obstacles, the rod rocks with impacts dissipating system energy. It is quite consequent to use the rocking rod for testing rigid contact and impact modeling on flexible multi-body systems. Moreover, a flexible model can be used to identify restitution coefficients for the contacts of a rigid body model.

Mechanical Setup A planar model of the rocking rod is investigated, see figure 6.4(a): the rod is initialized in a free and undeformed situation with the height h of the center of gravity above the level of the two pins 1 and 2. Table 6.2 defines the parameters of the system used for simulations. In addition to the flexible model



(a) System parametrization for initial configuration



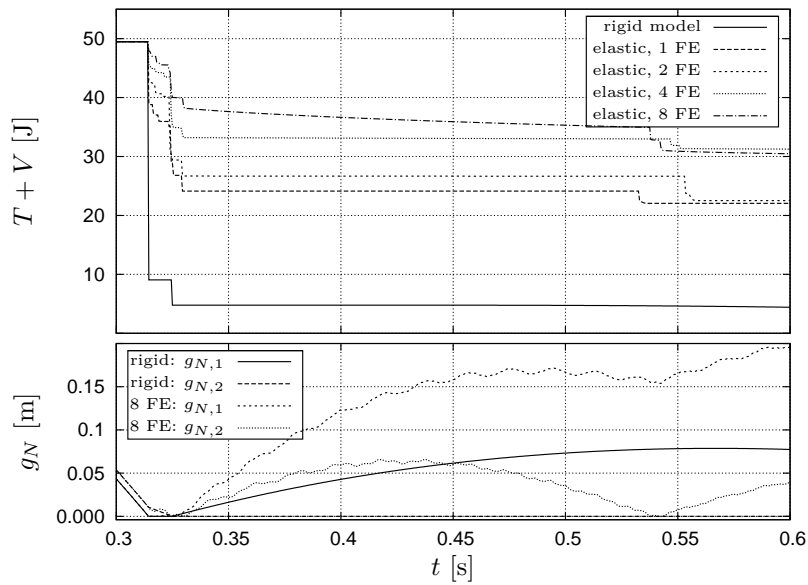
(b) Initial state

(c) First impact

Figure 6.4: Elastic rocking rod

Table 6.2: Parameters of the rocking rod

| specification | symbol | value |
|---------------------------------------|------------------------|--|
| modulus of elasticity | E | $2.1 \cdot 10^9 \text{ N/m}^2$ up to $2.1 \cdot 10^{11} \text{ N/m}^2$ |
| mass density | ρ | $7.88 \cdot 10^3 \text{ kg/m}^3$ |
| rod length | l | 0.8 m |
| cross sectional height and width | h, w | $20.0 \cdot 10^{-3} \text{ m}, 80.0 \cdot 10^{-3} \text{ m}$ |
| cross sectional moment of inertia | $I = \frac{h^3 w}{12}$ | |
| half distance between point obstacles | a | 0.1 m |
| gravity | g | 9.81 m/s^2 |
| friction coefficient | μ | 0.3 |
| initial values | h | 0.5 m |
| | φ_0 | 3.0° |
| parameters of θ -integrator | $\Delta t, \theta$ | $1 \cdot 10^{-6} \text{ s}, 0.5$ |

**Figure 6.5:** Energy and normal distances for various discretizations, $E = 2.1 \cdot 10^{10} \text{ N/m}^2$

discretized by RCM finite elements for beams, section 4.2.3, a rigid body model is used for comparisons. All contacts are modeled rigid without impact restitution and considering COULOMB-friction. The θ -time-stepping method is used to allow for equal constant time-step size Δt for all parameter sets and spatial discretizations.

Simulation Results In a first step, the influence of the spatial discretization on the impact behavior is investigated. The second analysis compares models with different specific stiffnesses parametrized by the modulus of elasticity E . Concluding remarks glance at rigid body models with elastic impact modeling.

Refinement of the Spatial Discretization Models with one, two, four and eight finite elements (FE) are used for the rod with $E = 2.1 \cdot 10^{10} \text{ N/m}^2$. Figure 6.5 compares the system energy, which is sum of the kinetic energy T and all potentials V , for the various discretizations and the rigid body model: for models, an instantaneous

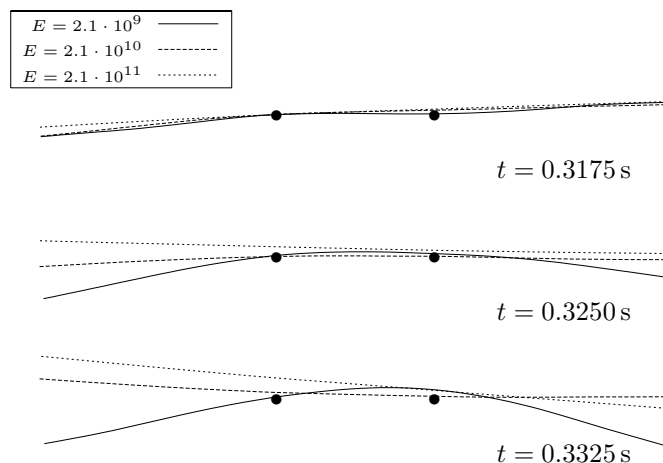


Figure 6.6: Frames of impact for rods with different modulus E of elasticity

energy loss is regarded with the closing of contacts, first at $t \approx 0.313$ s on pin 1. For a finite time span, vibration impacts occur in contact 1 until pin 2 gets in contact leading to the second major discrete decay in the system energy. The normal distances $g_{N,i}$ of both contacts i are depicted for the rigid model and the discretization using eight elements: contacts 1 and 2 close in quick succession. Unlike for the rigid model, both contacts of the flexible rods reopen rather fast due to the structural elasticity. The high frequent oscillations in the gap distances g_N reflect the structural oscillations of the beam. Energy transferred to these elastic waves are lost for the rigid body model because of the modeling assumptions.

The mass proportion involved in the impact via the projection \mathbf{G} decreases with refining the spatial discretization, compare to section 3.3.3: for the present model, the normal post-impact conditions claim zero velocity for the projected masses \mathbf{G} . Consequently, the energy loss decreases for finer spatial discretization and has an upper extremum set by the rigid model, see the decay of $T + V$ in figure 6.5 at $t \approx 0.313$ s. Refining the spatial discretization concurrently increases the frequency range of the model. For system frequencies in order of magnitude of the time step size Δt , an additional energy loss is regarded due to the implicit integration scheme. The θ -time-stepping scheme ensures A-stability for arbitrary large Δt but does not resolve the high frequencies of the eight element model: the slight numerical dissipation can be seen for the total energy during the free flight phase $t \in [0.34 \text{ s}, 0.53 \text{ s}]$.

Variation of Structural Stiffness Figure 6.6 depicts frames of the impact transition of the flexible model using 8 FE for various modulus E of elasticity. The beam with $E = 2.1 \cdot 10^9 \text{ N/m}^2$ deforms with large deflections and almost symmetric with respect to the obstacles: the impact response is comparatively slow. It is obvious that the stiffest model $E = 2.1 \cdot 10^{11} \text{ N/m}^2$ gives the fastest response and smallest deflections. For increasing structural stiffnesses, the changeover to classic rigid body modeling lays at hands: the fast contact dynamics of very stiff bodies can be approximated by non-vanishing restitution coefficients $\varepsilon > 0$: this can be used to control both the energy loss and local rebound effects for rigid body contact situations.

ZANDER ET AL. [65] investigate the approximation of structural flexibility by describing impacts for the rigid body model with a restitution coefficient: using numerical optimization, ε is estimated by comparative simulations. With $\varepsilon > 0$ the contact of the rigid model reopens instantaneously whereas the contact of the elastic body model stays closed for a finite time span. This behavior can be interpreted as time delay between both models and must be kept in mind when considering the overall system behavior. Using real system experiments and detailed finite element modeling for substructures, SEIFRIED [53] performs comprehensive investigations for the identification and interpretation of restitution coefficients in multi-body systems.

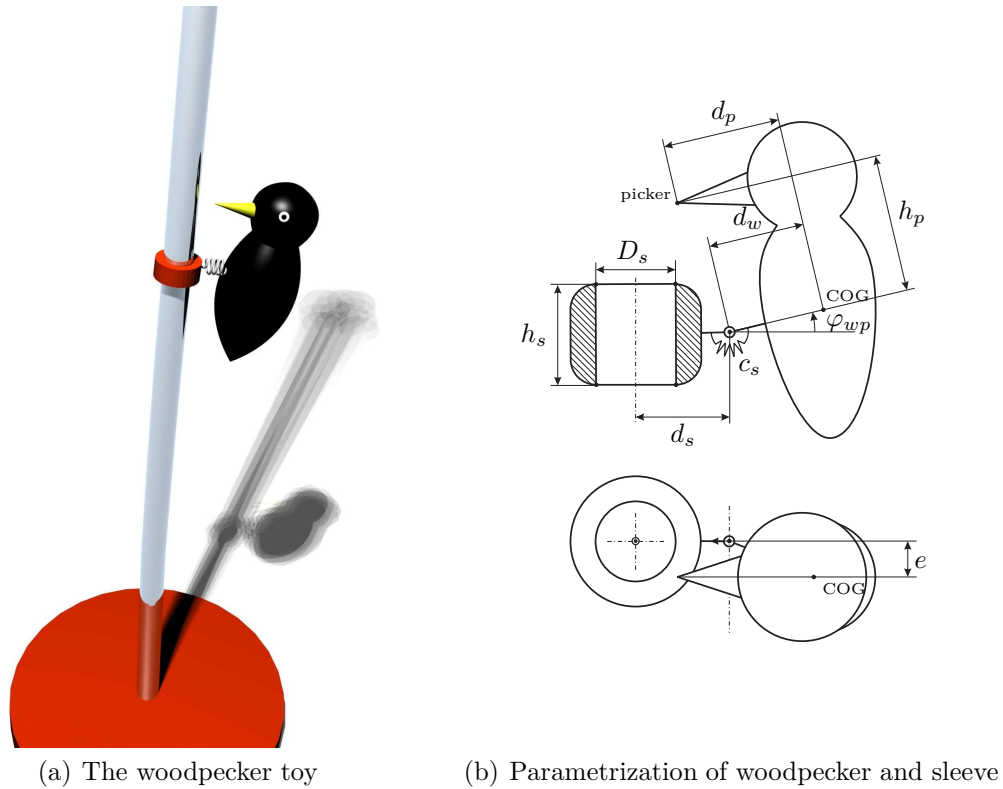
6.3 The Woodpecker Toy

The woodpecker toy is a second example for non-smooth multi-body systems often named in literature, see for example PFEIFFER [44] and LEINE AND GLOCKER [39]. Figure 6.7(a) depicts the woodpecker: hammering down the pole, the system uses gravity as energy source and stick-slip effects between the guiding sleeve and the pole as switch between free and constrained motion. With the sleeve sticking, the spring forces the woodpecker back towards picking the pole.

Mechanical Setup A planar rigid model and two models comprising an elastic pole – one regarding planar motion and one with spatial dynamics – are regarded. For all models the bird and the sleeve are represented by rigid bodies. The spring connecting the woodpecker to the sleeve, which comprises all planar or spatial degrees of freedom, is abstracted by a revolute joint with one relative freedom and a discrete elasticity. Parameters for the model with a solid circular pole are given in table 6.3 corresponding to figure 6.7(b). Rigid unilateral contacts are modeled between the pole and the sleeve as well as between the pole and the picker, which is reduced to a discrete point. A unitary coefficient μ of COULOMB-friction is assumed for all contacts. The simulations are initialized with an upright undeformed pole, a concentric sleeve and a horizontal bird. To start the system's self-excitation, the bird is released with the relative velocity $\dot{\varphi}_{wp,0}$. Again, the θ -time-stepping is used.

For planar flexible modeling, the pole is discretized by eight RCM-finite elements, section 4.2.3. The inertial clamping is described by bilateral constraints analogous to the cantilever beam of example 6.1. The pole surface is reduced to a left and a right planar curve: the rigid pole is described by inertially fixed straight lines, the elastic according to the deformation approximations. The four projected corners represent the sleeve's hole for point-to-continuum contacts with the pole.

For the spatial configuration, the flexible pole is modeled by a spatial bending-torsional beam using a finite-element formulation. Based on the EULER-BERNOULLI theory, small deformations with superposed torsion are accounted for. Contacts occur between the picker and the pole as well as between the two circles defining the sleeve and the deformed circular pole. To enforce the spatial character of the system, the woodpecker is attached with the eccentricity e to the sleeve.



(a) The woodpecker toy

(b) Parametrization of woodpecker and sleeve

Figure 6.7: Model of the woodpecker-toy**Table 6.3:** Parameters of the woodpecker model

| specification | symbol | value |
|------------------------------------|--|--|
| pole length | L | 0.5 m |
| pole radius | r_p | $2.5 \cdot 10^{-3}$ m |
| modulus of elasticity | E | $7.0 \cdot 10^{10}$ N/m ² |
| POISSON-ratio | ν | 0.3 |
| mass density | ρ | $2.3 \cdot 10^3$ kg/m ³ |
| clearance | γ | $0.1 \cdot 10^{-3}$ m |
| diameter sleeve | $D_s = 2r_p + \gamma$ | |
| height sleeve | h_s | $6.0 \cdot 10^{-3}$ m |
| mass sleeve | m_s | $5.0 \cdot 10^{-3}$ kg |
| inertia sleeve | $J_{s,1} = 2 J_{s,2} = J_{s,3}$ | $125.0 \cdot 10^{-9}$ kgm ² |
| distance joint | d_s | $10.0 \cdot 10^{-3}$ m |
| stiffness joint-spring | c_s | 0.05 Nm |
| eccentricity of woodpecker | e | $1.0 \cdot 10^{-3}$ m |
| distance center of gravity (COG) | d_w | $14.0 \cdot 10^{-3}$ m |
| mass woodpecker | m_w | $60.0 \cdot 10^{-3}$ kg |
| inertia woodpecker | $J_{w,1} = 10 J_{w,2} = J_{w,3}$ | $12.0 \cdot 10^{-6}$ kgm ² |
| distance picker | d_p | $20.0 \cdot 10^{-3}$ m |
| height picker | h_p | $20.0 \cdot 10^{-3}$ m |
| friction coefficient all contacts | μ | 0.15 |
| gravity in pole direction | g | 9.81 m/s ² |
| initial values | $\varphi_{wp,0}, \dot{\varphi}_{wp,0}$ | $0.0, -\pi$ s ⁻¹ |
| | $y_{wp,0}$ | 0.475 m |
| parameters of θ -integrator | $\Delta t, \theta$ | $2.5 \cdot 10^{-6}$ s, 0.5 |

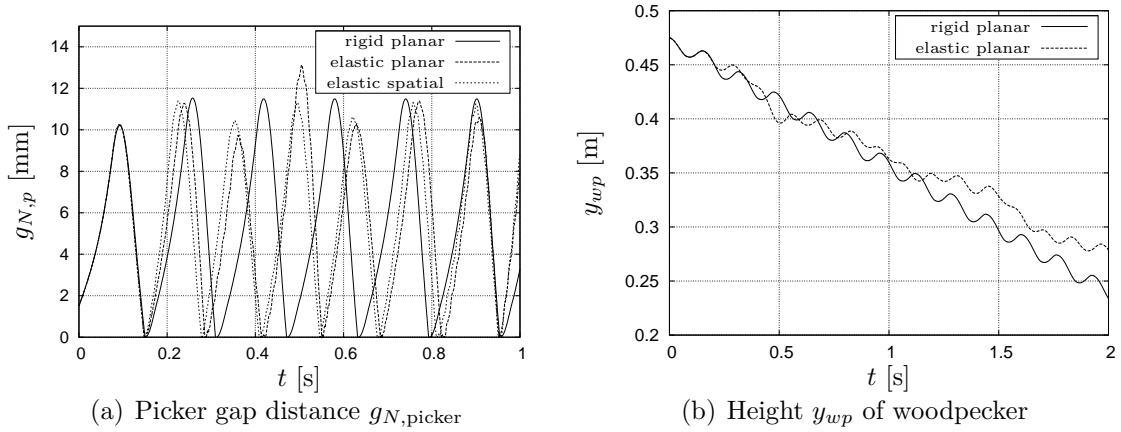


Figure 6.8: Motion of the woodpecker toy

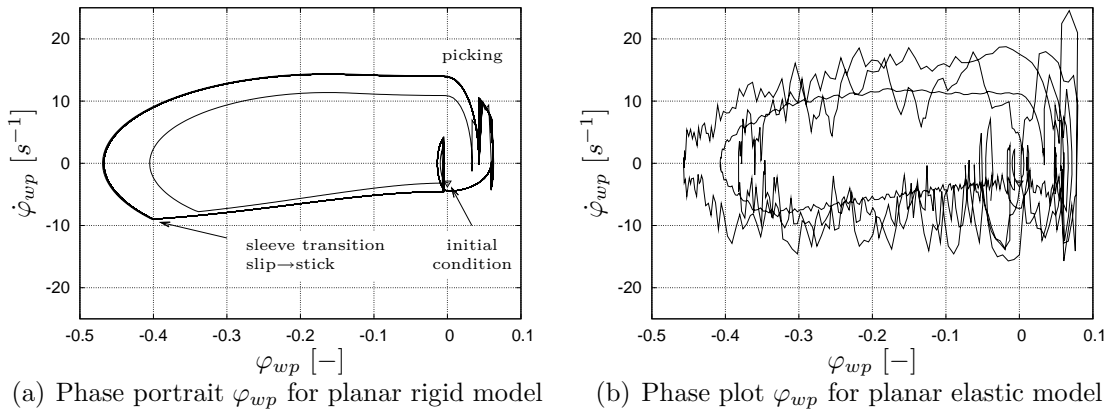


Figure 6.9: Motion of the woodpecker toy: phase plots

Simulation Results Figure 6.8(a) displays the gap distance $g_{N,p}$ between the picker and the pole for all simulations. It is evident that the rigid model gives periodic results whereas amplitudes and intervals change during the woodpecker's decent on the elastic poles. Consistent results are plotted in figure 6.8(b) for the height y_{wp} of the planar models. The figures 6.9 show phase space diagrams for the relative angle φ_{wp} between woodpecker and sleeve for the first three picking cycles: only the rigid model ends up in a stable limit cycle (compare literature, e.g. [39]). The elasticity of the pole leads to interferences between the dynamics of the woodpecker and of the elastic structure: no stable limit cycle is reached on elastic poles. Moreover, the characteristic frequencies of the model change with the varying position of the woodpecker on the pole, also causing small and large decent per cycle, see figure 6.8(b). Like for the example 6.2 of the rocking rod, the flexible modeling results in a partly elastic impact behavior: the re-opening velocity $\dot{g}_{N,p}$ of the picker contact is larger than for the rigid model leading to a higher picking frequency (comp. fig. 6.8(a)). Again, a restitution coefficient might be used for an adaption of the rigid model.

For the spatial configuration, the figures 6.10 show that the impact of the picker on the pole – marked by the picker gap distance $g_{N,p} = 0$ – induces rotations to both

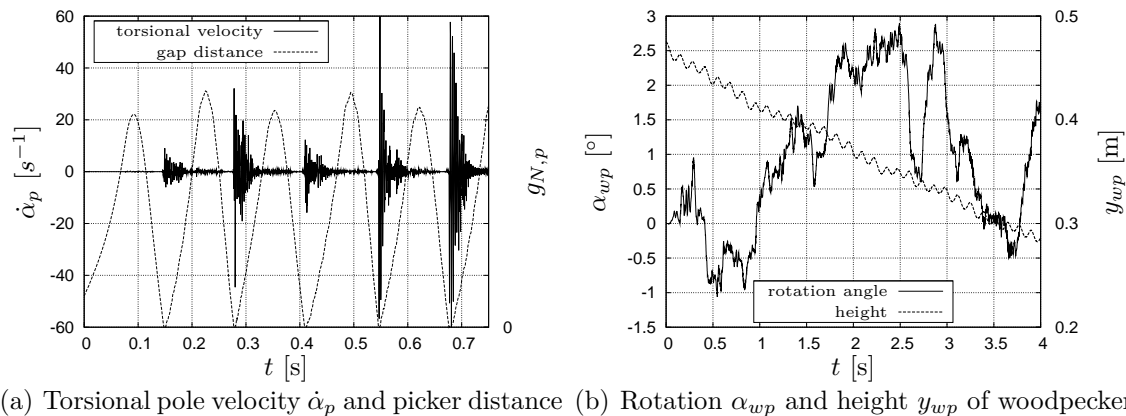


Figure 6.10: Torsional and tumbling motion induced by eccentric picking

the elastic pole and the woodpecker. Thereby, the torsion α_p of the pole tip occurs in high frequency oscillations. As a result of the spatial configuration, a tumbling rotation motion α_{wp} of the woodpecker around the vibrating pole occurs.

6.4 Elastic Bowl of Dice

Numerous rigid dice falling into an elastic bowl are the first example for a system with numerous contacts to a flexible structure. The modeling of the bowl is performed as idealization giving structures like an external pre-process. A subsequent interpolation between nodes describes the continuous surface. The figures 6.11 show a snap-shot of the falling dice and the bowl surface supported by 16 nodes.

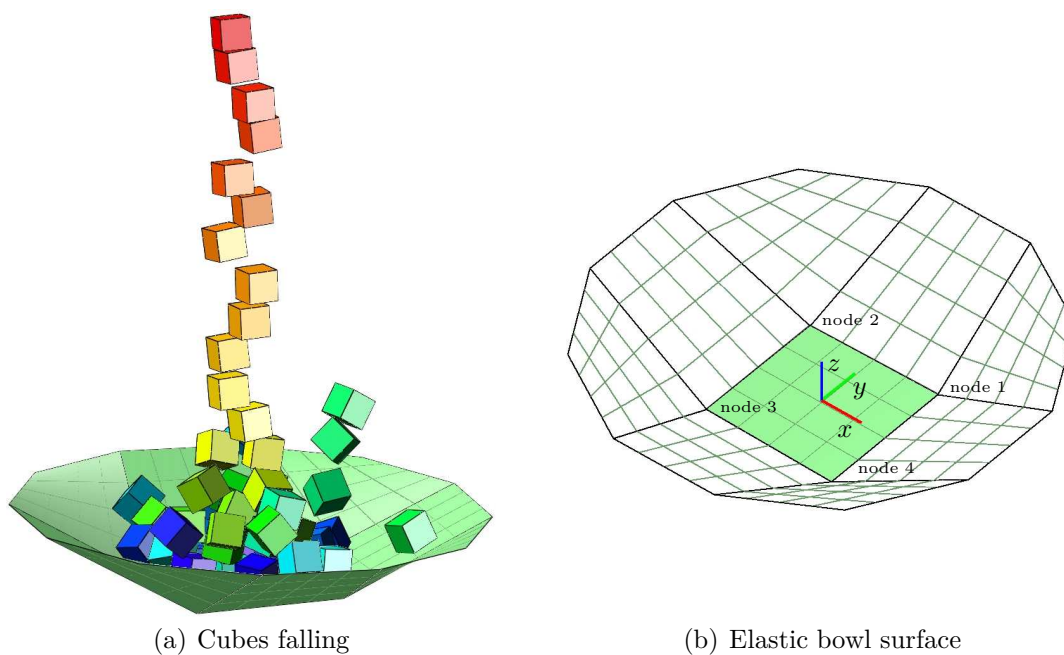


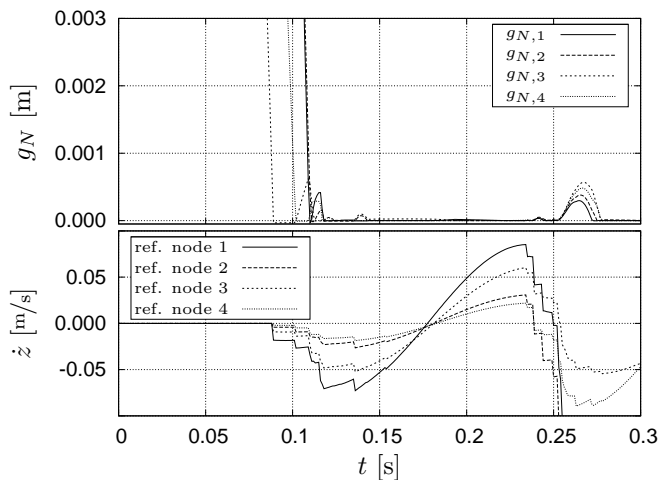
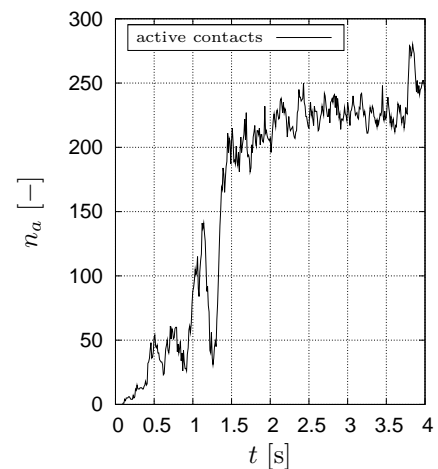
Figure 6.11: Cubes falling into an elastic bowl

Table 6.4: Parameters of the bowl and dice

| specification | symbol | value |
|---|---|-----------------------|
| nodal mass | m_n | 1.0 kg |
| nodal stiffness | k_n | 750.0 N/m |
| edge-length central square | l | 1.0 m |
| mass of dice | m_d | 0.1 kg |
| edge-length of dice | l_d | 0.1 m |
| inertias of the dice | $J_{11} = J_{22} = J_{33} = \frac{ml^2}{6}$ | |
| friction coefficient for all contacts | μ | 0.3 |
| gravity | g | 9.81 m/s ² |
| time step size for semi-explicit integrator | Δt | $5 \cdot 10^{-5}$ s |

Mechanical Setup Parameters for the system are given in table 6.4: to concentrate on surface and contact description, identity matrices are used for mass- and stiffness-matrix scaled by the nodal mass m_n and stiffness k_n . The surface is modeled piecewise by bi-linear interpolations supported by four nodes each, see figure 6.11(b). The central square has edge-length l . The 50 dice of mass m_d and edge-length l_d are released above the bowl with all contacts open. Two dice comprise the possibilities for contacts between the twelve edges pairwise and of the eight corners to six faces of each dice, giving $12 \cdot 12 + 2 \cdot 6 \cdot 8 = 240$ possible contact pairings. Including the contacts to the surface segments of the bowl, the system comprises 297 600 possible contacts between basic shape elements. Bounding sphere tests for all body pairings reduce the computational effort to 1275 trivial preliminary tests: the exact contact kinematics is evaluated only in case of intersection. All contacts are modeled rigid regarding dry friction, the gravity direction is normal on the undeformed central surface of the bowl. The simulation uses the semi-explicit time-stepping.

Simulation Results For the dice impacting on the bowl first, figure 6.12 displays the gap distances $g_{N,i}$ of the corners. At the times of closing contacts ($g_{N,i} = 0$ and $\dot{g}_{N,i} < 0$ at approximately $t_i \in \{0.08\text{s}, 0.1\text{s}, 0.11\text{s}, \dots\}$), jumps occur for the

**Figure 6.12:** Gap distances and velocities of the nodes supporting the central surface**Figure 6.13:** Number n_a of active contacts

vertical velocities \dot{z} of the four nodes supporting the central surface. The magnitude of the impact is simultaneously distributed on all nodes whereas the nodal portions are set by the interpolation weights according to the shape position, compare equation (3.49), page 53. The successive jumps in the velocities are related to closing contacts of other dice. Residual vibrations remain during the time of simulation leading to ongoing changes of the contact situation and frictional dissipation. In spite of the high number of up to $n_a = 270$ closed contacts – each comprising one normal and two frictional set-valued reactions – the system can be simulated successfully.

6.5 Push-Belt Continuous Variable Transmission

Continuous variable transmissions (CVT) are used in automobiles to allow for running the engines at the optimal operation point for various driving speeds. A transmission medium, either a belt or a chain, runs on pairs of conic sheaves being mounted on the axes. Using a hydraulic actuation, the axial distances between the sheaves can be varied causing a continuous change in the running radii and therewith modification of the transmission ratio. Friction is utilized for the power submission between the sheaves and the transmission medium.

Figure 6.14 shows the push-belt CVT manufactured by Bosch-VDT, Netherlands: the belt is composed of two packages of elastic steel rings guiding approximately 400 steel elements, compare 6.14(b). Due to their minor thickness and high number, these elements provide multi contact to the sheaves minimizing polygonal effects commonly known for classic chains. Using the words of SCHINDLER ET AL. [51] this setup provides “A Non-Smooth Challenge” for multi-body simulations.

The modeling of the complete transmission system is beyond the scope of the present work and topic of several successive thesis at the Institute of Applied Mechanics. Only the aspect of modeling the push-belt assembly is regarded here: the guiding of the rigid elements on the flexible ring-packages can either be abstracted by bilateral constraints or by a relative kinematic description. Closing up, references are given to comprehensive investigations covering the complete bush-belt CVT.

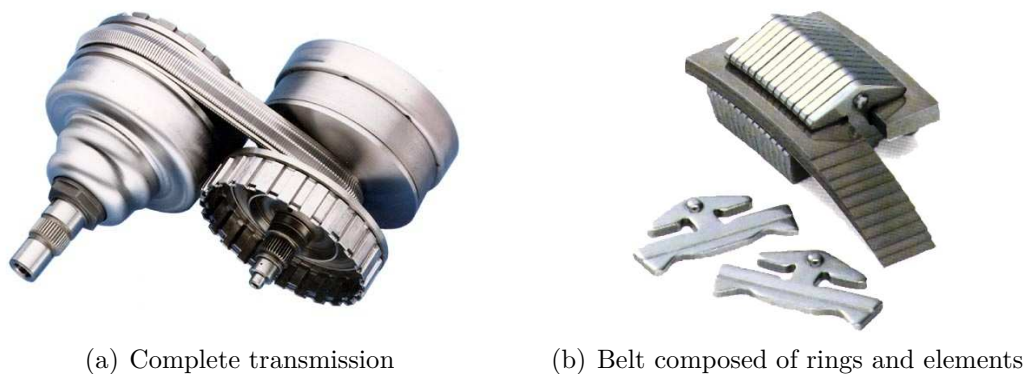


Figure 6.14: Push-belt continuous variable transmission

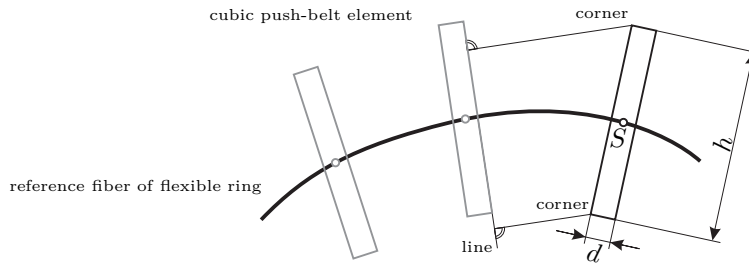


Figure 6.15: Abstraction of the push-belt

Table 6.5: Parameters of the push-belt

| specification | symbol | value |
|---|------------|--------------------------------------|
| ring package circumference | l | 1.0 m |
| modulus of elasticity | E | $2.5 \cdot 10^{10} \text{ N/m}^2$ |
| mass density | ρ | $2.5 \cdot 10^3 \text{ kg/m}^3$ |
| cross sectional area | A | $25.0 \cdot 10^{-6} \text{ m}^2$ |
| cross sectional moment of inertia | I | $50.0 \cdot 10^{-12} \text{ m}^4$ |
| mass element | m | $25.0 \cdot 10^{-3} \text{ kg}$ |
| inertia element | J_{zz} | $0.840 \cdot 10^{-6} \text{ kg m}^2$ |
| gravity | g | 9.81 m/s^2 |
| time step size for semi-explicit integrator | Δt | $1 \cdot 10^{-6} \text{ s}$ |

Modeling the Ring-Package

The model is reduced to planar dynamics. Figure 6.15 shows an abstraction of the original push-belt, compare figure 6.14(b): instead of describing the complex contact geometry of the elements, plain cuboids are used. Contacts are described pairwise between the two corners of one and the face represented by a line of the other cuboid. Two different modeling approaches are studied for the bilateral constraint motion of the elements on one virtual ring-package: either the absolute parametrization of both the dynamics of the ring and the elements can be supplemented by constraint equations; alternatively, the elements can be described with relative kinematics on the ring, which is parametrized absolute, compare to section 4.1.2.

Mechanical Setup For both modeling approaches, 24 RCM finite elements are used, see section 4.2.3, leading to $f_f = 120$ degrees of freedom for the ring package. Table 6.5 gives the parameters for the simulation. A belt with $n_e = 60$ rigid elements is investigated: the absolute parametrization needs $f_e^{\text{abs}} = 3n_e = 180$ degrees of freedom for the elements, the relative description $f_e^{\text{rel}} = 2n_e = 120$. Additionally, the modeling with bilateral constraints involves $c_b^{\text{abs}} = n_e = 60$ constraint equations ensuring the guidance of the elements on the flexible ring.

The belt is simulated with unilateral frictionless rigid contacts in-between the elements. For the simulation, one single element is translational fixated inertially: gravity causes a swinging motion of the belt, see figure 6.16. Another element is marked in different color for further considerations. The system is initialized in idle state with equal distances between all elements on a circular ring. Note that the

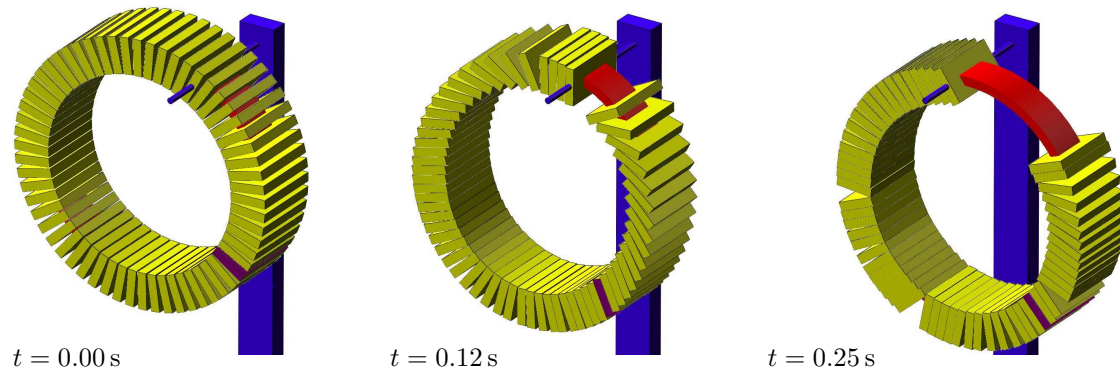


Figure 6.16: Frames of the push-belt swinging under gravity

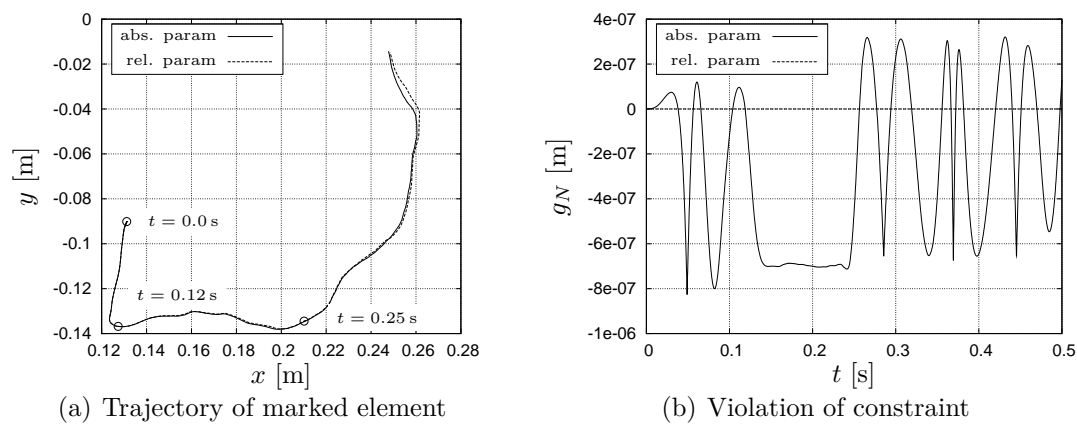


Figure 6.17: Kinematic comparison of element parametrization

setup has an unrealistic large collected clearance between the elements, visible as large gap in the right frame of figure 6.16. Time integration is performed using semi-explicit time-stepping with equal step-size Δt for both models.

Simulation Results Figure 6.16 shows the swinging motion around the fixated element. Concurrently, the other elements slide along the guiding ring with contacts closing impulsively. Good agreement can be seen for both modeling approaches looking for example at the trajectory of the marked element, figure 6.17(a). The relative kinematic description provides analytic compliance for all constraints; for the bilateral constrained system figure 6.17(b) depicts small violations $g_N \neq 0$ due to numerical drift related to the marked element.

High numbers of up to $n_a = 140$ active contacts for the absolute parametrization with bilateral constraints and $n_a = 80$ active contacts for the relative description are plotted in figure 6.18(a): except for the inertial fixation giving two constraint reactions, each of these contacts comprises one LAGRANGE multiplier. The processor time T_{CPU} needed for simulation of the relative kinematic parametrization is larger by 15% to 20% compared to the formulation using bilateral constraints, see figure 6.18(b): this higher computational effort of the relative description is related

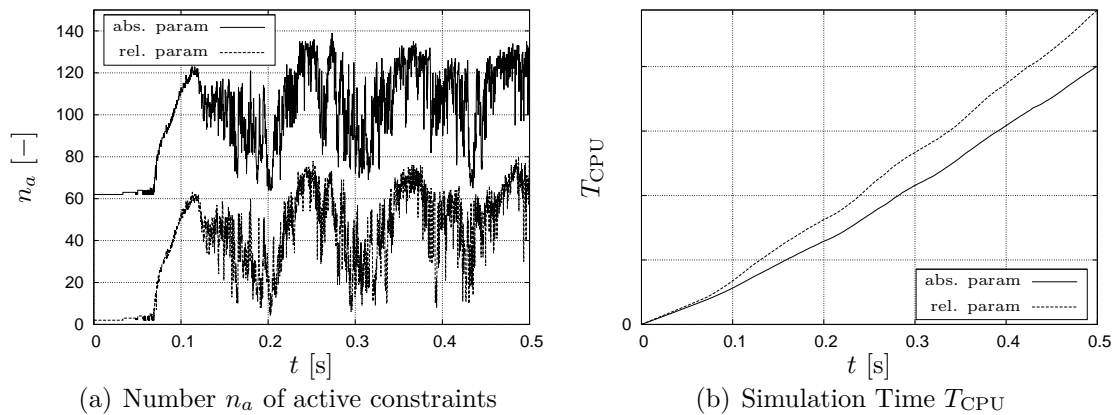


Figure 6.18: Algorithmic comparison of element parametrization

to the higher accuracy. The time-stepping formulation gives only linear approximation of the constraints evaluating only the JACOBI-matrices; in contrast, the analytic evaluation of the sliding contact needs evaluation for example of curvatures and time derivatives of the JACOBIANS being of highest computational effort. To ensure accuracy, a stronger limitation on the time-step size Δt being equal for both approaches is set by the absolute parametrized model. In addition, the relative kinematic description would allow for arbitrary numerical integration schemes for ordinary differential equations when no other rigid contacts than the relative guiding need to be described.

Industrial System

In his PhD-thesis [25] GEIER develops a planar model for the transient behavior of the push-belt CVT. The ring-packages are modeled elastic using the planar beam model discussed within the current work. The guiding of the elements is described by bilateral constraints; quasi-static deformations are regarded for the conic sheaves. Reducing the model to approximately 1500 degrees of freedom, 3500 contact reactions for impenetrability and friction need to be determined. A linear implicit EULER-scheme, what equals $\theta = 1$ of the θ -time-stepping, is used for time integration. A modular and mixed formulation allows for rigid as well as flexible contact models including friction between all components. The model captures all important effects and shows excellent agreement with measurements performed by Honda. Additionally, SCHINDLER ET AL. [50] validate the model by measurements of Bosch-VDT.

Further enhancement of this model towards three dimensional dynamics is provided by SCHINDLER ET AL. [51]. Especially the description of the ring-packages with spatial large translational and rotational deflections is subject of intensive investigation. An additional challenge arises with the complex spatial contact situations.

7 Conclusion

The increasing request for detailed multi-body simulations includes demands for rigid contact description on flexible bodies. While both rigid contact and flexible body modeling are well established working fields that provide results efficiently also in the context of industrial and high dimensional investigations, the description of set-valued force laws applied to flexible bodies lacks for comprehensive studies. The present work provides a framework for this application.

Referring to fundamental contributions in literature, a general mathematical basis for the description of MBS including non-smooth characteristics is established in chapter 2. An introductory discussion of variational approaches for dynamic systems with unilateral constraints in mind prepares the application to flexible systems. The modular derivation of the kinematic and the kinetic part of contacts later on allows for a structured implementation in a simulation environment. The formulation by proximal functions for the set-valued force laws – these represent the rigid contacts – is utilized during time integration of the non-smooth dynamic systems.

Chapter 3 starts with resuming the framework commonly used for the description of flexible MBS: kinematic and kinetic assumptions allow for the derivation of partial differential equations describing the transient deformation behavior. Before the spatial discretization is introduced, which is needed for most computational simulations, the non-smooth characteristic is discussed in the context of a spatial continuum: a time discrete jump in the velocity of a singular point concurrently induces a spatial discrete discontinuity. Even though this effect is blurred by every spatial discretization, it needs to be regarded during the selection of proper shape functions. Here, opposite extremals are set by a modal and a finite element discretization: while the first aims for representing the steady-state behavior of the entire body, the second yields a local focus by spatial division. Therefore, the modal approach is best suited for fixed configurations without structural variance like closing contacts: only systems with constant structure provide constant eigenforms. Contrasting, finite elements preserve the local character of contact modeling also for sliding bilateral and unilateral constraints but may only weakly approximate eigendynamics for very coarse discretizations. Having established continuous shapes for the discretized flexible bodies, the contact formulations of chapter 2 can be applied entirely. Thereby, formulating a rigid contact means that the basic kinematic assumptions are preserved, for example undeformable cross sections of a slender beam, and impenetrability is regarded excluding contact flexibility.

Among the constraint formulations named within this thesis, the bilateral contact is the only one that provides constant dimension of the minimal parametrization. Simultaneously, it is of major relevance for many MBS simulations. In a first

part, chapter 4 addresses the analytic incorporation of equality restrictions for tree-structured systems: a rigid body on a flexible predecessor is discussed in detail. The exact compliance for the constraint is accompanied by the need for evaluating the entire nonlinear kinematic relations up to acceleration level.

Being of similar mathematical structure, a redundant parametrization of the body's kinematics can be used to allow for a selective modeling of special physical effects with good computational performance. Here, a finite element formulation for beams with large deflections is derived utilizing both connectivity of nodal coordinates and effect-based modeling like for moving frame of reference formulations.

Some special aspects concerning the numerics of flexible MBS with contacts are addressed in chapter 5. Implying contacts at velocity level, a scaled linear implicit time-stepping integrator is formulated providing A-stability: the time-step size can be chosen independent from the spatial discretization of flexible systems. During simulation the contact kinematics implies the unitary identification of the pairing potential contact points: a bounding volume hierarchy might be used for a reduction of the computational effort by pre-selection and for capturing all regions of possible interactions. This can complement root-finding algorithms in identifying the contact points and ensure validity of the solutions.

Chapter 6 provides examples spanning from academic to industrial, from single to multi-impact problems. Thereby, MBSIM is used as simulation platform: the module for flexible bodies results of the work presented within this thesis and provides interfaces to further implementations of specific flexible body models.

As expected, impacts to flexible structures excite the entire modeled frequency range. Concurrently, rigid body impacts show partly flexible characteristics due to the modeled structural flexibility but depending upon the spatial discretization: the finer the local resolution the lower are the instantaneous losses of kinetic energy for impacts; instead local deformations occur rapidly. For the relative motion of masses applied to a flexible body, shifts and interfaces in the characteristic frequencies and modes of the system might result from the changes in the mass distribution. Using proper time-integration schemes, even high dimensional problems with numerous contacts can be simulated efficiently including flexible bodies.

Summing up, the present work shows the applicability of rigid contact formulations including dry friction to flexible multi-body systems. This is of interest since functional formulations like penalty approaches can be avoided: these tend to be numerically stiff when decreasing mass ratios are included in contacts for refined spatial discretizations. Nevertheless, the definition of the system is a crucial point, especially the discretization of flexible components: systems with constant structure allow for highly specialized model approaches; structure variance on flexible bodies, like closing unilateral contacts or contacts with relative motion, yields the necessity for modular modeling concepts as well as approximations with a sharp local focus.

Bibliography

- [1] ACARY, V. ; BROGLIATO, B. : *Numerical methods for nonsmooth dynamical systems*. Berlin, Heidelberg, New York : Springer, 2008
- [2] ALART, P. ; CURNIER, A. : A mixed formulation for frictional contact problems prone to NEWTON like solution methods. In: *Computer Methods in Applied Mechanics and Engineering* 92 (1991), S. 353–375
- [3] AMBRÓSIO, J. A. C. ; NIKRAVESH, P. E.: Elasto-plastic deformations in multibody dynamics. In: *Nonlinear Dynamics* (1992), Nr. 3, S. 85–104
- [4] AMBRÓSIO, J. A. C.: *Advances in Computational Multibody Systems*. Berlin, Heidelberg, New York : Springer, 2005
- [5] BACHMAYER, M. ; ZANDER, R. ; ULBRICH, H. : Numerical approaches for residual vibration free positioning of elastic robots. In: *Proceedings of the ACE-X 2008*. Barcelona, Spain : ACE-X, 2008
- [6] BATHE, K. : *Finite Element Procedures*. Prentice Hall, 1996
- [7] BELYTSCHKO, T. ; SCHWER, L. : Large Displacement Transient Analysis of Space Frames. In: *International Journal for Numerical Methods in Engineering* 11 (1977), S. 65–84
- [8] BONNANS, J. F. ; GILBERT, J. C. ; LEMARÉCHAL, C. ; SAGASTIZÁBAL, C. A.: *Numerical optimization*. Berlin, Heidelberg, New York : Springer, 2006
- [9] BRANDL, H. ; JOHANNI, R. ; OTTER, M. : An Algorithm for the Simulation of Multibody Systems with Kinematic Loops. In: *Proceedings of the 7th World Congress on the Theory of Machines and Mechanisms*, 1987
- [10] BREMER, H. ; PFEIFFER, F. : *Elastische Mehrkörpersysteme*. Wiesbaden : Teubner Verlag, 1992
- [11] BROGLIATO, B. ; TEN DAM, A. A. ; PAOLI, L. ; GÉNOT, F. ; ABADIE, M. : Numerical simulation of finite dimensional multibody nonsmooth mechanical systems. In: *ASME Applied Mechanics Reviews* 55 (2002), S. 107–150
- [12] BROGLIATO, B. : *Nonsmooth Mechanics*. Berlin, Heidelberg, New York : Springer, 1999
- [13] CLARKE, F. H.: *Optimization and nonsmooth analysis*. Repr. SIAM, 1990
- [14] CRISFIELD, M. A. ; GALVANETTO, U. ; JELENÍČ, G. : Dynamics of 3-D Co-rotational Beams. In: *Computational Mechanics* 20 (1997), S. 507–519
- [15] EBERHARD, P. : *Kontaktuntersuchungen druch hybride Mehrkörpersystem / Finite Element Simulationen*. Aachen : Shaker Verlag, 2000
- [16] EBRAHIMI, S. : *A Contribution to Computational Contact Procedures in Flexible Multibody Systems*. Aachen, Institut für Technische und Numerische Mechanik, Universität Stuttgart, Diss., 2007

- [17] ENGELHARDT, T. : *Dynamik von Steuer- und Ventiltrieben*. Düsseldorf, Lehrstuhl für Angewandte Mechanik, TU München, Diss., 2007
- [18] FETECAU, R. C. ; MARSDEN, J. E. ; ORTIZ, M. ; WEST, M. : Nonsmooth Lagrangian Mechanics and Variational Collision Integrators. In: *SIAM Journal of Applied Dynamical Systems* 2 (2003), S. 381–416
- [19] FÖRG, M. : *Mehrkörpersysteme mit mengenwertigen Kraftgesetzen – Theorie und Numerik*. Düsseldorf, Lehrstuhl für Angewandte Mechanik, TU München, Diss., 2007
- [20] FÖRG, M. ; ENGELHARDT, T. ; ULBRICH, H. : Analysis of different time-integration methods applied to a non-smooth industrial problem. In: *Proceedings of the ENOC Fifth EUROMECH Nonlinear Dynamics Conference*. Eindhoven, Netherlands, 2005
- [21] FÖRG, M. ; NEUMANN, L. ; GEIER, T. ; ULBRICH, H. : r-factor Strategies for the Augmented Lagrangian Approach in Multi-Body Contact Mechanics. In: *Proceedings of the III European Conference on Computational Mechanics*. Lisbon, Portugal : Springer, 2006
- [22] FÖRG, M. ; ZANDER, R. ; ULBRICH, H. : A Framework for the Efficient Simulation of Spatial Contact Problems. In: *Proceedings of the ECCOMAS Conference on Multi-Body Systems*. Milano, Italy : ECCOMAS, 2007
- [23] FRÉMOND, M. : *Non-smooth thermomechanics*. Berlin, Heidelberg, New York : Springer, 2002
- [24] FUNK, K. : *Simulation eindimensionaler Kontinua mit Unstetigkeiten*. Düsseldorf, Lehrstuhl für Angewandte Mechanik, TU München, Diss., 2004
- [25] GEIER, T. : *Dynamics of Push Belt CVTs*. Düsseldorf, Lehrstuhl für Angewandte Mechanik, TU München, Diss., 2007
- [26] GÉRADIN, M. ; CARDONA, A. : *Flexible Multibody Systems*. Chichester : John Wiley Inc., 2001
- [27] GERSTMAYR, J. : The Absolute Coordinate Formulation with Elasto-Plastic Deformations. In: *Multibody System Dynamics* 12 (2004), S. 363–383
- [28] GINZINGER, L. ; ZANDER, R. ; ULBRICH, H. : Controller Design for a Rubbing Rotor. In: *Proceedings of the 4th International Conference, Mechatronic Systems and Materials (MSM 2008)*. Białystok, Poland, 2008
- [29] GLOCKER, C. : *Set-valued force laws, Dynamics of non-smooth systems*. Berlin, New York : Springer, 2001. – Lecture notes in applied mechanics 1
- [30] GLOCKER, C. : Concepts for modeling impacts without friction. In: *Acta Mechanica* 168 (2004), S. 1–19
- [31] GROSS, D. ; HAUGER, W. ; SCHNELL, W. ; WRIGGERS, P. : *Technische Mechanik 4*. Berlin, Heidelberg, New York : Springer, 1999
- [32] HAIRER, E. ; NORSETT, S. P. ; WANNER, G. : *Solving Ordinary Differential Equations I. Nonstiff problems*. Berlin, Heidelberg, New York : Springer, 1987
- [33] HAIRER, E. ; WANNER, G. : *Solving Ordinary Differential Equations II. Stiff and Differential-Algebraic Problems*. Berlin, Heidelberg, New York : Springer, 1991
- [34] HIBBELER, R. C. : *Mechanics of materials*. Prentice Hall, 2003

- [35] HIPPMANN, G. : An Algorithm for Compliant Contact between Complexly Shaped Surfaces in Multibody Dynamics. In: *Proceedings of the ECCOMAS Conference on Multi-Body Systems*. Lisbon, Portugal : ECCOMAS, 2003
- [36] HIPPMANN, G. : *Modellierung von Kontakten komplex geformter Körper in der Mehrkörperdynamik*, Technische Universität Wien, Diss., 2004
- [37] HUBER, R. ; ULBRICH, H. : Simulation of a Valve Train Using Non-Smooth Mechanics. In: *Proceedings of the SAE 2008 World Congress*. Detroit, USA, 2008
- [38] JEAN, M. : The nonsmooth contact dynamics method. In: *Computer Methods in Applied Mechanics and Engineering* 177 (1999), S. 235–257
- [39] LEINE, R. I. ; GLOCKER, C. : A set-valued force law for spatial COULOMB-CONTENSOU friction. In: *European Journal of Mechanics* 22 (2003), S. 193–216
- [40] MAGNUS, K. : *Dynamics of multibody systems*. Berlin, Heidelberg, New York : Springer, 1978
- [41] MARSDEN, J. E. ; RATIU, T. S.: *Introduction to Mechanics and Symmetry*. Berlin, Heidelberg, New York : Springer, 1999
- [42] MOREAU, J. J.: Unilateral Contact and Dry Friction in Finite Freedom Dynamics. In: *International Centre for Mechanical Sciences, Courses and Lectures*. Bd. 302. Montpellier, France : Springer, 1988
- [43] PANAGIOTOPOULOS, P. : Variational Principles for Contact Problems Including Impact Phenomena. In: *Contact Mechanics* Bd. 168. Wien, New York : Springer, 1994, S. 431–440
- [44] PFEIFFER, F. : *Einführung in die Dynamik*. Wiesbaden : Teubner Verlag, 1997
- [45] PFEIFFER, F. ; GLOCKER, C. : *Multibody Dynamics with Unilateral Contacts*. New York : John Wiley Inc., 1996
- [46] PIEGL, L. A. ; TILLER, W. : *The NURBS book*. Berlin, Heidelberg, New York : Springer, 1997
- [47] RITZ, W. : Über eine neue Methode zur Lösung gewisser Randwertaufgaben. In: *Journal für die reine und angewandte Mathematik* 135 (1908), S. 1–61
- [48] ROCKAFELLAR, R. T.: Augmented Lagrangians and applications of the proximal point algorithm in convex programming. In: *Mathematics of Operations Research* 1 (1976), S. 97–116
- [49] SCHIEHLEN, W. : Multibody System Dynamics: Roots and Perspectives. In: *Multibody System Dynamics* 1 (1997), S. 149–188
- [50] SCHINDLER, T. ; GEIER, T. ; ULBRICH, H. ; PFEIFFER, F. ; VELDE, A. van d. ; BRANDSMA, A. : Dynamics of Pushbelt CVTs. In: *VDI-Berichte 1997 - Umschlingungsgetriebe*. Berlin : VDI-Verlag, June 2007
- [51] SCHINDLER, T. ; ULBRICH, H. ; PFEIFFER, F. ; VELDE, A. van d. ; BRANDSMA, A. : Pushbelt CVTs – A Non-Smooth Challenge. In: *Proceedings of the ENOC Six EUROMECH Nonlinear Dynamics Conference*. St. Petersburg, Russia, 2008
- [52] SCHWERTASSEK, R. ; WALLRAPP, O. : *Dynamik flexibler Mehrkörpersysteme*. Vieweg, 1999

- [53] SEIFRIED, R. : *Numerische und experimentelle Stoßanalyse für Mehrkörpersysteme*. Aachen, Institut für Technische und Numerische Mechanik, Universität Stuttgart, Diss., 2005
- [54] SHABANA, A. A.: Constrained Motion of Deformable Bodies. In: *International Journal for Numerical Methods in Engineering* 32 (1991), S. 1813–1831
- [55] SHABANA, A. A.: Definition of the Slopes and the Finite Element Absolute Nodal Coordinate Formulation. In: *Nonlinear Dynamics* 1 (1997), S. 339–348
- [56] SHABANA, A. A.: *Dynamics of Multibody Systems*. 3rd Edition. Cambridge ; New York : Cambridge University Press, 2005
- [57] STIEGELMEYR, A. : *Zur numerischen Berechnung strukturvarianter Systeme*. Düsseldorf, Lehrstuhl für Angewandte Mechanik, TU München, Diss., 2001
- [58] STUDER, C. : *Augmented time-stepping integration of non-smooth dynamical systems*, ETH Zurich, Diss., 2008.
http://www.zfm.ethz.ch/dynamY/index_download.html
- [59] TESCHNER, M. ; KIMMERLE, S. ; HEIDELBERGER, B. ; ZACHMANN, G. ; RAGHUPATHI, L. ; FUHRMANN, A. ; CANI, M. ; FAURE, F. ; MAGNENAT-THALMANN, N. ; STRASSER, W. ; VOLINO, P. : Collision Detection for Deformable Objects. (2005). <http://citeseer.ist.psu.edu/teschner04collision.html>
- [60] ULBRICH, H. : *Maschinendynamik*. Wiesbaden : Teubner Verlag, 1996
- [61] VERESHCHAGIN, A. F.: Computer simulation of the dynamics of complicated mechanisms of robot manipulators. In: *Engineering Cybernetics* 6 (1974), S. 65–70
- [62] WASFY, T. M. ; NOOR, A. K.: Computational strategies for flexible multibody systems. In: *Applied Mechanics Reviews* (2002), S. 553–613
- [63] WELGE-LÜSSEN, T. : *Design of a Passively Actuated Robot Manipulator*, ETH Zurich, Diss., 2008
- [64] WRIGGERS, P. : *Computational Contact Mechanics*. Chichester : John Wiley Inc., 2002
- [65] ZANDER, R. ; FÖRG, M. ; ULBRICH, H. : Impacts on beam structures: Interactions of wave propagation and global dynamics. In: *IUTAM – Multiscale Problems in Multibody System Contacts*. Berlin, Heidelberg, New York : Springer, 2007
- [66] ZANDER, R. ; SCHINDLER, T. ; FRIEDRICH, M. ; HUBER, R. ; FÖRG, M. ; ULBRICH, H. : Non-smooth dynamics in academia and industry: recent work at TU München. In: *Acta Mechanica* (2008), S. 167–183
- [67] ZANDER, R. ; ULBRICH, H. : Free plain motion of flexible beams in MBS – A comparison of models. In: *Nonlinear Dynamics of Moving Structures – Journal of Mechanics Based Design of Structures and Machines* 34 (2006), Nr. 4, S. 365–387
- [68] ZANDER, R. ; ULBRICH, H. : Reference-free mixed FE-MBS approach for beam structures with constraints. In: *Nonlinear Dynamics* 46 (2006), Nr. 4, S. 349–361